IRF4 haploinsufficiency in a family with Whipple's disease

Antoine Guérin, M.Sc.,[1,2] Gaspard Kerner, M.Sc.,[1,2,*] Nico Marr, Ph.D.,[3,*]
Janet G. Markle, Ph.D.,[4,§] Florence Fenollar, M.D., Ph.D.,[5,§] Natalie Wong, B. Sc. (Hons),[6,7,§]
Sabri Boughorbel, Ph.D.,[3,§] Danielle T. Avery, B. Sc.,[6,7,§] Cindy S. Ma, Ph.D.,[6,7,§]
Salim Bougarn,Ph.D.,[3,§] Matthieu Bouaziz, Ph.D.,[1,2] Vivien Beziat, Ph.D.,[1,2]
Erika Della Mina, Ph.D.,[1,2] Tomi Lazarov, B.Sc.,[8] Lisa Worley, B.Sc. (Hons),[6,7]
Tina Nguyen, B.Sc. (Hons),[6,7] Etienne Patin, Ph.D.,[9,10,11] Caroline Deswarte, M.Sc.,[1,2]
Rubén Martinez-Barricarte, Ph.D.,[4] Soraya Boucherit, M.D.,[1,2] Xavier Ayral, M.D.,[12]
Sophie Edouard, PharmD.,[5] Stéphanie Boisson-Dupuis, Ph.D.,[1,2,4] Vimel Rattina, M.Sc.,[1,2]
Benedetta Bigio, M.Sc.,[4] Guillaume Vogt, Ph.D.,[2] Frédéric Geissmann, M.D., Ph.D.,[8,13,°]
Lluis Quintana-Murci, Ph.D.,[9,10,11,°] Damien Chaussabel, Ph.D.,[3,°] Stuart G. Tangye, Ph.D.,[6,7,°]
Didier Raoult, M.D., Ph.D.,[5,#] Laurent Abel, M.D., Ph.D.,[1,2,4,#]
Jacinta Bustamante, M.D., Ph.D.,[1,2,4,14,#] and Jean-Laurent Casanova, M.D., Ph.D.[1,2,4,15,16,#,@]

1. Laboratory of Human Genetics of Infectious Diseases, Necker Branch, INSERM U1163, 75015 Paris, France, EU.
2. Paris Descartes University, Imagine Institute, 75015 Paris, France, EU.
3. Sidra Medical and Research Center, Doha, Qatar.
4. St. Giles Laboratory of Human Genetics of Infectious Diseases, Rockefeller Branch, The Rockefeller University, New York, NY 10065, USA.
5. Research Unit of Infectious and Tropical Emerging Diseases, University Aix-Marseille, URMITE, UM63, CNRS 7278, IRD 198, 13005 Marseille, France, EU.
6. Immunology Division, Garvan Institute of Medical Research, Darlinghurst, NSW 2010, Australia.
7. St Vincent's Clinical School, Faculty of Medicine, UNSW Sydney NSW 2010, Australia.
8. Immunology Program and Ludwig Center, Memorial Sloan Kettering Cancer Center, New York, NY 10065, USA.
9. Human Evolutionary Genetics, Department of Genomes & Genetics, Institut Pasteur, Paris 75015, France, EU.
10. CNRS URA3012, 75015 Paris, France, EU.
11. Center of Bioinformatics, Biostatistics and Integrative Biology, Institut Pasteur, 75015 Paris, France, EU.
12. Rheumatology Unit, Cochin Hospital, 75014 Paris, France, EU.
13. Weill Cornell Graduate School of Medical Sciences, New York, NY 10065, USA.
14. Center for the Study of Primary Immunodeficiencies, Assistance Publique-Hôpitaux de Paris, Necker Hospital for Sick Children, 75015 Paris, France, EU.
15. Pediatric Hematology and Immunology Unit, Assistance Publique-Hôpitaux de Paris, Necker Hospital for Sick Children, 75015 Paris, France, EU.
16. Howard Hughes Medical Institute, New York, NY 10065 USA.

*,§,°,# Equal contributions

@ Correspondence: casanova@rockefeller.edu

Keywords: Whipple's disease, primary immunodeficiency, IRF4, haploinsufficiency

Running title: Whipple's disease and IRF4 deficiency

Conflict of interest statement: The authors have no conflict of interest to declare.

Abstract

The pathogenesis of Whipple's disease (WD) remains largely unknown, as WD strikes only a very small minority of the individuals infected with *Tropheryma whipplei* (Tw). Asymptomatic carriage of Tw is less rare. We studied a large multiplex French kindred, containing four otherwise healthy WD patients (mean age: 76.7 years) and five healthy carriers of Tw (mean age: 55 years). We used a strategy combining genome-wide linkage analysis and whole-exome sequencing to test the hypothesis that WD is inherited in an autosomal dominant (AD) manner, with age-dependent incomplete penetrance. WD was linked to 12 genomic regions covering 27 megabases in the four patients. These regions contained only one very rare non-synonymous variation: the R98W variant of *IRF4*. The five Tw carriers were heterozygous for R98W. Interferon regulatory factor 4 (IRF4) is a transcription factor with pleiotropic roles in immunity. We showed that R98W was a loss-of-function allele, like only five other exceedingly rare *IRF4* alleles of a total of 39 rare and common non-synonymous alleles tested. Furthermore, heterozygosity for R98W led to a distinctive pattern of transcription in leukocytes following stimulation with BCG or Tw. Finally, we found that *IRF4* had evolved under purifying selection and that R98W was not dominant-negative, suggesting that the IRF4 deficiency in this kindred was due to haploinsufficiency. Overall, haploinsufficiency at the *IRF4* locus selectively underlies WD in this multiplex kindred. This deficiency displays AD inheritance with incomplete penetrance, and chronic carriage probably precedes WD by several decades in Tw-infected heterozygotes.

Introduction

Whipple's disease (WD) was first described as an intestinal inflammatory disease by George H. Whipple in 1907 (1). Its infectious origin was suspected in 1961 (2), and the causal microbe, *Tropheryma whipplei* (Tw), a Gram-positive actinomycete, was detected by PCR in 1992 (3), and cultured in 2000 (4). Tw is probably transmitted between humans via the oro-oral or feco-oral routes. WD is a chronic condition with a late onset (mean age at onset: 55 years) (5) affecting multiple organs. The clinical manifestations of classical WD are arthralgia, diarrhea, abdominal pain, and weight loss (6-10). However, about 25% of WD patients display no gastrointestinal or osteoarticular symptoms, instead presenting with cardiac and/or neurological manifestations (8, 11-14). WD is fatal if left untreated, and relapses occur in 2 to 33% of treated cases, even after prolonged appropriate antibiotic treatment (15), (16). WD is rare and has been estimated to affect about one in a million individuals (6, 17, 18). However, about two thousand cases have been reported in at least nine countries worldwide, mostly in North America and Western Europe (11, 19-23). Chronic asymptomatic carriage of Tw is common in the general population, and this bacterium has been detected in feces, saliva, and intestinal mucosae. The prevalence of Tw carriage in the feces has been estimated at 2 to 11% for the general population, but can reach 26% in sewer workers and 37% in relatives of patients and carriers (11, 14, 17, 24-28).

Seroprevalence for specific antibodies against Tw in the general population varies from 50% in France to 70% in Senegal (4, 11, 14, 29). At least 75% of infected individuals clear Tw primary infections, but a minority (<25%) become asymptomatic carriers, a small proportion of whom develop WD (~0.01%) (30). Tw infection is therefore necessary, but not sufficient, for WD development and it is unclear whether prolonged asymptomatic carriage necessarily precedes WD. The hypothesis that WD results from the emergence of a more pathogenic clonal strain of Tw was not supported by bacterial genotyping (31). WD mostly affects individuals of

European origin, but does not seem to be favored by specific environments. WD is typically sporadic, but six multiplex kindreds have been reported, with cases often diagnosed years apart, suggesting a possible genetic component (8, 17, 32). WD patients are not prone to other severe infections (33). Moreover, WD has never been reported in patients with conventional primary immunodeficiencies (PIDs) (34). This situation is reminiscent of other sporadic severe infections, such as herpes simplex virus-1 encephalitis, severe influenza, recurrent rhinovirus infection, and severe varicella zoster disease, which are caused by single-gene inborn errors of immunity in some patients (35-38). We therefore hypothesized that WD might be due to monogenic inborn errors of immunity to Tw, with age-dependent incomplete penetrance.

Results

A multiplex kindred with WD

We investigated four related patients diagnosed with WD (P1, P2, P3, and P4) with a mean age at diagnosis of 58 years. They belong to a large non-consanguineous French kindred (Figure 1, A). The proband (P1), a 69-year-old woman, presented with right knee arthritis in 2011, after recurrent episodes of arthritis of the right knee since 1980. Tw was detected in the synovial fluid by PCR and culture, but not in saliva, feces, or small intestine tissue by PCR. Treatment with doxycycline and hydroxychloroquine was effective. At last follow-up, in 2016, P1 was well and Tw PCR on saliva and feces was negative. P2, a second cousin of P1, is a 76-year-old woman with classical WD diagnosed at 37 years of age in 1978 by periodic acid–Schiff (PAS) staining of a small intestine biopsy specimen. She was treated with sulfamethoxazole/trimethoprim. At last follow-up, in 2016, Tw PCR on saliva and feces was positive. P3, the father of P1, is a 92-year-old man with classical WD diagnosed at 62 years of age, in 1987, based on positive PAS staining of a small intestine biopsy specimen. Long-term

sulfamethoxazole/trimethoprim treatment led to complete clinical and bacteriological remission. P4, the brother of P2, is a 70-year-old man who consulted in 2015 for arthralgia of the knees and right ulna-carpal joints. PCR and culture did not detect Tw in saliva and feces, but serological tests for Tw were positive. Treatment with methotrexate and steroids was initiated before antibiotics, the effect of which is currently being evaluated. All four patients are otherwise healthy. Saliva and/or feces samples from 18 other members of the family were tested for Tw (Figure 1, A; table S1). Five individuals are chronic carriers (mean age: 55 years) and 13 tested negative (mean age: 38 years). Nine additional relatives could not be tested. The distribution of WD in this kindred was suggestive of an AD trait with incomplete penetrance.

A private heterozygous missense *IRF4* variant segregates with WD

We analyzed the familial segregation of WD by genome-wide linkage (GWL), using information from both genome-wide single-nucleotide polymorphism (SNP) microarrays and whole-exome sequencing (WES) (39). Multipoint linkage analysis was performed under an AD model with a very rare disease-causing allele ($<10^{-5}$) and age-dependent incomplete penetrance (see Supplementary Results). Twelve chromosomal regions linked to WD were identified on chromosomes 1 (x3), 2, 3, 6, 7, 8, 10, 11, 12 and 17, with a LOD score close (>1.90) to the maximum expected value (1.95) (Figure S1, A). These regions covered 27.18 Mb and included 263 protein-coding genes. WES data analysis for these 263 genes identified 54 heterozygous non-synonymous coding variants common to all four WD patients (Table S2). Only one, a variant of the *IRF4* gene encoding a transcription factor, member of the *IRF* family (40), and located in a 200 kb linked region on chromosome 6 (Figure S1 A, B), was very rare, and was even found to be private [not found in the GnomAD database, http://gnomad.broadinstitute.org, or in our own WES database (HGID)], whereas all other variants had a frequency >0.001, which

is inconsistent with the frequency of WD and our hypothesis of a very rare ($<10^{-5}$) deleterious heterozygous allele. The variant is a c.292 C>T substitution in exon 3 of *IRF4*, replacing the arginine residue in position 98 with a tryptophan residue (R98W) (Figure 1, A, B, C). IRF4 is a transcription factor with an important pleiotropic role in innate and adaptive immunity, at least in mice (41). Mice heterozygous for a null *Irf4* mutation have not been studied, but homozygous null mice have various T- and B-cell abnormalities and are susceptible to both *Leishmania* and lymphocytic choriomeningitis virus (see Supplementary Results) (42-47). We confirmed the *IRF4* R98W mutation by Sanger sequencing genomic DNA from the blood of the four WD patients (Figure 1, C). Thirteen relatives of the WD patients were WT/WT at the *IRF4* locus, and 10 of these relatives (77%) tested negative for Tw carriage. Eight other relatives were heterozygous for the *IRF4* R98W mutation, five of whom (62.5%) were Tw carriers (mean age: 55 years) (Figure 1, A; table S1). Overall, 12 individuals from the kindred, including the four patients, the five chronic carriers of Tw, two non-carriers of Tw and one relative not tested for Tw, were heterozygous for *IRF4* R98W (Figure 1, A; table S1). The familial segregation of the *IRF4* R98W allele was therefore consistent with an AD pattern of WD inheritance with incomplete penetrance. Chronic Tw carriage also followed an AD mode of inheritance.

R98W is predicted to be loss-of-function, unlike most other IRF4 variants

The R98 residue in the DNA-binding domain (DBD) of IRF4 is highly conserved in the 12 species for which *IRF4* was sequenced (Figure 1, B, D). It has been suggested that this residue is essential for IRF4 DNA-binding activity, because the R98A-C99A double mutant is loss-of-function (48, 49). The R98W mutation is predicted to be damaging by multiple programs (50); it has a CADD score of R98W (26.5), well above the mutation significance cutoff (MSC) of IRF4 (11.125) (Figure S2) (50, 51). The R98W variant was not present in the GnomAD database or our in-house HGID database of more than 4,000 exomes from patients

with various infectious diseases. The mutant allele was not found in the sequences for the CEPH-HGDP panel of 1,052 controls from 52 ethnic groups, or in 100 French controls, confirming that this variant was very rare, probably private to this kindred. Therefore, the minor allele frequency (MAF) of this private allele is $<4x10^{-6}$. Moreover, the *IRF4* gene has a gene damage index (GDI) of 2.85, a neutrality index score of 0.15 (52), and a purifying selection *f* parameter of 0.32 (among the <10% of genes in the genome subject to the greatest constraint; Figure S3A), strongly suggesting that *IRF4* has evolved under purifying selection (i.e., strong evolutionary constraints) (53). Biologically disruptive heterozygous mutations of *IRF4* are therefore likely to have clinical effects. We identified 156 other high-confidence heterozygous non-synonymous coding or splice variants of *IRF4* (Table S3) in public (GnomAD: 153 variants, all with MAF<0.009) and HGID (3 variants) databases: 147 were missense (two were also found in the homozygous state), four were frameshift indels, three were in-frame indels, one was a nonsense variant, and one was an essential splice variant. Up to 150 of the 156 variants are predicted to be benign, whereas only six were predicted to be potentially loss-of-function (LOF) according to the GnomAD classification. Comparison of the CADD score and MAF of these *IRF4* variants, showed R98W to have the second highest CADD score of the four variants with a MAF $< 4 \times 10^{-6}$ (Figure S2). These findings suggest that the private heterozygous *IRF4* variant of this kindred is biochemically deleterious, unlike most other rare (MAF<0.009) non-synonymous variants in the general population, 150 of 156 of which were predicted to be benign (54).

R98W is loss-of-function, unlike most other IRF4 variants

We first characterized IRF4 R98W production and function *in vitro*, in an overexpression system. We assessed the effect of the *IRF4* R98W mutation on IRF4 levels by transiently expressing WT or mutant R98W in HEK293-T cells. IRF4 R98A-C99A, which is

LOF for DNA-binding (49), was included as a negative control. In total cell extracts, mutant IRF4 proteins were more abundant than the WT protein, and had the expected molecular weight (MW) of 51 kDa, as shown by western blotting (Figure 2A). The R98 residue has been shown to be located in a nuclear localization signal, the complete disruption of which results in a loss of IRF4 retention in the nucleus (55). We therefore analyzed the subcellular distribution of IRF4 WT and R98W proteins, in total, cytoplasmic and nuclear extracts from transiently transfected HEK293-T cells. The R98W mutant was more abundant than the WT protein in total cell and cytoplasmic extracts, but these proteins were similarly abundant in nuclear extracts (Figure 2B). We performed luciferase reporter assays to assess the ability of the mutant IRF4 protein to induce transcription from interferon-stimulated response element (*ISRE*) motif-containing promoters. Unlike the WT protein, both R98W and R98A-C99A failed to activate the $(ISRE)_3$ promoter (Figure 2C). We observed no dominant-negative effect of the IRF4 R98W protein (Figure S4). We assessed the ability of R98W to bind DNA, in an electrophoretic mobility shift assay (EMSA) (Figure 2, D, E). Signal specificity was assessed by analyzing both supershift with an IRF4-specific antibody and by competition with an unlabeled competitor probe. The R98W mutation abolished IRF4 binding to the *ISRE cis* element (Figure 2D), and binding of the IRF4-PU.1 complex to interferon composite elements (EICEs) containing both IRF4 and PU.1 recognition motifs (Figure 2E). The R98W allele of *IRF4* is therefore LOF for both DNA binding and the induction of transcription. Next, we tested 39 of the 156 other *IRF4* variants, including all variants found in GnomAD with a MAF above $4.5x10^{-5}$ (sixteen variants), or with a CADD score above 30 (ten variants), variants predicted to be LOF (five variants including two with a CADD score above 30; the splice variant could not be tested) and variants in the HGID database (three private variants and seven also present in GnomAD) (Figure S3, B, C). Thirty one variants were normally expressed (two of them with higher molecular weight), the five predicted LOF tested were not detectable (as expected since the antibody epitope is in the

IRF4 C terminus), as well as three missense (Figure S5, A, B). When tested for $(ISRE)_3$ promoter activation, only four variants from public databases (P208Q, R259W, R376C and R376H, MAF between 4.1 $x10^{-6}$ and $7.2x10^{-5}$) and one from the HGID database (G279-H280 del, private to one family) were LOF (Figure S5, C, D). Our data show that the R98W *IRF4* allele is LOF, like only five very rare other non-synonymous *IRF4* variants out of the 39 variants tested.

AD IRF4 deficiency phenotypes in heterozygous EBV-B cells

We investigated the cellular phenotype of heterozygosity for the R98W allele in EBV-transformed B-cell lines (EBV-B cells) from patients. We performed reverse transcription-quantitative polymerase chain reaction (RT-qPCR) on EBV-B cells from P1, P3, two healthy heterozygous relatives (*IRF4* WT/R98W), four healthy *IRF4*-WT homozygous relatives, 25 patients from our WD cohort (with unknown genetic etiologies) and seven healthy unrelated individuals (*IRF4* WT/WT). Cells from individuals heterozygous for the R98W mutation (patients and healthy carriers) had higher *IRF4* mRNA levels than those from WT homozygous relatives, unrelated WD cohort patients and EBV-B cells from unrelated healthy controls (Figure S6, A). We compared the relative abundances of WT and R98W *IRF4* mRNA in EBV-B cells from heterozygous carriers of the mutation, by performing TA-cloning experiments on P1, P3, one healthy heterozygous relative, one relative homozygous for WT *IRF4*, and two previously tested unrelated controls. In heterozygous carriers of the mutation (patients and healthy relatives) 48.1%-60% of the total *IRF4* mRNA carried the R98W mutation, whereas the rest was WT (Figure S6, B). We evaluated the levels and distribution of IRF4 protein by western blot in EBV-B cells from P1, P2, P3, one healthy heterozygous relative, three healthy homozygous WT relatives and five unrelated healthy individuals. As in transfected HEK293-T

cells, IRF4 protein levels were high in both total cell and cytoplasmic extracts of EBV-B cells from heterozygous carriers (Figure S7, A, B). By contrast, IRF4 protein levels in EBV-B cell nuclei were similar in heterozygous mutation carriers and controls (Figure S7, C). As IRF4 is a transcription factor, we then analyzed the steady-state transcriptome of EBV-B cells from three healthy homozygous WT relatives and three WT/R98W heterozygotes (P1, P3, VI.6). We identified 37 protein-coding genes as differentially expressed between subjects heterozygous for *IRF4* and those homozygous WT for *IRF4* (18 upregulated and 19 downregulated; data not shown). We identified no marked pathway enrichment based on these genes. EBV-B cells from *IRF4*-heterozygous individuals had a detectable phenotype, in terms of IRF4 production and function, consistent with AD IRF4 deficiency underlying WD.

AD IRF4 deficiency phenotypes in heterozygous leukocytes

We assessed IRF4 levels in myeloid and lymphoid cells from healthy controls (see Supplementary Results). IRF4 levels were highest in $CD4^+$ T cells, particularly after stimulation with CD2/CD3/CD28 beads (see Supplementary Results). We therefore assessed the IRF4 protein expression profile in $CD4^+$ T cells from four controls, P1 and P3, with and without (non-stimulated, NS) stimulation with CD2/CD3/CD28-coated beads. The results were consistent with those for transfected HEK293-T and EBV-B cells, as IRF4 levels in total and cytoplasmic extracts were higher in $CD4^+$ T cells from P1 and P3, whereas IRF4 levels in the nucleus were similar in heterozygous mutation carriers and controls (Figure 3, A, B, C). We checked for transcriptomic differences associated with genotype and/or infection, by investigating the transcriptomes of peripheral mononuclear blood cells (PBMCs) from six *IRF4*-heterozygous individuals (three patients, P1-P3; and three healthy relatives, HET1-HET3) and six *IRF4* WT-homozygous individuals (four healthy relatives, WT1-WT4; and two unrelated controls, C1-

C2) with and without *in vitro* infection with Tw, or *Mycobacterium bovis*-Bacillus Calmette-Guerin (BCG) for 24 hours. We performed unsupervised hierarchical clustering of the differentially expressed (DE) transcripts (infected versus uninfected) to analyze the overall responsiveness of PBMCs from individual subjects to BCG and Tw infections *in vitro*. Heterozygous individuals clearly clustered separately from homozygous WT individuals (Figure 4, A), revealing a correlation between genotype and response to infection. In homozygous WT subjects, 402 transcripts from 193 unique genes were responsive to BCG infection, and 119 transcripts from 29 unique genes were responsive to Tw infection (Table S4 A, B). Due to the small number of Tw-responsive transcripts linked to unique genes, we were unable to detect any pathway enrichment in this specific condition. However, we identified 24 canonical pathways as enriched after the exposure of PBMCs to BCG. We ranked these pathways according to the difference in mean *z*-score between homozygous WT and heterozygous subjects (Figure 4, B). The top 10 pathways included the interferon signaling network, the Th1 pathway network, the HMGB1 signaling network, the p38 MAPK signaling network, the NF-κB signaling network, the dendritic cell maturation network and the network responsible for producing nitric oxide and reactive species. These pathways were highly ranked mostly due to *IFNG* and *STAT1*, which were strongly downregulated in *IRF4* heterozygotes, particularly in P1, P2 and P3, relative to WT homozygotes. IRF4 is predicted to bind the promoter regions of 47% of the genes identified in the BCG study (91 of 193 genes), including those of *IFNG* and *STAT1*. Subjects heterozygous for *IRF4* also had lower levels of *LTA* expression and lower levels of *IL2RA* expression were observed specifically in patients (Table S4). These data suggest a general impairment of the T-cell response in subjects heterozygous for *IRF4* upon BCG infection *in vitro*. Moreover, the lower levels of *CD80* expression suggest a possible impairment of myeloid and/or antigen-presenting cell function upon BCG infection in patients but not in healthy heterozygous or homozygous WT subjects (Table S4). Peripheral

leukocytes from *IRF4*-heterozygous individuals therefore had a phenotype in terms of IRF4 production and function.

Discussion

WD was initially described as an inflammatory disease (1), but subsequently shown to be infectious (2-4). We provide evidence that WD is also a genetic disorder. We show here that, in a large multiplex kindred, heterozygosity for the private, loss-of-function R98W mutation of *IRF4* underlies an AD form of WD with incomplete penetrance. The causal relationship between *IRF4* genotype and WD was demonstrated as follows. First, the *IRF4* R98W mutation is the only non-synonymous rare variant segregating with WD in this kindred. Second, the mutation was demonstrated experimentally to be loss-of-function, unlike 34 of 39 other non-synonymous *IRF4* variants in the general population, including all eight variants with a MAF greater than 0.0001. Only six of the 156 identified *IRF4* variants were predicted to be LOF, five of which were experimentally tested and shown not to be LOF. Moreover, *IRF4* has evolved under purifying selection, suggesting that deleterious heterozygous variants of this gene entail fitness costs (56-58). Third, EBV-B cell lines heterozygous for *IRF4* R98W have a distinctive phenotype, particularly for IRF4 expression. This mutation also has a strong functional impact on the gene expression of *IRF4* R98W-heterozygous PBMCs stimulated with BCG or Tw. These findings unequivocally show that heterozygosity for the R98W allele of *IRF4* is the genetic etiology of WD in this kindred. Other patients may also develop WD due to inborn errors of immunity. WD is a late-onset infectious disease. This observation therefore extends our model, in which life-threatening infectious diseases striking otherwise healthy individuals during primary infection can result from single-gene inborn errors of immunity (35, 36).

In this kindred with AD IRF4 deficiency, haploinsufficiency was identified as the key mechanism, although IRF4 protein levels in the cytoplasmic compartment were higher in patients with the mutation than in wild-type homozygotes. The protein was not more abundant in the nucleus, where IRF4 exerts its effects on transcription. Moreover, not only is *IRF4* subject to purifying selection, but the R98W mutation is itself LOF, with no detectable dominant-

negative effect at cell level. Haploinsufficiency is an increasingly recognized mechanism underlying AD inborn errors of immunity (58, 59). It is commonly due to loss-of-expression alleles, contrasting with the negative dominance typically exerted by expressed proteins, but many mutations are known to cause haploinsufficiency without actually preventing protein production (58-60). Incomplete penetrance is common in conditions resulting from haploinsufficiency. In this kindred, incomplete penetrance may result from a lack of Tw infection, or a lack of WD development in infected individuals. All five chronic carriers of Tw were heterozygous, suggesting that AD IRF4 deficiency also favors the development of chronic Tw carriage, also with incomplete penetrance. The five asymptomatic carriers were 24 to 82 years old, whereas the four patients were 69 to 92 years old. All were heterozygous. The impact of IRF4 R98W may therefore increase with age, initially facilitating chronic carriage in Tw-infected individuals, and subsequently predisposing chronic carriers to WD. Future studies will attempt to define the cellular basis of WD in individuals with *IRF4* mutations. The apparently normal development and function of all myeloid and lymphoid blood subsets studied in patients (see Supplementary Results), and the selective predisposition of these individuals to WD suggest that the disease mechanism is subtle and specifically affects protective immunity to Tw, and that it may act in the gastrointestinal tract.

Materials and Methods

Informed consent was obtained from all family members, and the study was approved by the national ethics committee.

Genome-wide analysis

Genome-wide linkage analysis was performed by combining genome-wide array and whole-exome sequencing (WES) data (39). In total, nine family members were genotyped with the Genome-Wide Human SNP Array 6.0. Genotype calling was achieved with the Affymetrix Power Tools Software Package (http://www.affymetrix.com/estore/partners_programs/programs/developer/tools/powertools.affx). SNPs were selected with population-based filters (61), resulting in the use of 905,420 SNPs for linkage analysis. WES was performed as described in the corresponding section, in four family members, P1, P2, P3 and P4. In total, 64,348 WES variants were retained after application of the following filtering criteria: genotype quality (GQ) > 40, minor read ratio (MRR) > 0.3, individual depth (DP) > 20x, retaining only diallelic variants with an existing RS number and a call rate of 100%. Parametric multipoint linkage analysis was performed with the Merlin program (62), using the combined set of 960,267 variants. We assumed an AD mode of inheritance with a frequency of the deleterious allele of 10^{-5} and a penetrance varying with age (0.8 above the age of 65 years, and 0.02 below this threshold). Data for the family and for Europeans from the 1000G project were used to estimate allele frequencies and to define linkage clusters, with an r^2 threshold of 0.4.

The method used for WES have been described elsewhere (63, 64). Briefly, genomic DNA extracted from the patients' blood cells was sheared with a Covaris S2 Ultrasonicator (Covaris). An adapter-ligated library was prepared with the Paired-End Sample Prep kit V1

(Illumina). Exome capture was performed with the SureSelect Human All Exon kit (71 Mb version - Agilent Technologies). Paired-end sequencing was performed on an Illumina Genome Analyzer IIx (Illumina), generating 72- or 100-base reads. We used a BWA-MEM aligner (65) to align the sequences with the human genome reference sequence (hg19 build). Downstream processing was carried out with the Genome analysis toolkit (GATK) (66) SAMtools (67), and Picard Tools (http://picard.sourceforge.net). Substitution calls were made with a GATK UnifiedGenotyper, whereas indel calls were made with a SomaticIndelDetectorV2. All calls with a read coverage <2x and a Phredscaled SNP quality <20 were filtered out. Single-nucleotide variants (SNV) were filtered on the basis of dbSNP135 (http://www.ncbi.nlm.nih.gov/SNP/) and 1000 Genomes (http:browser.1000genomes.org/index.html) data. All variants were annotated with ANNOVAR (68). All *IRF4* mutations identified by WES were confirmed by Sanger sequencing.

Tw detection

PCR and serological tests for Tw were performed as previously described (29).

Cell culture and subpopulation separation

PBMCs were isolated by Ficoll-Hypaque density centrifugation (GE Healthcare) from cytopheresis or whole-blood samples obtained from healthy volunteers and patients, respectively. PBMCs and EBV-B cells were cultured in RPMI medium supplemented with 10% FBS, whereas HEK293-T cells were cultured in DMEM medium supplemented with 10%

FBS. Subsets were separated by MACS, using magnetic beads conjugated with the appropriate antibody (Miltenyi Biotec) according to the manufacturer's protocol.

Site-directed mutagenesis and transient transfection

The full-length cDNA of *IRF4* and *PU.1* was inserted into the pcDNA™ 3.1D/V5-His-TOPO® vector with the directional TOPO expression kit (Thermo Fisher Scientific). Constructs carrying mutant alleles were generated from this plasmid by mutagenesis with a site-directed mutagenesis kit (QuikChangeII XL; Agilent Technologies), according to the manufacturer's instructions. HEK293 T cells were transiently transfected with the various constructs, using the Lipofectamine LTX kit (Thermo Fisher Scientific) in accordance with the manufacturer's instructions.

Cell lysis and western blotting

Total protein extracts were prepared by mixing cells with lysis buffer (50 mM Tris-HCl pH 7.4, 150 mM NaCl, 0.5% Triton X-100, and 2 mM EDTA supplemented with protease inhibitors (Complete, Roche) and phosphatase inhibitor cocktail (PhoStop, Roche), 0.1 mM dithiothreitol DTT (Life Technologies, California, USA), 10 µg/ml pepstatin A (Sigma, #P4265), 10 µg/ml leupeptin (Sigma, #L2884), 10 µg/ml antipain dihydrochloride (Sigma, #A6191) and incubating for 40 minutes on ice. A two-step extraction was performed to separate the cytoplasmic and nuclear content of the cells; cells were first mixed with a membrane lysis buffer (10 mM Hepes pH 7.9, 10 mM KCl, 0.1 mM EDTA, 0.1 mM EGTA, 0.05 % NP40, 25 mM NaF supplemented with 1 mM PMSF, 1 mM DTT, 10 µg/ml leupeptin, 10 µg/ml aprotinin) and incubated for 30 minutes on ice. The lysate was centrifuged at 10,000 x *g*. The supernatant, corresponding to the cytoplasm-enriched fraction, was collected and the nuclear pellet was

mixed with nuclear lysis buffer (20 mM Hepes pH 7.9, 0.4 M NaCl, 1,mM EDTA, 1, mM EGTA, 25% glycerol supplemented with 1 mM PMSF, 1 mM DTT, 10 µg/ml leupeptin, 10 µg/ml aprotinin). Equal amounts of protein, according to a Bradford protein assay (BioRad, Hercules, California, USA), were resolved by SDS-PAGE in a Criterion™ TGX™ 10% precast gel (Biorad) and transferred to a low-fluorescence PVDF membrane. Membranes were probed with unconjugated antibody: anti-IRF4 (Santa Cruz, M-17) antibody was used at a dilution of 1:1000 and antibodies against GAPDH (Santa Cruz, FL-335), topoisomerase I (Santa Cruz, C-21), and lamin A/C (Santa Cruz, H-110) were used as loading controls. The appropriate HRP-conjugated or infrared dye (IRDye)-conjugated secondary antibodies were incubated with the membrane for the detection of antibody binding by the ChemiDoc MP (Biorad) or Licor Odyssey CLx system (Li-Cor, Lincoln, Nebraska, USA) respectively.

EMSA

Double-stranded unlabeled oligonucleotides (cold probes) were generated by annealing in TE buffer (pH 7.9) supplemented with 33.3 mM NaCl and 0.67 mM $MgCl_2$. The annealing conditions were 100°C for 5 minutes, followed by cooling overnight at room temperature. After centrifugation at 3,000 x *g* centrifugation at 4°C for 30 minutes, the pellet was suspended in water. We labeled 0.1 µg of cold probe in Klenow buffer supplemented with 9.99 mM dNTP without ATP, 10 U Klenow fragment (NEB) and 50 µCi d-ATP-^{32}P, at 37°C for 60 minutes. Labeled probes were purified on Illustra MicroSpin G-25 Columns (GE Healthcare Life Sciences) according to the manufacturer's protocol. We incubated10 µg of nuclear protein lysate for 30 minutes on ice with ^{32}P-labeled (a-dATP) *ISRE* probe (5' – gat cGG GAA AGG GAA ACC GAA ACT GAA-3') designed on the basis of the *ISG15* promoter or λB probe (5'-gat cGC TCT TTA TTT TCC TTC ACT TTG GTT AC-3') described by Brass et al. in 1999

(49). For supershift assays, nuclear protein lysates were incubated for 30 minutes on ice with 2 µg of anti-IRF4 (Santa Cruz, M-17) antibody or anti-goat Ig (Santa Cruz) antibody. Protein/oligonucleotide mixtures were then subjected to electrophoresis in 12.5% acrylamide/bis-acrylamide 37.5:1 gels in 0.5% TBE migration buffer for 80 minutes at 200 mA. Gels were dried on Whatman paper at 80°C for 30 minutes and placed in a phosphor-screen cassette for five days. Radioactivity levels were analyzed with the Fluorescent Image Analyzer FLA-3000 system (Fujifilm). For oligonucleotide probes tagged at the 5' end with a fluorescent IRD700 tag (Metabion), fluorescence was measured with the Licor Odyssey CLx system (Li-Cor, Lincoln, Nebraska, USA) immediately after electrophoresis of the protein/oligonucleotide mixture as described above.

Luciferase reporter assays

The $(ISRE)_3$ reporter plasmid, which contains three repeats of the *ISRE* sequence separated by spacers was kindly provided by Prof. Aviva Azriel (Department of Biotechnology and Food Engineering, Technion-Israel Institute of Technology). HEK293 T cells were transiently transfected with the $(ISRE)_3$ reporter plasmid (100 ng/well for a 96-well plate), the pRL-SV40 vector (40 ng/well) and a *IRF4* WT or mutant pcDNA™ 3.1D/V5-His-TOPO® plasmid (25 ng/well, made up to 50 ng with empty plasmid), with the Lipofectamine LTX kit (Thermo Fisher Scientific), according to the manufacturer's instructions. Cells were used for luciferase assays 24 h after transfection, with the Dual-Luciferase® 1000 assay system kit (Promega), according to the manufacturer's protocol. Signal intensity was determined with a Victor™ X4 plate reader (Perkin Elmer). Experiments were performed in triplicate and $(ISRE)_3$ reporter activity is expressed as fold induction relative to cells transfected with the empty vector. Negative dominance was assessed by performing the same protocol with the following modifications: $(ISRE)_3$ reporter plasmid (100 ng/well for a 96-well plate), pRL-SV40 vector

(40 ng/well) WT and mutant plasmids were used to cotransfect cells, with a constant amount of WT plasmid (25 ng/well) but various amounts of mutant plasmid (25 ng/well alone made up to 50 ng with empty plasmid or 25 ng/well, 12.5 ng/well, or 6.25 ng/well made up to 25 ng with empty plasmid) for a total amount of 190 ng/well.

Microarrays

For the microarray analysis of PBMCs, cells from six *IRF4*-heterozygous individuals (three patients, P1-P3; and three healthy relatives, HET1-HET3) and six *IRF4* WT-homozygous individuals (four healthy relatives, WT1-WT4; and two unrelated controls, C1-C2) were dispensed into a 96-well plate at a density of 200,000 cells/well and were infected *in vitro* with live Tw at a multiplicity of infection (MOI) of 1, or with live BCG (*M. bovis*-BCG, Pasteur substrain) at a MOI of 20, or were left uninfected (mock). Two wells per condition were combined 24 h post-infection for total RNA isolation with the ZR RNA Microprep™ kit (Zymo Research). For the microarray on EBV-B cells, we used 400,000 cells from three *IRF4*-heterozygous mutation carriers and three WT individuals from the kindred for total RNA isolation with the ZR RNA Microprep™ kit (Zymo Research). Microarray experiments on both PBMCs and EBV-B cells were performed with the Affymetrix GeneChip Human Transcriptome Array 2.0. Raw expression data were normalized by the robust multi-array average expression (RMA) method implemented in the affy R package (69, 70). Normalized expression data were processed as follows, to select transcripts substantially affected by *in vitro* infection of PBMC samples obtained from the subjects described above with BCG or with Tw. First, fold-changes in expression between mock-infected and BCG-infected or Tw-infected conditions were calculated for each individual separately. For each set of conditions, transcripts were further filtered based on a minimal 1.5-fold change (FC) in expression (up- or downregulation), with a minimum absolute difference in expression of more than 150 relative

to unstimulated samples. In a final filtering stage, transcripts satisfying the previous filters in four of the six homozygous individuals with a normal genotype (WT and HET) for each *in vitro* infection condition were retained for downstream analysis and production of the corresponding figures. We analyzed the relative response, by counting the number of probes for which differences were observed between heterozygous individuals and subjects with a WT homozygous genotype. We calculated the number of probes affected by stimulation in samples from control subjects, for the same stimulus. The overall transcriptional responsiveness of individual subjects to both Tw and BCG is depicted as a heatmap, and individual subjects were grouped by unsupervised hierarchical clustering. Responsive transcripts were further analyzed with Ingenuity Pathway Analysis (IPA) Software, Version 28820210 (QIAGEN) (71) for functional interpretation. In brief, the FC values for each individual and treatment were used as input data for the identification of canonical pathway enrichment (*z*-score cut-off was set at 0.1). The activation *z*-score values calculated for the identified pathways were exported from IPA and used to calculate mean values and differences between WT homozygote and heterozygotes and for graphical representation, with Microsoft Excel and GraphPad Prism Version 7.0, respectively. The direction of the difference was not considered further. Negative mean difference values were converted into positive values before the ranking of the canonical pathways according to the difference between the genotypes. The microarray data used in this study have been deposited in the NCBI Gene Expression Omnibus (GEO), under accession number GSE102862.

***IRF4* qPCR**

Total RNA was prepared from the EBV-B cells of patients heterozygous for *IRF4* mutations and WT family members or unrelated individuals (healthy control and a patient with Tw carriage). RNA was prepared from 500,000 cells with the RNeasy Micro kit, according to

the manufacturer's instructions (Qiagen). A mixture of random octamers and oligo dT-16 was used with the MuLV reverse transcriptase (High-Capacity RNA-to-cDNA™ kit, Thermo Fisher Scientific), to generate cDNA. Quantitative real-time PCR was performed with the TaqMan® Universal PCR Master Mix (Roche), the *IRF4*-specific primer (Hs01056533_m1, Thermo Fisher Scientific) and the endogenous human β-glucuronidase (*GUSB*) as a control (4326320E, Thermo Fisher Scientific). Data were analyzed by the ΔΔCt method, with normalization against *GUSB*.

IRF4 TA-cloning

The full-length cDNA generated from the EBV-B cells of heterozygous and WT-homozygous individuals was used for the PCR amplification of exon 3 of *IRF4*. The products obtained were cloned with the TOPO TA cloning kit (pCR2.1®-TOPO® TA vector, Thermo Fisher Scientific), according to the manufacturer's instructions. They were then used to transform chemically competent bacteria, and 100 clones per individual were Sanger-sequenced with M13 primers (forward and reverse).

Ex vivo naïve and effector/memory CD4$^+$ T-cell stimulation

CD4$^+$ T cells were isolated as previously described (72). Briefly, cells were labeled with anti-CD4, anti-CD45RA, and anti-CCR7 antibodies, and naïve (defined as CD45RA$^+$ CCR7$^+$ CD4$^+$) T cells or effector/memory T cells (defined as CD45RA$^-$CCR7$^\pm$ CD4$^+$) were isolated (> 98% purity) with a FACS Aria cell sorter (BD Biosciences). Purified naïve or effector/memory CD4$^+$ T cells were cultured with T-cell activation and expansion beads (anti-CD2/CD3/CD28; Miltenyi Biotec) for 5 days; culture supernatants were then used to assess the secretion of IL-

2, IL-4, IL-5, IL-6, IL-9, IL-10, IL-13, IL-17A, IL-17F, IFNγ and TNFα with a cytometric bead array (BD) and the secretion of IL-22, by ELISA.

In vitro differentiation of naïve CD4$^+$ T cells

Naïve CD4$^+$ T cells (CD45RA$^+$CCR7$^+$) were isolated (> 98% purity) from healthy controls or patients, with a FACS Aria sorter (BD Biosciences). They were cultured under polarizing conditions, as previously described (72). Briefly, cells were cultured with T-cell activation and expansion beads (anti-CD2/CD3/CD28; Miltenyi Biotec) alone or under Th1 (IL-12 [20 ng/ml; R&D Systems]) or Th17 (TGFβ, IL-1β [20 ng/ml; Peprotech], IL-6 [50 ng/ml; PeproTech], IL-21 [50 ng/ml; PeproTech], IL-23 [20 ng/ml; eBioscience], anti-IL-4 [5 μg/ml], and anti-IFN-γ [5 μg/ml; eBioscience]) polarizing conditions. After five days, culture supernatants were used to assess the secretion of the cytokines indicated, by ELISA (IL-22), or with a cytometric bead array (all other cytokines).

Acknowledgments

We thank the patients and their families for participating in the study. We thank Yelena Nemirovskaya, Tatiana Kochetkov, Lahouari Amar, Cécile Patissier, Céline Desvallées, Dominick Papandrea, Mark Woollett, and Amy Gall for technical and secretarial assistance and all members of the Laboratory of Human Genetics of Infectious Diseases for helpful discussions. We acknowledge the use of the biological resources of the Imagine Institute DNA biobank (BB-33-00065). A.G. was supported by ANR-IFNPHOX (ANR-13-ISV3-0001-01) and Imagine Institute. The Laboratory of Human Genetics of Infectious Diseases is supported in part by grants from the St. Giles Foundation, The Rockefeller University, Institut National de la Santé et de la Recherche Médicale (INSERM), Paris Descartes University, and the European Research Council (ERC), the Integrative Biology of Emerging Infectious Diseases Laboratory of Excellence (ANR-10-LABX-62-IBEID) and the French National Research Agency (ANR) under the "Investments for the future" program (grant number ANR-10-IAHU-01), ANR-IFNPHOX (ANR-13-ISV3-0001-01, to J.B.), ANR-GENMSMD (ANR-16-CE17-0005-01, to J.B.). Research in the Quintana-Murci laboratory was supported by the Pasteur Institute, the Centre National de la Recherche Scientifique (CNRS), the French Government's Investissement d'Avenir program, (ANR-10-LABX-62-IBEID), IEIHSEER (ANR-14-CE14-0008-02) and TBPATHGEN (ANR-14-CE14-0007-02), and the European Union's Seventh Framework Program (FP/2007–2013)/ERC Grant Agreement No. 281297. S.G.T. and C.S.M. are supported by grants and fellowship awarded by the National Health and Medical Research Council of Australia (1113904, 1042925) and the Office of Health and Medical Research of the New South Wales State Government. T.N. and L.W. are supported by Australian Postgraduate Research Awards from the University of NSW.

Supplementary Results

Case report

All members of the multiplex kindred studied, the pedigree of which is shown in Figure 1, live in France and are of French descent.

Patient 1 (P1, proband) was born in 1948 and presented arthritis of the right knee in 2011, after recurrent episodes of arthritis of this joint associated with effusion since 1980. *Tropheryma whipplei* (Tw) was detected in synovial fluid by PCR and culture in 2011, but was not detected by PCR in saliva, feces, and small-bowel biopsy specimens. Physical examination revealed a large effusion of the right knee, limiting mobility. The fluid aspirated from this joint contained 4,000 erythrocytes/mm^3 and 8,800 leukocytes/mm^3, but no crystals or evidence of microbes. Synovial hypertrophy of the right knee and a narrowing of the right internal femoro-tibial joint were detected on MRI. X ray showed an extension of the right femoro-tibial joint and erosion of the posterior part of the femoro-tibial joint. However, erythrocyte sedimentation rate (ESR) (3 mm/h) and C-reactive protein (CRP) (1.8 mg/l) determinations gave negative results. P1 received methotrexate (15 mg/week) for four months, without remission. Antibiotic treatment with doxycycline (200 mg/day) was then initiated immediately. The arthralgia resolved, but right knee effusion persisted. Hydroxychloroquine was therefore added to the treatment regimen. At last follow-up, in 2016, the patient was well and PCR for Tw was negative for saliva and feces samples.

P2, a second cousin of P1, was born in 1941 and was diagnosed with classical WD and digestive problems in 1978, based on positive periodic acid–Schiff (PAS) staining of a small intestine biopsy specimen. She was treated with sulfamethoxazole/trimethoprim. At last follow-up, in 2016, Tw PCR was positive for the saliva and feces.

P3, the father of P1, was born in 1925 and was diagnosed with classical WD in 1987 on the basis of positive PAS staining of a small intestine biopsy specimen. Clinical manifestations

included diarrhea, abdominal pain and weight loss. P3 displayed no extraintestinal manifestations. He was successfully treated with sulfamethoxazole/trimethoprim, with complete clinical and bacteriological remission.

P4, the brother of P2, was born in 1947 and sought medical advice in 2015 for arthralgia affecting the knees and right ulna-carpal joints. The other joints were unaffected. A culture of the joint fluid was negative for bacteria, but Tw was not sought. Tw was not detected in the saliva and feces by PCR or culture, but serological tests for Tw were positive. P4 had no rheumatoid factor, anti-cyclic citrullinated peptide antibodies (anti-CCP), or anti-nuclear antibodies. The fluid aspirated from the right knee contained 4,800 erythrocytes/mm^3 and 10,900 leukocytes/mm^3 (91% neutrophils and 9% lymphocytes) without crystals. Synovial fluid culture was negative for bacteria, but Tw was not sought. Blood tests revealed an ESR of 30 mm/h and a CRP concentration of 50 mg/l, with no rheumatoid factor, anti-cyclic citrullinated peptide antibodies (anti-CCP) or anti-nuclear antibodies. An X ray revealed a narrowing of the joint space in the knees and vertebral hyperostosis were visible. The joints of the hands were unaffected. The patient was treated with anti-inflammatory drugs, without success. Treatment with methotrexate and steroids was introduced, followed by antibiotics, the effect of which is currently being evaluated.

Saliva and/or feces samples from 18 other members of the family were checked for the presence of Tw, by a PCR specifically targeting *T. whipplei*, as previously described (Figure 1, A) (73). Five individuals were found to be chronic carriers (mean age: 55 years) and 13 were not (mean age: 38 years). Testing was not possible for nine other relatives. The overall distribution of WD in this kindred was suggestive of an AD trait with incomplete penetrance.

Production and function of IRF4 in the patients' peripheral leukocytes

We investigated IRF4 levels by western blotting on total cell lysates from peripheral blood mononuclear cells (PBMCs) and their subpopulations isolated from six healthy controls. We showed that IRF4 was produced in large amounts in total B lymphocytes ($CD19^+$), but also naïve and memory B lymphocytes ($CD19^+CD27^-$ and $CD19^+CD27^+$, respectively; Figure S8). IRF4 was less strongly expressed in $CD3^+$ T lymphocytes and was not detectable in $CD14^+$ monocytes or $CD56^+$ natural killer (NK) cells. IRF4 levels were low in naïve $CD3^+$ T cells and $CD4^+$ T cells, but not detectable in naïve $CD8^+$ T cells in the basal state, relative to controls cells (western blot, data not shown). We showed, in $CD3^+$ T cells and $CD4^+$ T cells, that phorbol myristate acetate (PMA)-ionomycin stimulation induced the production of even larger amounts of IRF4 expression following activation with CD2/CD3/CD28-coated beads (data not shown). We therefore assessed the pattern of IRF4 protein production in $CD4^+$ T cells from four controls, P1 and P3, either non-stimulated (NS) or stimulated with CD2/CD3/CD28-coated beads. Our results are consistent with our findings for HEK293 T cells, as IRF4 production by P1 and P3 $CD4^+$ T cells was stronger than that by $CD4^+$ T cells from unrelated controls, in total cell lysates (4.5 times higher for P1 and 2.1 times higher for P3 in NS conditions; 1.9 times higher for P1 and 1.3 times higher for P3 under stimulation), in the cytoplasmic compartment (3 times higher for P1 and 3.7 times higher for P3 in NS conditions; 7.7 times higher for P1 and 2.3 times higher for P3 under stimulation) and in the nuclear compartment in NS conditions (2 times higher for P1 and 3 times higher for P3) but not under stimulation (2 times higher for P1 and 0.6 times higher for P3) (Figure 3, A, B, C). Analyses of the overall pattern of IRF4 expression in the cells of controls and patients showed that the patients' $CD4^+$ T lymphocytes had higher total IRF4 levels and that a higher proportion of IRF4 was located in the cytoplasm than in controls, as observed for EBV-B cells and with the overexpression system.

We characterized the transcriptomic differences linked to genotype and/or to infection, by performing microarray studies on PBMCs (at early time points or in the absence of stimulation for 24 h (NS)) from six *IRF4*-heterozygous individuals (three patients, P1-P3; and three healthy relatives, HET1-HET3) and six individuals homozygous for the WT *IRF4* allele (four healthy relatives, WT1-WT4; and two unrelated controls, C1-C2). A comparison of NS samples from the *IRF4*-heterozygous and *IRF4* WT-homozygous groups showed that differentially regulated transcripts could be detected only at an early time point (49 genes upregulated and 16 downregulated in the heterozygous group relative to the WT homozygotes), but not after 24 h. It was not, therefore, possible to distinguish genes differentially regulated due to the *IRF4* mutation from those differentially regulated as a result of a systemic immune response in the patients.

Expression and function of IRF4 in the patients' myeloid cells

An analysis of the three main subsets of DCs present in human blood —CD303$^+$ pDCs (CD123$^+$ CD303$^+$ HLA-DR$^+$ Lin$^-$ CD14$^-$ CD16$^-$), CD1c$^+$ cDCs (CD1c$^+$ CD11c$^+$ HLA-DR$^+$ Lin$^-$ CD14$^-$ CD16$^-$) and CD141$^+$ cDCs (CD141$^+$ CD11c$^+$ HLA-DR$^+$ Lin$^-$ CD14$^-$ CD16$^-$) — showed that the frequencies of these subsets in P1 were similar to those in controls (Figure S9). We assessed IRF4 expression levels and the effect of IRF4 deficiency in myeloid cells, by first studying monocyte-derived dendritic cells (MDDCs) from controls, in which IRF4 was produced after stimulation with LPS but not after stimulation with IFN-γ. IRF4 was not produced by immature MDDC (data not shown). We also generated monocyte-derived macrophages (MDMs) for controls and patients, using different conditions of differentiation and activation to obtain M1-like and M2-like MDMs. We found that IRF4 was present in similar amounts in MDMs from patients and controls, regardless of the differentiation or activation conditions used (Figure S10, A and B). FACS analysis of MDMs with common and specific

markers (for M1-like and M2-like MDMs) showed that CD11b, CD86, CD206, CD209 and HLA-DR expression was similar for MDMs from patients and MDMs from controls (Figure S10, C and D). Thus, all the myeloid subsets studied developed and functioned normally in the patient, suggesting a subtle disease mechanism.

Lymphoid immunological phenotype

We then assessed the potential impact of heterozygosity for the R98W mutation of *IRF4* on the development and function of lymphoid subsets. In mice, Irf4 plays a major role in the generation, differentiation and functions of various immune cells, including T and B lymphocytes (74, 75). We analyzed peripheral leukocytes from the three patients (P1, P2, P3) and from the P1's healthy dizygotic twin sister (WT). All subjects had normal numbers and percentages of T, B, and NK cells for age (table S5). We also performed deeper B-cell immunophenotyping by flow cytometry. The frequency of memory B cells within the total B-cell population was normal, as was the frequency of class-switched B cells in the memory compartment in cells from the patients (P1, P2 and P3), as shown by comparisons with healthy controls (Figure S11, A). We assessed *ex vivo* cytokine production by differentiated memory $CD4^+$ Th cells. Cells from the patients (P2 and P3) produced more IL-9 and less IL-17A and IL-17F than cells from controls (Figure. S11, B). We found no significant difference in the production of IL-2, IL-4, IL-5, IL-10, IL-13, IL-22, IFN-γ and tumor necrosis factor-alpha (TNF-α) between patients and controls (Figure S11, B). Analyses of $CD4^+$ T-cell differentiation *in vitro* showed that, contrary to the *ex vivo* data obtained for memory $CD4^+$ T cells, naïve $CD4^+$ T cells from the patients were able to produce relatively normal amounts of IL-17-A/F (Figure S11, C). The *in vitro* production of IFN-γ, IL-10 and IL-21 by naïve $CD4^+$ T cells from patients was also unimpaired (Figure S11, C). Furthermore, studies of the *in vitro* function of naïve and total memory B cells upon costimulation with CD40 ligand (CD40L) and IL-21 showed that

cells from patients (P2 and P3) produced similar amounts of IgA, IgG and IgM to cells from healthy controls (data not shown). Thus, overall, in the experimental conditions tested, the *IRF4* R98W mutation has no global effect on the development or function of adaptive immune system lymphocytes, suggesting that haploinsufficiency for IRF4 does not underlie WD through adaptive immune responses.

Additional information concerning the mouse model

Irf4-deficient homozygous mice have lymphoid defects relating to differentiation (Th1, B cells), proliferation (T and B cells), Ig levels (IgG and IgM) and activity (abolition of IL-4 and IFN-γ production by $CD4^+$ T cells after infection with *Leishmania major*). They also display splenomegaly, adenomegaly, lower counts of plasmacytoid dendritic cells (pDCs) in the spleen and thymus, of the abolition of plasma cells in the spleen and abnormal class-switch recombination. Moreover, homozygous mice have no germinal center in the spleen and lymph nodes and are more susceptible to *Leishmania* and lymphocytic choriomeningitis virus (42-47). Mice heterozygous for an *Irf4*-null mutation have not been studied.

References

1. Whipple GH. A hitherto undescribed disease characterized anatomically by deposits of fat and fattyacids in the intestinal and mesentericlymphatic tissues. Bull Johns Hopkins Hosp. 1907;18(5):382.
2. Yardley JH, Hendrix TR. Combined electron and light microscopy in Whipple's disease. Demonstration of "bacillary bodies" in the intestine. Bull Johns Hopkins Hosp. 1961;109:80-98. Epub 1961/08/01.
3. Relman DA, Schmidt TM, MacDermott RP, Falkow S. Identification of the uncultured bacillus of Whipple's disease. N Engl J Med. 1992;327(5):293-301. Epub 1992/07/30.
4. Raoult D, Birg ML, La Scola B, Fournier PE, Enea M, Lepidi H, et al. Cultivation of the bacillus of Whipple's disease. N Engl J Med. 2000;342(9):620-5. Epub 2000/03/04.
5. Braubach P, Lippmann T, Raoult D, Lagier JC, Anagnostopoulos I, Zender S, et al. Fluorescence In Situ Hybridization for Diagnosis of Whipple's Disease in Formalin-Fixed Paraffin-Embedded Tissue. Frontiers in medicine. 2017;4:87. Epub 2017/07/12.
6. Dobbins WOI. Whipple's disease. Thomas Books. 1987;Springfield, IL.
7. Maizel H, Ruffin JM, Dobbins WO, 3rd. Whipple's disease: a review of 19 patients from one hospital and a review of the literature since 1950. Medicine (Baltimore). 1970;49(3):175-205. Epub 1970/05/01.
8. Durand DV, Lecomte C, Cathebras P, Rousset H, Godeau P. Whipple disease. Clinical review of 52 cases. The SNFMI Research Group on Whipple Disease. Societe Nationale Francaise de Medecine Interne. Medicine (Baltimore). 1997;76(3):170-84. Epub 1997/05/01.
9. Fleming JL, Wiesner RH, Shorter RG. Whipple's disease: clinical, biochemical, and histopathologic features and assessment of treatment in 29 patients. Mayo Clinic proceedings. 1988;63(6):539-51. Epub 1988/06/01.
10. Mahnel R, Kalt A, Ring S, Stallmach A, Strober W, Marth T. Immunosuppressive therapy in Whipple's disease patients is associated with the appearance of gastrointestinal manifestations. Am J Gastroenterol. 2005;100(5):1167-73. Epub 2005/04/22.
11. Schneider T, Moos V, Loddenkemper C, Marth T, Fenollar F, Raoult D. Whipple's disease: new aspects of pathogenesis and treatment. Lancet Infect Dis. 2008;8(3):179-90. Epub 2008/02/23.
12. Fenollar F, Lepidi H, Raoult D. Whipple's endocarditis: review of the literature and comparisons with Q fever, Bartonella infection, and blood culture-positive endocarditis. Clin Infect Dis. 2001;33(8):1309-16. Epub 2001/09/21.
13. Gubler JG, Kuster M, Dutly F, Bannwart F, Krause M, Vogelin HP, et al. Whipple endocarditis without overt gastrointestinal disease: report of four cases. Ann Intern Med. 1999;131(2):112-6. Epub 1999/07/27.
14. Fenollar F, Lagier JC, Raoult D. Tropheryma whipplei and Whipple's disease. J Infect. 2014;69(2):103-12. Epub 2014/06/01.
15. Marumganti AR, Murphy TF. Whipple's disease: neurological relapse presenting as headache for two years. Journal of general internal medicine. 2008;23(12):2131-3. Epub 2008/09/12.
16. Lagier JC, Fenollar F, Lepidi H, Raoult D. Evidence of lifetime susceptibility to Tropheryma whipplei in patients with Whipple's disease. J Antimicrob Chemother. 2011;66(5):1188-9. Epub 2011/03/12.
17. Fenollar F, Puechal X, Raoult D. Whipple's disease. N Engl J Med. 2007;356(1):55-66. Epub 2007/01/05.
18. Dobbins WO, 3rd. Is there an immune deficit in Whipple's disease? Digestive diseases and sciences. 1981;26(3):247-52. Epub 1981/03/01.
19. Desnues B, Al Moussawi K, Fenollar F. New insights into Whipple's disease and Tropheryma whipplei infections. Microbes Infect. 2010;12(14-15):1102-10. Epub 2010/08/17.
20. Fenollar F, Laouira S, Lepidi H, Rolain JM, Raoult D. Value of Tropheryma whipplei quantitative polymerase chain reaction assay for the diagnosis of Whipple disease: usefulness of saliva and stool specimens for first-line screening. Clin Infect Dis. 2008;47(5):659-67. Epub 2008/07/30.

21. Puechal X. Whipple's arthritis. Joint, bone, spine : revue du rhumatisme. 2016;83(6):631-5. Epub 2016/08/10.
22. Lagier JC, Fenollar F, Lepidi H, Raoult D. Failure and relapse after treatment with trimethoprim/sulfamethoxazole in classic Whipple's disease. J Antimicrob Chemother. 2010;65(9):2005-12. Epub 2010/07/20.
23. Bakkali N, Fenollar F, Biswas S, Rolain JM, Raoult D. Acquired resistance to trimethoprim-sulfamethoxazole during Whipple disease and expression of the causative target gene. J Infect Dis. 2008;198(1):101-8. Epub 2008/05/27.
24. Ehrbar HU, Bauerfeind P, Dutly F, Koelz HR, Altwegg M. PCR-positive tests for Tropheryma whippelii in patients without Whipple's disease. Lancet. 1999;353(9171):2214. Epub 1999/07/07.
25. Amsler L, Bauernfeind P, Nigg C, Maibach RC, Steffen R, Altwegg M. Prevalence of Tropheryma whipplei DNA in patients with various gastrointestinal diseases and in healthy controls. Infection. 2003;31(2):81-5. Epub 2003/04/12.
26. Maibach RC, Dutly F, Altwegg M. Detection of Tropheryma whipplei DNA in feces by PCR using a target capture method. J Clin Microbiol. 2002;40(7):2466-71. Epub 2002/06/29.
27. Street S, Donoghue HD, Neild GH. Tropheryma whippelii DNA in saliva of healthy people. Lancet. 1999;354(9185):1178-9. Epub 1999/10/08.
28. Rolain JM, Fenollar F, Raoult D. False positive PCR detection of Tropheryma whipplei in the saliva of healthy people. BMC Microbiol. 2007;7:48. Epub 2007/05/31.
29. Fenollar F, Amphoux B, Raoult D. A paradoxical Tropheryma whipplei western blot differentiates patients with whipple disease from asymptomatic carriers. Clin Infect Dis. 2009;49(5):717-23. Epub 2009/07/29.
30. Fenollar F, Trani M, Davoust B, Salle B, Birg ML, Rolain JM, et al. Prevalence of asymptomatic Tropheryma whipplei carriage among humans and nonhuman primates. J Infect Dis. 2008;197(6):880-7. Epub 2008/04/19.
31. Li W, Fenollar F, Rolain JM, Fournier PE, Feurle GE, Muller C, et al. Genotyping reveals a wide heterogeneity of Tropheryma whipplei. Microbiology. 2008;154(Pt 2):521-7. Epub 2008/01/30.
32. Ponz de Leon M, Borghi A, Ferrara F, Contri M, Roncucci L. Whipple's disease in a father-son pair. Internal and emergency medicine. 2006;1(3):254-6. Epub 2006/11/24.
33. Marth T, Moos V, Muller C, Biagi F, Schneider T. Tropheryma whipplei infection and Whipple's disease. Lancet Infect Dis. 2016;16(3):e13-22. Epub 2016/02/10.
34. Picard. C, Gaspar. HB, Al-Herz. W, Bousfiha. A, Casanova. J-L, Chatila. T, et al. International Union of Immunological Societies 2017 Primary Immunodeficiency Diseases Committee report on Inborn Errors of Immunity. Journal of Clinical Immunology. 2017;*In Press*.
35. Casanova JL. Severe infectious diseases of childhood as monogenic inborn errors of immunity. Proc Natl Acad Sci U S A. 2015;112(51):E7128-37. Epub 2015/12/02.
36. Casanova JL. Human genetic basis of interindividual variability in the course of infection. Proc Natl Acad Sci U S A. 2015;112(51):E7118-27. Epub 2015/12/02.
37. Lamborn IT, Jing H, Zhang Y, Drutman SB, Abbott JK, Munir S, et al. Recurrent rhinovirus infections in a child with inherited MDA5 deficiency. J Exp Med. 2017;214(7):1949-72. Epub 2017/06/14.
38. Ogunjimi B, Zhang SY, Sorensen KB, Skipper KA, Carter-Timofte M, Kerner G, et al. Inborn errors in RNA polymerase III underlie severe varicella zoster virus infections. J Clin Invest. 2017;127(9):3543-56. Epub 2017/08/08.
39. Belkadi A, Pedergnana V, Cobat A, Itan Y, Vincent QB, Abhyankar A, et al. Whole-exome sequencing to analyze population structure, parental inbreeding, and familial linkage. Proc Natl Acad Sci U S A. 2016;113(24):6713-8. Epub 2016/06/02.
40. Ikushima H, Negishi H, Taniguchi T. The IRF family transcription factors at the interface of innate and adaptive immune responses. Cold Spring Harbor symposia on quantitative biology. 2013;78:105-16. Epub 2013/10/05.

41. Shaffer AL, Emre NC, Romesser PB, Staudt LM. IRF4: Immunity. Malignancy! Therapy? Clinical cancer research : an official journal of the American Association for Cancer Research. 2009;15(9):2954-61. Epub 2009/04/23.
42. Tominaga N, Ohkusu-Tsukada K, Udono H, Abe R, Matsuyama T, Yui K. Development of Th1 and not Th2 immune responses in mice lacking IFN-regulatory factor-4. International immunology. 2003;15(1):1-10. Epub 2002/12/28.
43. Tamura T, Tailor P, Yamaoka K, Kong HJ, Tsujimura H, O'Shea JJ, et al. IFN regulatory factor-4 and -8 govern dendritic cell subset development and their functional diversity. J Immunol. 2005;174(5):2573-81. Epub 2005/02/25.
44. Suzuki S, Honma K, Matsuyama T, Suzuki K, Toriyama K, Akitoyo I, et al. Critical roles of interferon regulatory factor 4 in CD11bhighCD8alpha- dendritic cell development. Proc Natl Acad Sci U S A. 2004;101(24):8981-6. Epub 2004/06/09.
45. Mittrucker HW, Matsuyama T, Grossman A, Kundig TM, Potter J, Shahinian A, et al. Requirement for the transcription factor LSIRF/IRF4 for mature B and T lymphocyte function. Science. 1997;275(5299):540-3. Epub 1997/01/24.
46. Lohoff M, Mittrucker HW, Prechtl S, Bischof S, Sommer F, Kock S, et al. Dysregulated T helper cell differentiation in the absence of interferon regulatory factor 4. Proc Natl Acad Sci U S A. 2002;99(18):11808-12. Epub 2002/08/22.
47. Klein U, Casola S, Cattoretti G, Shen Q, Lia M, Mo T, et al. Transcription factor IRF4 controls plasma cell differentiation and class-switch recombination. Nat Immunol. 2006;7(7):773-82. Epub 2006/06/13.
48. Escalante CR, Brass AL, Pongubala JM, Shatova E, Shen L, Singh H, et al. Crystal structure of PU.1/IRF-4/DNA ternary complex. Mol Cell. 2002;10(5):1097-105. Epub 2002/11/28.
49. Brass AL, Zhu AQ, Singh H. Assembly requirements of PU.1-Pip (IRF-4) activator complexes: inhibiting function in vivo using fused dimers. EMBO J. 1999;18(4):977-91. Epub 1999/02/18.
50. Kircher M, Witten DM, Jain P, O'Roak BJ, Cooper GM, Shendure J. A general framework for estimating the relative pathogenicity of human genetic variants. Nat Genet. 2014;46(3):310-5. Epub 2014/02/04.
51. Itan Y, Shang L, Boisson B, Ciancanelli MJ, Markle JG, Martinez-Barricarte R, et al. The mutation significance cutoff: gene-level thresholds for variant predictions. Nature methods. 2016;13(2):109-10. Epub 2016/01/29.
52. Itan Y, Shang L, Boisson B, Patin E, Bolze A, Moncada-Velez M, et al. The human gene damage index as a gene-level approach to prioritizing exome variants. Proc Natl Acad Sci U S A. 2015;112(44):13615-20. Epub 2015/10/21.
53. Eilertson KE, Booth JG, Bustamante CD. SnIPRE: selection inference using a Poisson random effects model. PLoS computational biology. 2012;8(12):e1002806. Epub 2012/12/14.
54. Lek M, Karczewski KJ, Minikel EV, Samocha KE, Banks E, Fennell T, et al. Analysis of protein-coding genetic variation in 60,706 humans. Nature. 2016;536(7616):285-91. Epub 2016/08/19.
55. Lau JF, Parisien JP, Horvath CM. Interferon regulatory factor subcellular localization is determined by a bipartite nuclear localization signal in the DNA-binding domain and interaction with cytoplasmic retention factors. Proc Natl Acad Sci U S A. 2000;97(13):7278-83. Epub 2000/06/22.
56. Quintana-Murci L, Clark AG. Population genetic tools for dissecting innate immunity in humans. Nat Rev Immunol. 2013;13(4):280-93. Epub 2013/03/09.
57. Barreiro LB, Quintana-Murci L. From evolutionary genetics to human immunology: how selection shapes host defence genes. Nature reviews Genetics. 2010;11(1):17-30. Epub 2009/12/03.
58. Rieux-Laucat F, Casanova JL. Immunology. Autoimmunity by haploinsufficiency. Science. 2014;345(6204):1560-1. Epub 2014/09/27.
59. Afzali B, Gronholm J, Vandrovcova J, O'Brien C, Sun HW, Vanderleyden I, et al. BACH2 immunodeficiency illustrates an association between super-enhancers and haploinsufficiency. Nat Immunol. 2017;18(7):813-23. Epub 2017/05/23.

60. Perez de Diego R, Sancho-Shimizu V, Lorenzo L, Puel A, Plancoulaine S, Picard C, et al. Human TRAF3 adaptor molecule deficiency leads to impaired Toll-like receptor 3 response and susceptibility to herpes simplex encephalitis. Immunity. 2010;33(3):400-11. Epub 2010/09/14.
61. Purcell S, Neale B, Todd-Brown K, Thomas L, Ferreira MA, Bender D, et al. PLINK: a tool set for whole-genome association and population-based linkage analyses. Am J Hum Genet. 2007;81(3):559-75. Epub 2007/08/19.
62. Abecasis GR, Cherny SS, Cookson WO, Cardon LR. Merlin--rapid analysis of dense genetic maps using sparse gene flow trees. Nat Genet. 2002;30(1):97-101. Epub 2001/12/04.
63. Bogunovic D, Byun M, Durfee LA, Abhyankar A, Sanal O, Mansouri D, et al. Mycobacterial Disease and Impaired IFN-gamma Immunity in Humans with Inherited ISG15 Deficiency. Science. 2012. Epub 2012/08/04.
64. Byun M, Abhyankar A, Lelarge V, Plancoulaine S, Palanduz A, Telhan L, et al. Whole-exome sequencing-based discovery of STIM1 deficiency in a child with fatal classic Kaposi sarcoma. J Exp Med. 2010;207(11):2307-12. Epub 2010/09/30.
65. Li H, Durbin R. Fast and accurate short read alignment with Burrows-Wheeler transform. Bioinformatics. 2009;25(14):1754-60. Epub 2009/05/20.
66. McKenna A, Hanna M, Banks E, Sivachenko A, Cibulskis K, Kernytsky A, et al. The Genome Analysis Toolkit: a MapReduce framework for analyzing next-generation DNA sequencing data. Genome Res. 2010;20(9):1297-303. Epub 2010/07/21.
67. Li H, Handsaker B, Wysoker A, Fennell T, Ruan J, Homer N, et al. The Sequence Alignment/Map format and SAMtools. Bioinformatics. 2009;25(16):2078-9. Epub 2009/06/10.
68. Wang K, Li M, Hakonarson H. ANNOVAR: functional annotation of genetic variants from high-throughput sequencing data. Nucleic acids research. 2010;38(16):e164. Epub 2010/07/06.
69. Gautier L, Cope L, Bolstad BM, Irizarry RA. affy--analysis of Affymetrix GeneChip data at the probe level. Bioinformatics. 2004;20(3):307-15. Epub 2004/02/13.
70. Irizarry RA, Hobbs B, Collin F, Beazer-Barclay YD, Antonellis KJ, Scherf U, et al. Exploration, normalization, and summaries of high density oligonucleotide array probe level data. Biostatistics. 2003;4(2):249-64. Epub 2003/08/20.
71. Alsina L, Israelsson E, Altman MC, Dang KK, Ghandil P, Israel L, et al. A narrow repertoire of transcriptional modules responsive to pyogenic bacteria is impaired in patients carrying loss-of-function mutations in MYD88 or IRAK4. Nat Immunol. 2014;15(12):1134-42. Epub 2014/10/27.
72. Ma CS, Avery DT, Chan A, Batten M, Bustamante J, Boisson-Dupuis S, et al. Functional STAT3 deficiency compromises the generation of human T follicular helper cells. Blood. 2012;119(17):3997-4008. Epub 2012/03/10.
73. Edouard S, Fenollar F, Raoult D. The rise of Tropheryma whipplei: a 12-year retrospective study of PCR diagnoses in our reference center. J Clin Microbiol. 2012;50(12):3917-20. Epub 2012/09/28.
74. Shukla V, Lu R. IRF4 and IRF8: Governing the virtues of B Lymphocytes. Frontiers in biology. 2014;9(4):269-82. Epub 2014/12/17.
75. Huber M, Lohoff M. IRF4 at the crossroads of effector T-cell fate decision. Eur J Immunol. 2014;44(7):1886-95. Epub 2014/05/02.

A

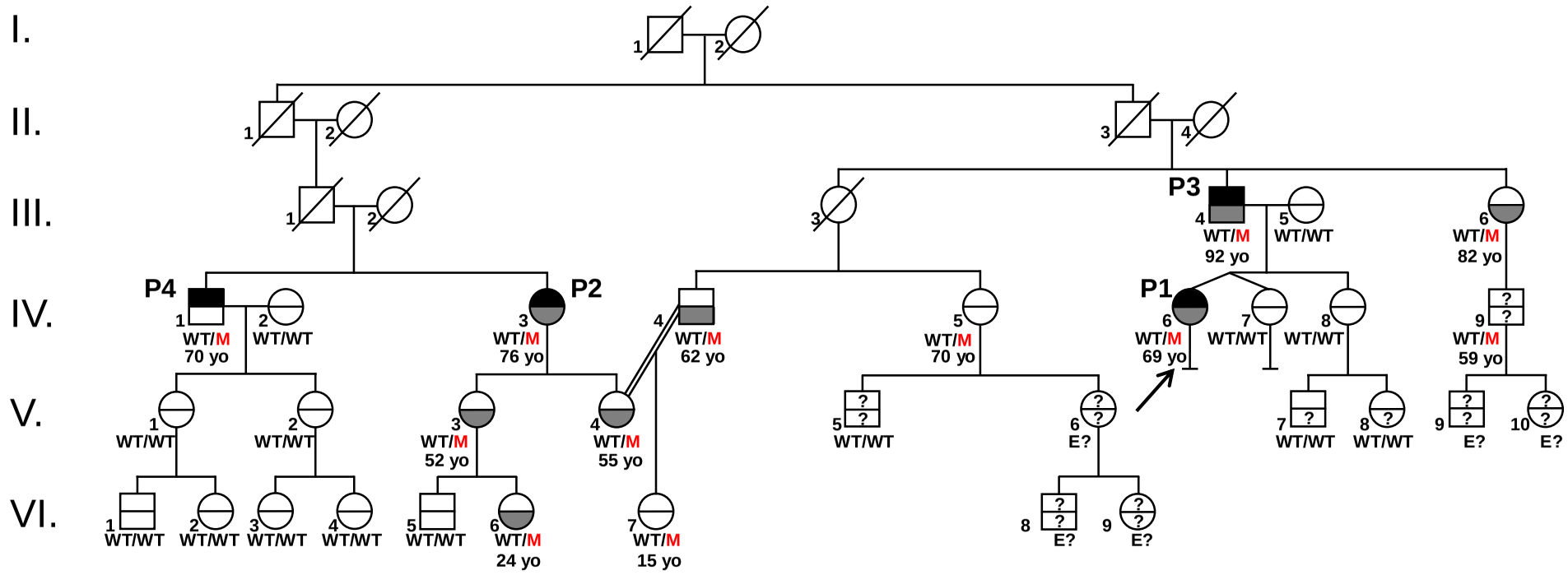
I.
II.
III.
IV.
V.
VI.
P4
P2
P3
P1
WT/M
70 yo
WT/WT
WT/M
76 yo
WT/M
62 yo
WT/M
70 yo
WT/M
92 yo
WT/WT
WT/M
82 yo
WT/M
69 yo
WT/WT
WT/WT
WT/M
59 yo
WT/WT
WT/M
52 yo
WT/M
55 yo
E?
WT/WT
WT/WT
WT/WT
WT/WT
WT/WT
WT/M
24 yo
WT/M
15 yo
E?
E?
E?
E?

B

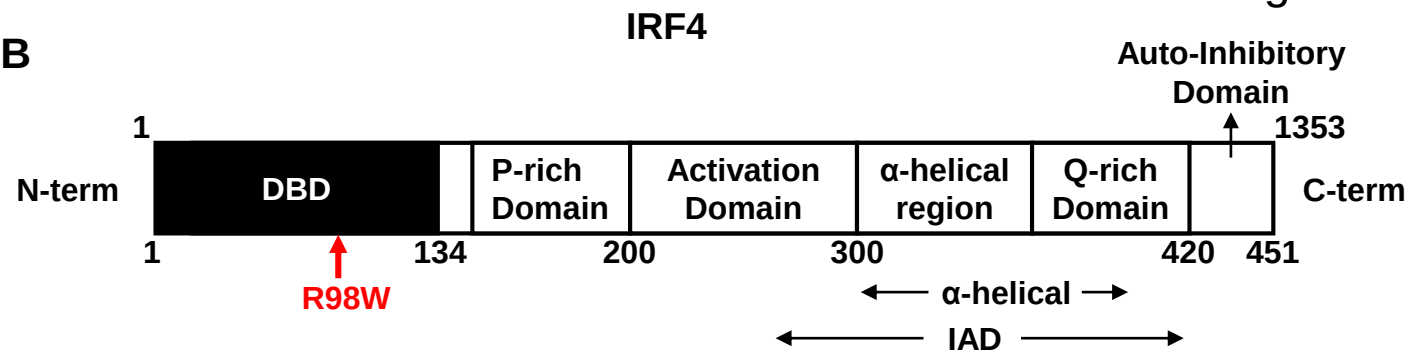

C

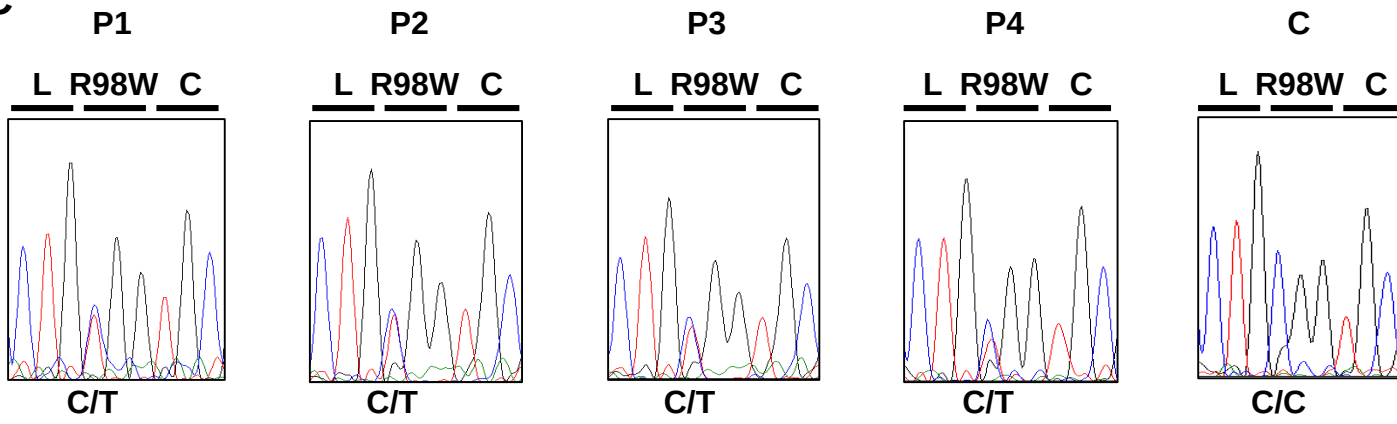

D

Homo sapiens	AWALFKGKFREGIDKPDPPTWKTRLRCALNKSNDFEELVERSQLDISDPYKVYRIVPEGAKKG
Pan troglodytes	AWALFKGKFREGIDKPDPPTWKTRLRCALNKSNDFEELVERSQLDISDPYKVYRIVPEGAKKG
Nomascus leucogenys	AWALFKGKFREGIDKPDPPTWKTRLRCALNKSNDFEELVERSQLDISDPYKVYRIVPEGAKKG
Macaca mulatta	AWALFKGKFREGIDKPDPPTWKTRLRCALNKSNDFEELVERSQLDISDPYKVYRIVPEGAKKG
Rattus norvegicus	AWALFKGKFREGIDKPDPPTWKTRLRCALNKSNDFEELVERSQLDISDPYKVYRIVPEGAKKG
Mus musculus	AWALFKGKFREGIDKPDPPTWKTRLRCALNKSNDFEELVERSQLDISDPYKVYRIVPEGAKKG
Canis familiaris	AWALFKGKFREGIDKPDPPTWKTRLRCALNKSNDFEELVERSQLDISDPYKVYRIVPEGAKKG
Ornithorhynchus anaticus	AWALFKGKFREGIDKPDPPTWKTRLRCALNKSNDFEELVERSQLDISDPYKVYRIVPEGAKKG
Gallus gallus	AWALFKGKFREGIDKPDPPTWKTRLRCALNKSNDFEELVERSQLDISDPYKVYRIVPEGAKKG
Xenopus tropicalis	AWALFKGKYREGIDKPDPPTWKTRLRCALNKSNDFEELVERSQLDISDPYKVYKIIPEGSKKG
Tetraodon nigroviridis	AWALFKGKFREGIDKPDPPTWKTRLRCALNKSNDFEELVDRSQLDISDPYKVYRIVPGGCQKK
Danio rerio	AWALFKGKFREGVDKPDPPTWKTRLRCALNKSNDFEEIVERSQLDISDPYKVYRIVPEGSKKG

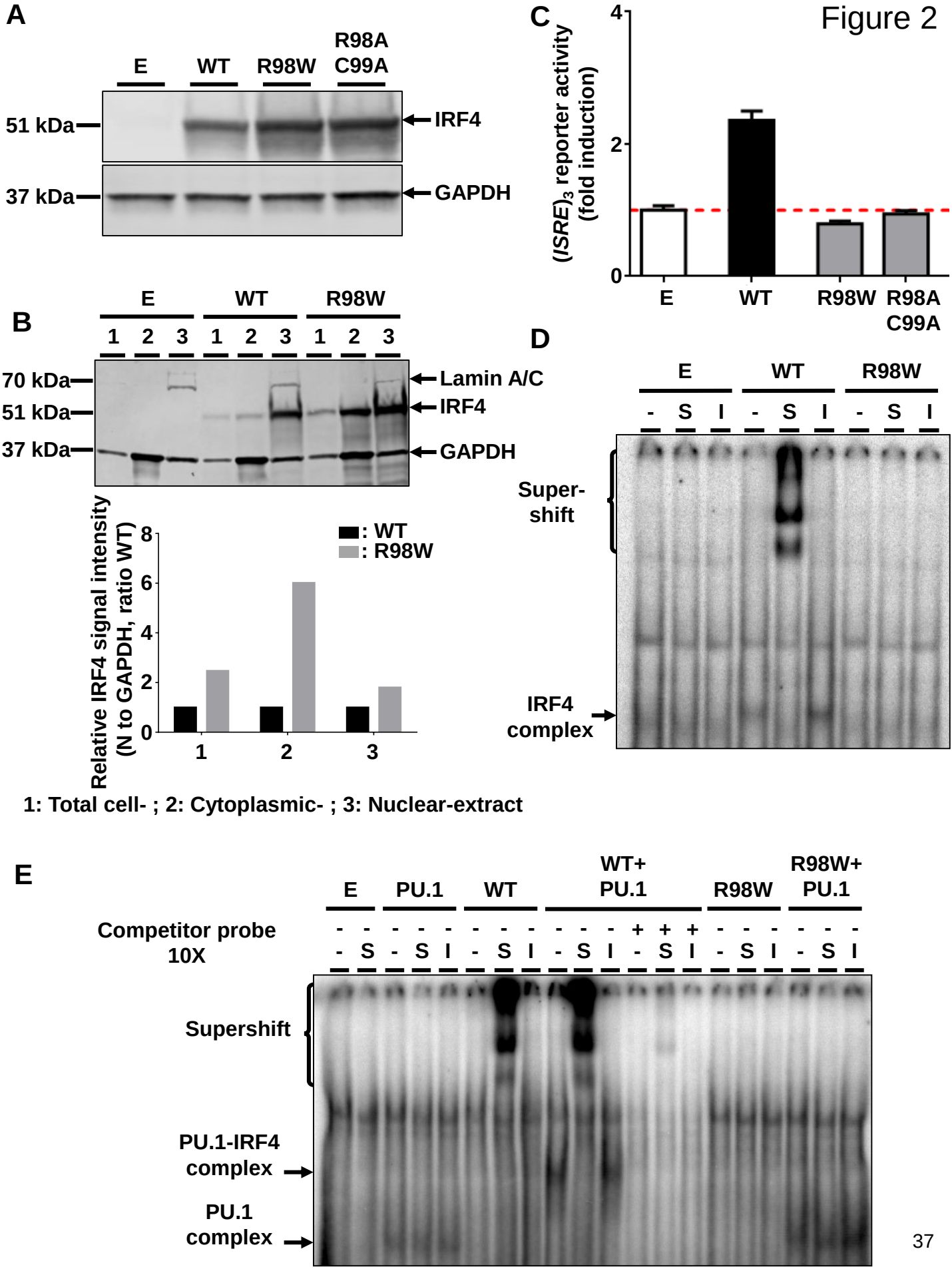
A
E
WT
R98W
R98A C99A
51 kDa
IRF4
37 kDa
GAPDH
C
(ISRE)3 reporter activity (fold induction)
4
2
0
E
WT
R98W
R98A C99A
B
E
WT
R98W
1 2 3 1 2 3 1 2 3
70 kDa
51 kDa
37 kDa
Lamin A/C
IRF4
GAPDH
Relative IRF4 signal intensity (N to GAPDH, ratio WT)
: WT
: R98W
8
6
4
2
0
1
2
3
D
E
WT
R98W
- S I - S I - S I
Super-shift
IRF4 complex
1: Total cell- ; 2: Cytoplasmic- ; 3: Nuclear-extract
E
E
PU.1
WT
WT+ PU.1
R98W
R98W+ PU.1
Competitor probe 10X
- - - - - - - - - - - + + + - - - - - -
- S - S I - S I - S I - S I - S I - S I
Supershift
PU.1-IRF4 complex
PU.1 complex

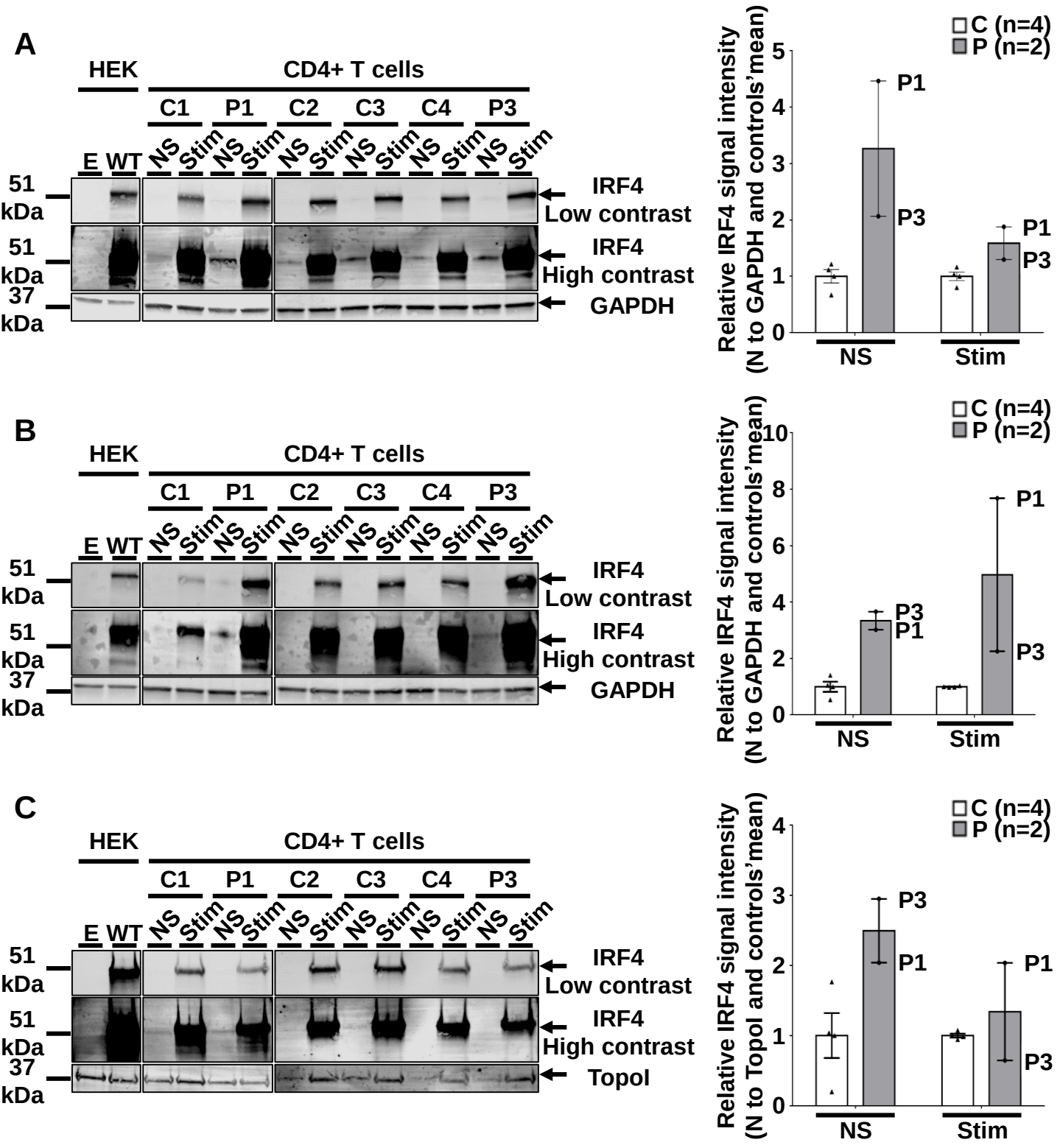
A
HEK
CD4+ T cells
C1
P1
C2
C3
C4
P3
E WT
NS
Stim
51 kDa
IRF4
Low contrast
IRF4
High contrast
37 kDa
GAPDH
Relative IRF4 signal intensity (N to GAPDH and controls'mean)
C (n=4)
P (n=2)
P1
P3
NS
Stim
B
HEK
CD4+ T cells
C1
P1
C2
C3
C4
P3
E WT
NS
Stim
51 kDa
IRF4
Low contrast
IRF4
High contrast
37 kDa
GAPDH
Relative IRF4 signal intensity (N to GAPDH and controls'mean)
C (n=4)
P (n=2)
P1
P3
NS
Stim
C
HEK
CD4+ T cells
C1
P1
C2
C3
C4
P3
E WT
NS
Stim
51 kDa
IRF4
Low contrast
IRF4
High contrast
37 kDa
Topol
Relative IRF4 signal intensity (N to Topol and controls'mean)
C (n=4)
P (n=2)
P1
P3
NS
Stim

A

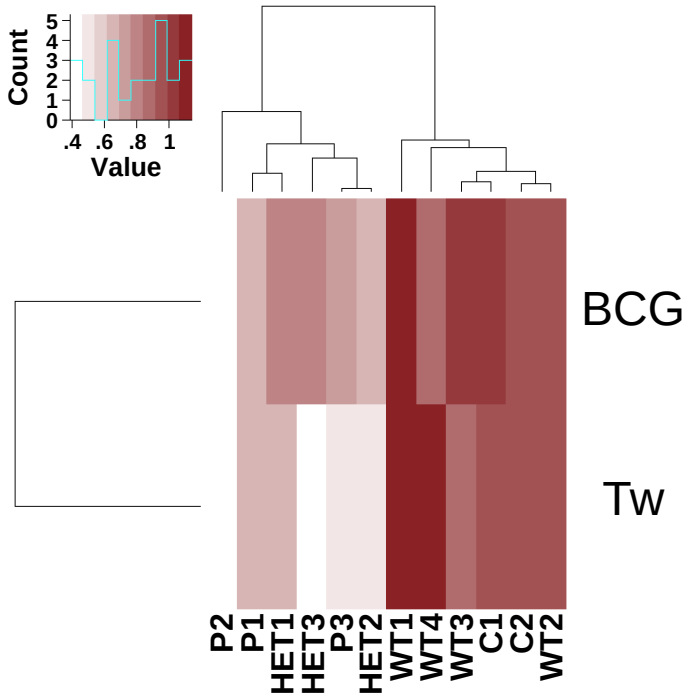
Count
5
4
3
2
1
0
.4 .6 .8 1
Value
BCG
Tw
P2
P1
HET1
HET3
P3
HET2
WT1
WT4
WT3
C1
C2
WT2

B

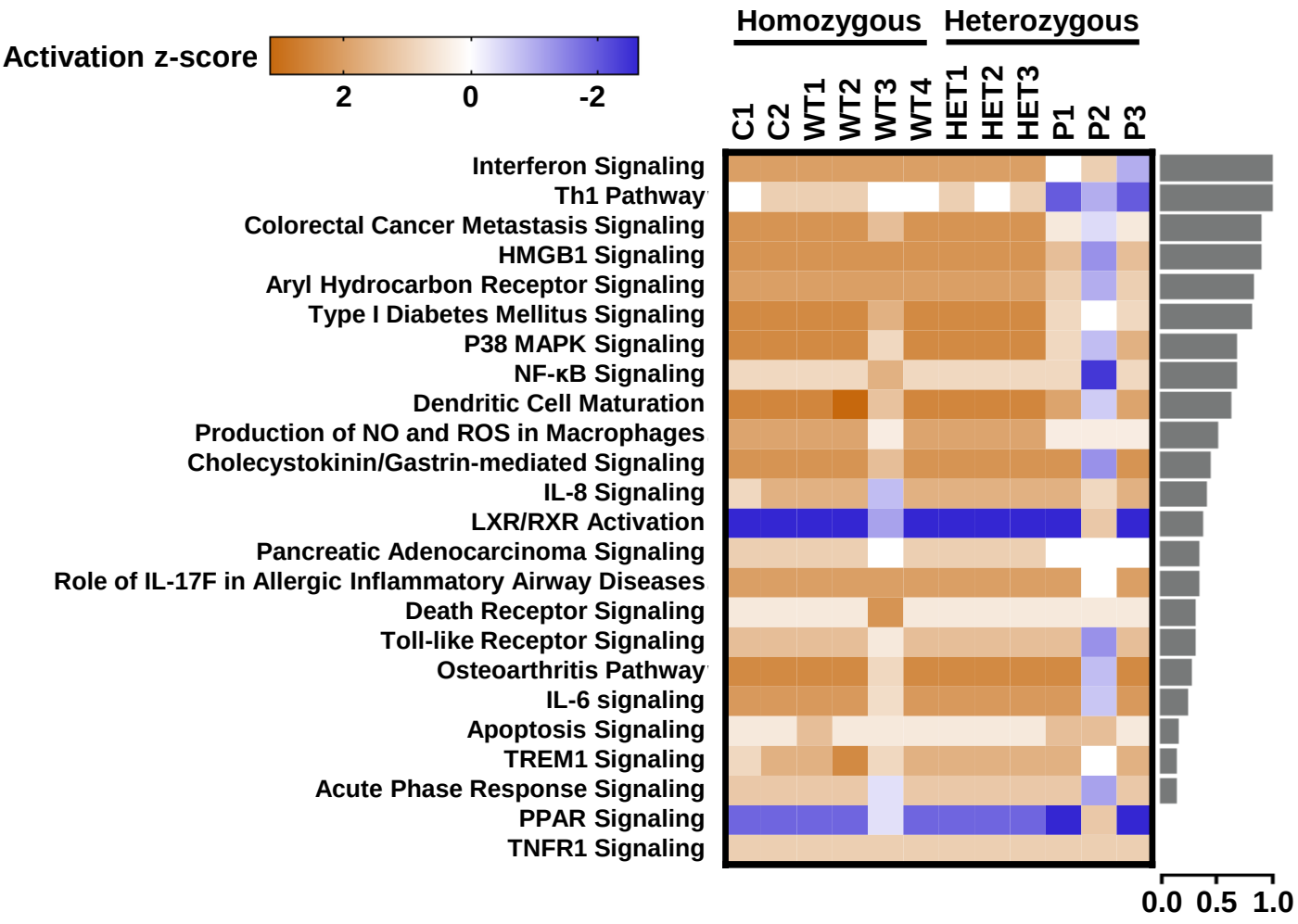
Activation z-score
2
0
-2
Homozygous
Heterozygous
C1
C2
WT1
WT2
WT3
WT4
HET1
HET2
HET3
P1
P2
P3
Interferon Signaling
Th1 Pathway
Colorectal Cancer Metastasis Signaling
HMGB1 Signaling
Aryl Hydrocarbon Receptor Signaling
Type I Diabetes Mellitus Signaling
P38 MAPK Signaling
NF-κB Signaling
Dendritic Cell Maturation
Production of NO and ROS in Macrophages
Cholecystokinin/Gastrin-mediated Signaling
IL-8 Signaling
LXR/RXR Activation
Pancreatic Adenocarcinoma Signaling
Role of IL-17F in Allergic Inflammatory Airway Diseases
Death Receptor Signaling
Toll-like Receptor Signaling
Osteoarthritis Pathway
IL-6 signaling
Apoptosis Signaling
TREM1 Signaling
Acute Phase Response Signaling
PPAR Signaling
TNFR1 Signaling
0.0 0.5 1.0

A

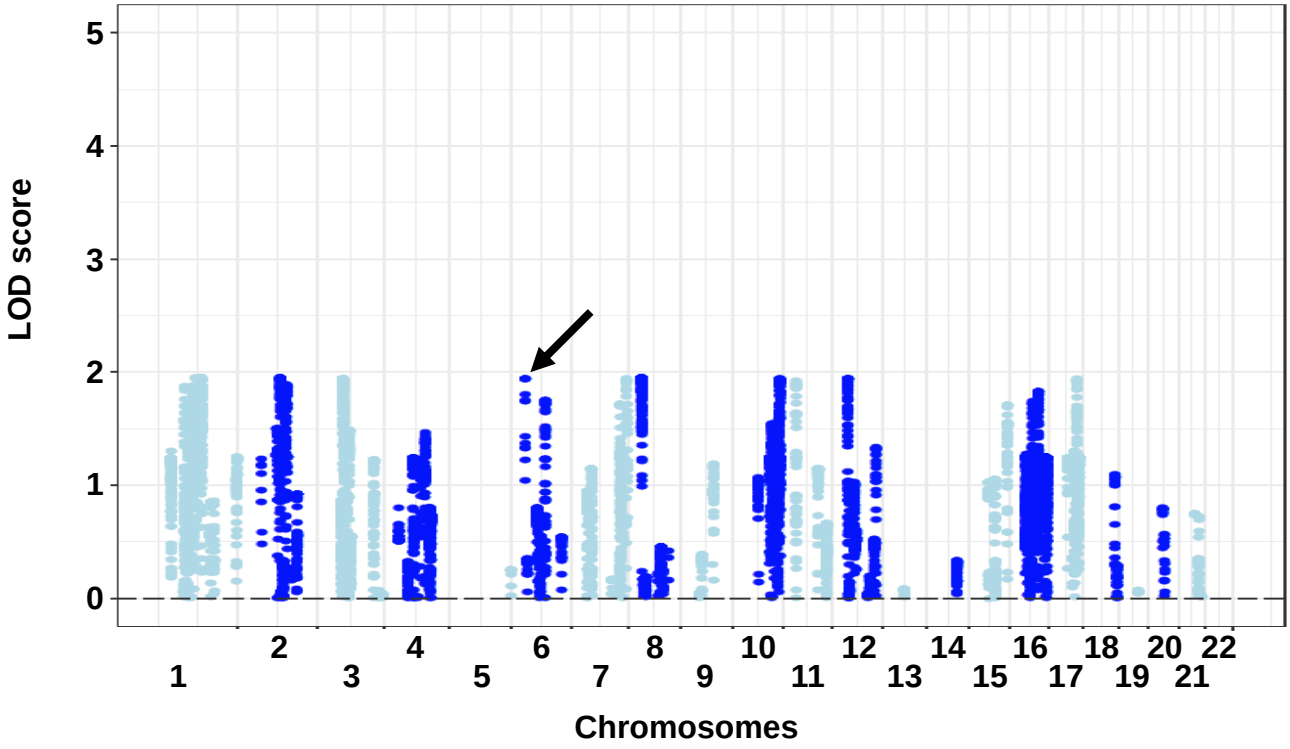
LOD score
0
1
2
3
4
5
1
2
3
4
5
6
7
8
9
10
11
12
13
14
15
16
17
18
19
20
21
22
Chromosomes

B

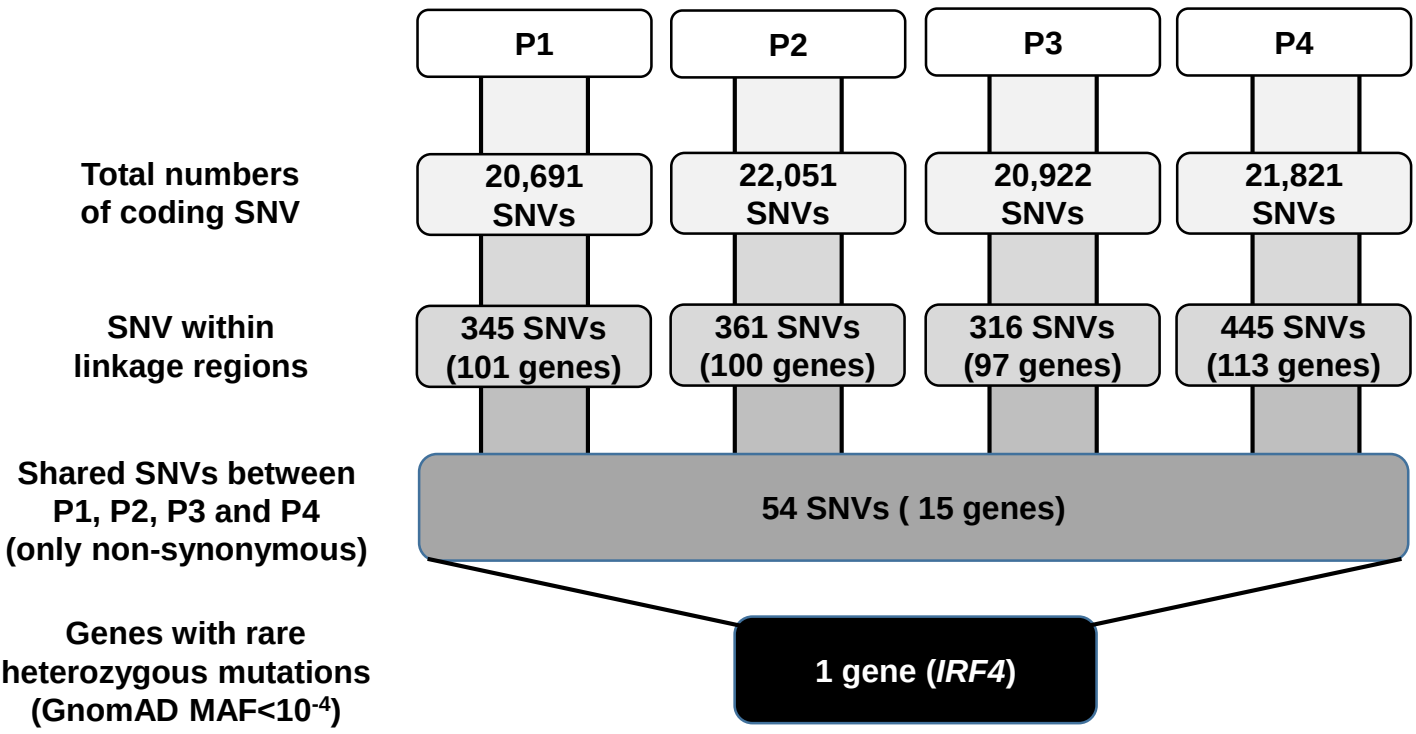
P1
P2
P3
P4
Total numbers of coding SNV
20,691 SNVs
22,051 SNVs
20,922 SNVs
21,821 SNVs
SNV within linkage regions
345 SNVs (101 genes)
361 SNVs (100 genes)
316 SNVs (97 genes)
445 SNVs (113 genes)
Shared SNVs between P1, P2, P3 and P4 (only non-synonymous)
54 SNVs (15 genes)
Genes with rare heterozygous mutations (GnomAD MAF<10-4)
1 gene (IRF4)

Figure S2

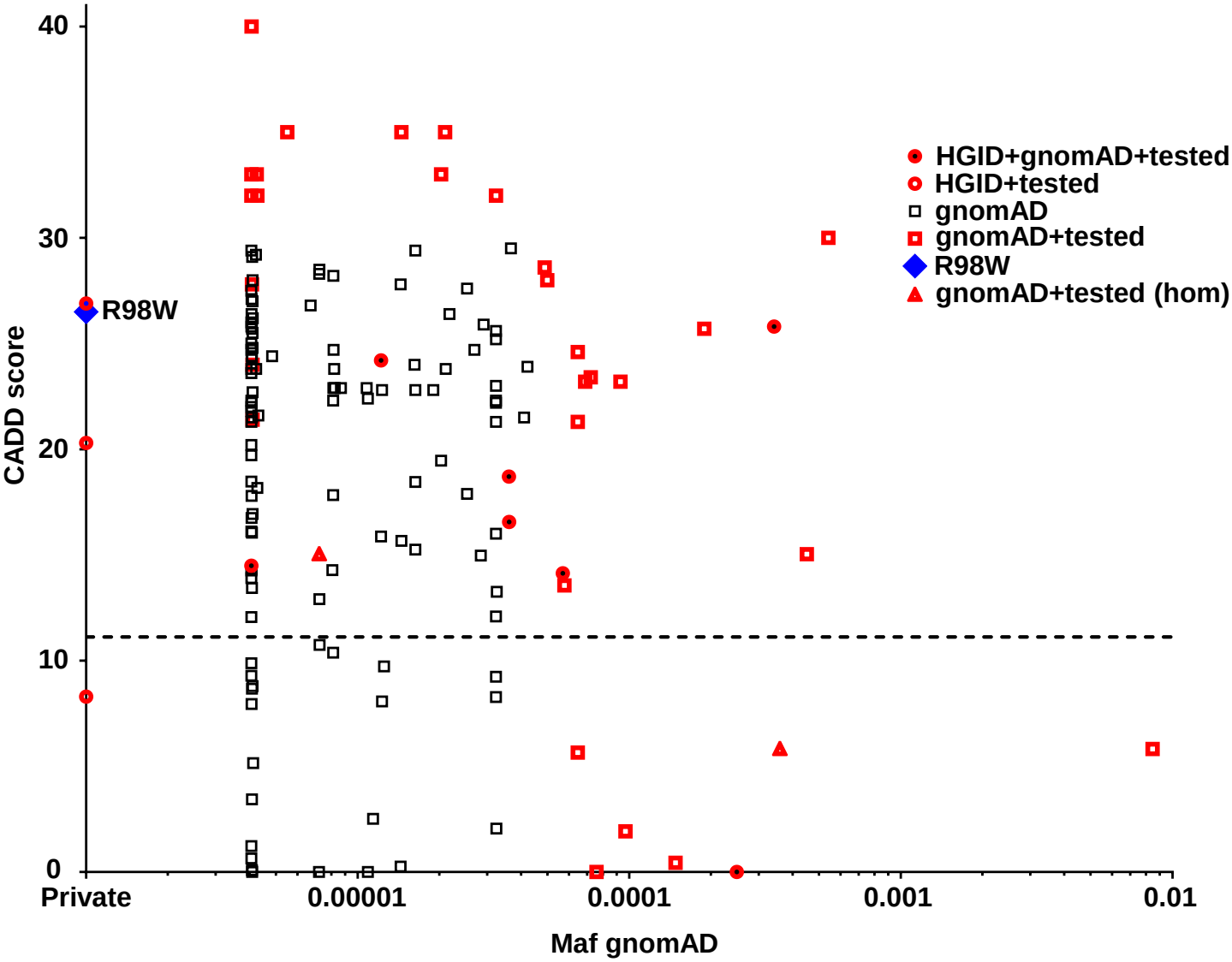
40
30
20
10
0
CADD score
R98W
Private
0.00001
0.0001
0.001
0.01
Maf gnomAD
HGID+gnomAD+tested
HGID+tested
gnomAD
gnomAD+tested
R98W
gnomAD+tested (hom)

A

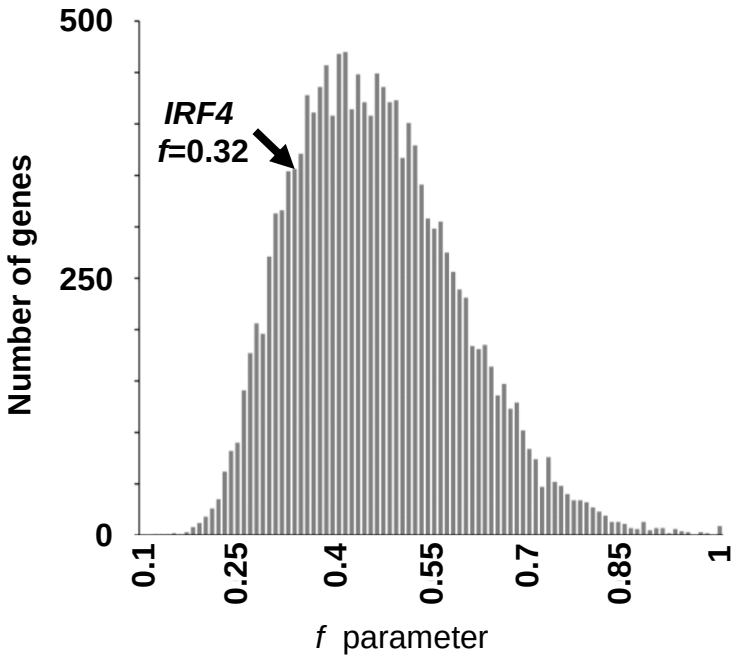

B

Protein Variants	CADD score	MAF
p.(R8L)	28	4.99E-05
p.(R8Q)	25.7	1.89E-04
p.(W27Yfs)	35	5.51E-06
p.(W74Gfs)	40	4.07E-06
p.(R82*)	24	4.10E-06
p.(P88A)	18.71	3.61E-05
p.(P88L)	33	4.06E-06
p.(P88Q)	30	5.41E-04
p.(N105S)	13.56	5.77E-05
p.(R113W)	32	4.06E-06
p.(S149N)	5.825	8.45E-03
p.(Y152Lfs)	27.8	4.08E-06
p.(S160Rfs)	21.4	4.10E-06
p.(V182I)	14.49	4.06E-06
p.(R201H)	24.2	1.22E-05
p.(G202S)	0.004	7.58E-05
p.(P208Q)	23.4	7.22E-05
p.(C214F)	16.56	3.61E-05
p.(P225T)	24.6	6.46E-05
p.(R259W)	33	4.07E-06
p.(R275W)	32	3.23E-05
p.(D283E)	0.003	2.49E-04
p.(A284T)	14.13	5.69E-05
p.(A284V)	21.3	6.46E-05
p.(N298S)	0.434	1.48E-04
p.(A326V)	23.2	6.88E-05
p.(A341V)	25.8	3.42E-04
p.(A370V)	15.04	4.51E-04
p.(R376C)	33	2.03E-05
p.(R376H)	28.6	4.88E-05
p.(L406P)	5.648	6.46E-05
p.(R411K)	23.2	9.29E-05
p.(I434F)	1.929	9.69E-05
p.(R445C)	35	2.10E-05
p.(S447F)	33	4.25E-06
p.(S448F)	32	4.27E-06

C

Protein variants	CADD score	MAF
p.M170V	8.301	Private
p.(R442G)	26.9	Private
p.(G279_H280del)	20.3	Private

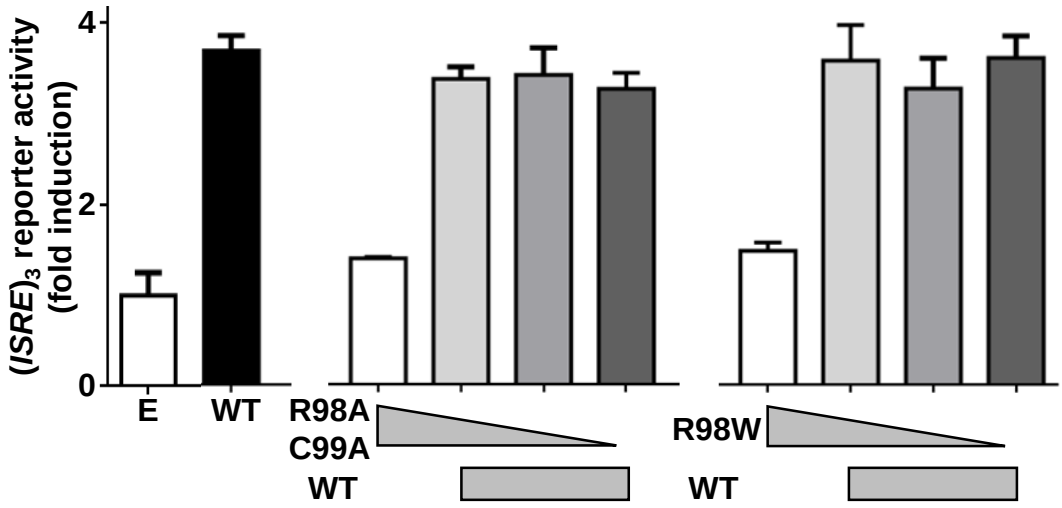
(ISRE)3 reporter activity
(fold induction)
4
2
0
E
WT
R98A
C99A
WT
R98W
WT

A

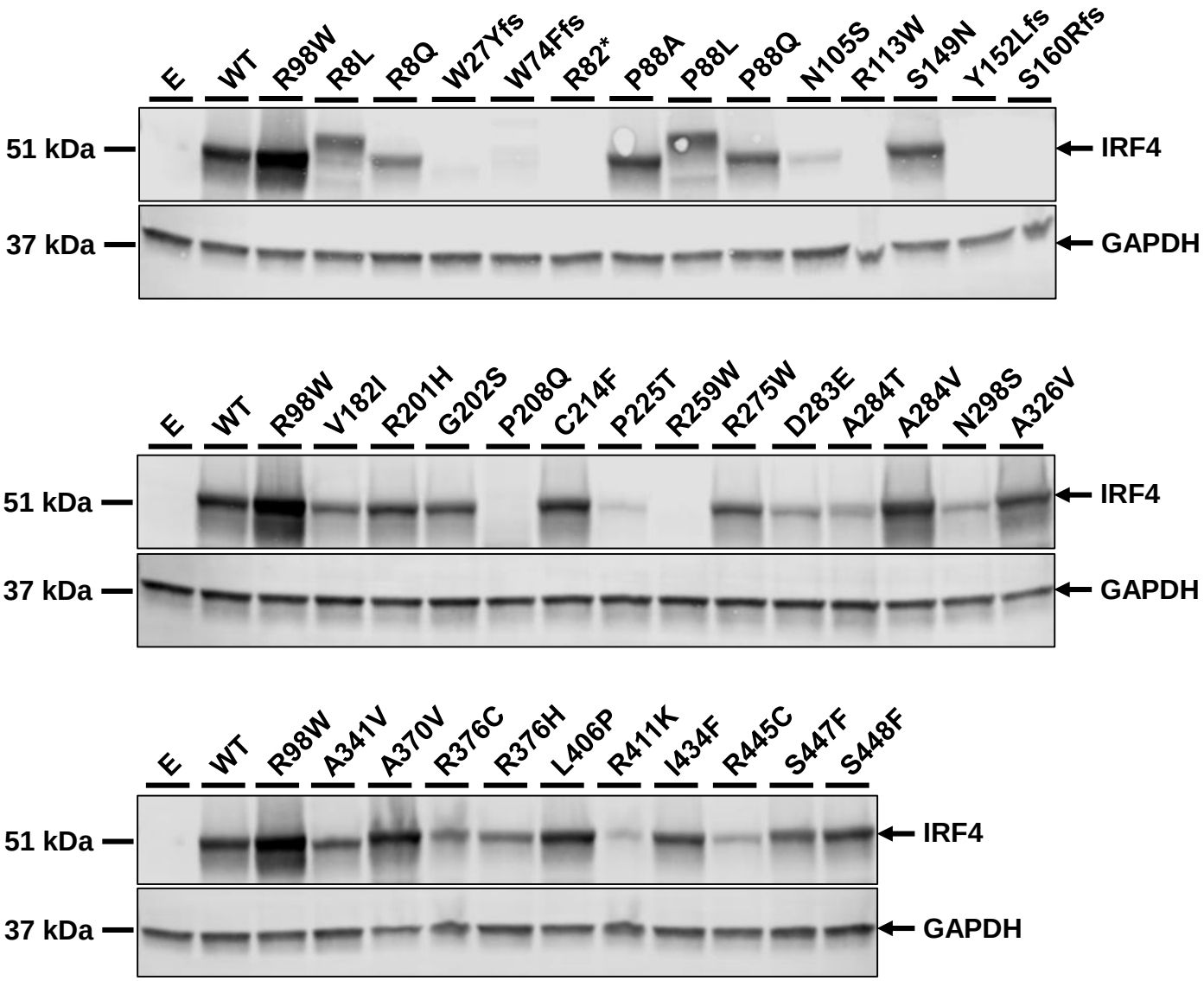
E
WT
R98W
R8L
R8Q
W27Yfs
W74Ffs
R82*
P88A
P88L
P88Q
N105S
R113W
S149N
Y152Lfs
S160Rfs
51 kDa
IRF4
37 kDa
GAPDH
E
WT
R98W
V182I
R201H
G202S
P208Q
C214F
P225T
R259W
R275W
D283E
A284T
A284V
N298S
A326V
51 kDa
IRF4
37 kDa
GAPDH
E
WT
R98W
A341V
A370V
R376C
R376H
L406P
R411K
I434F
R445C
S447F
S448F
51 kDa
IRF4
37 kDa
GAPDH

B

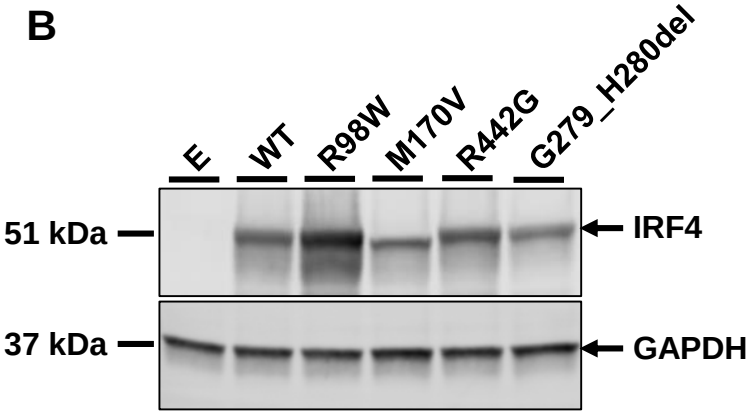
E
WT
R98W
M170V
R442G
G279_H280del
51 kDa
IRF4
37 kDa
GAPDH

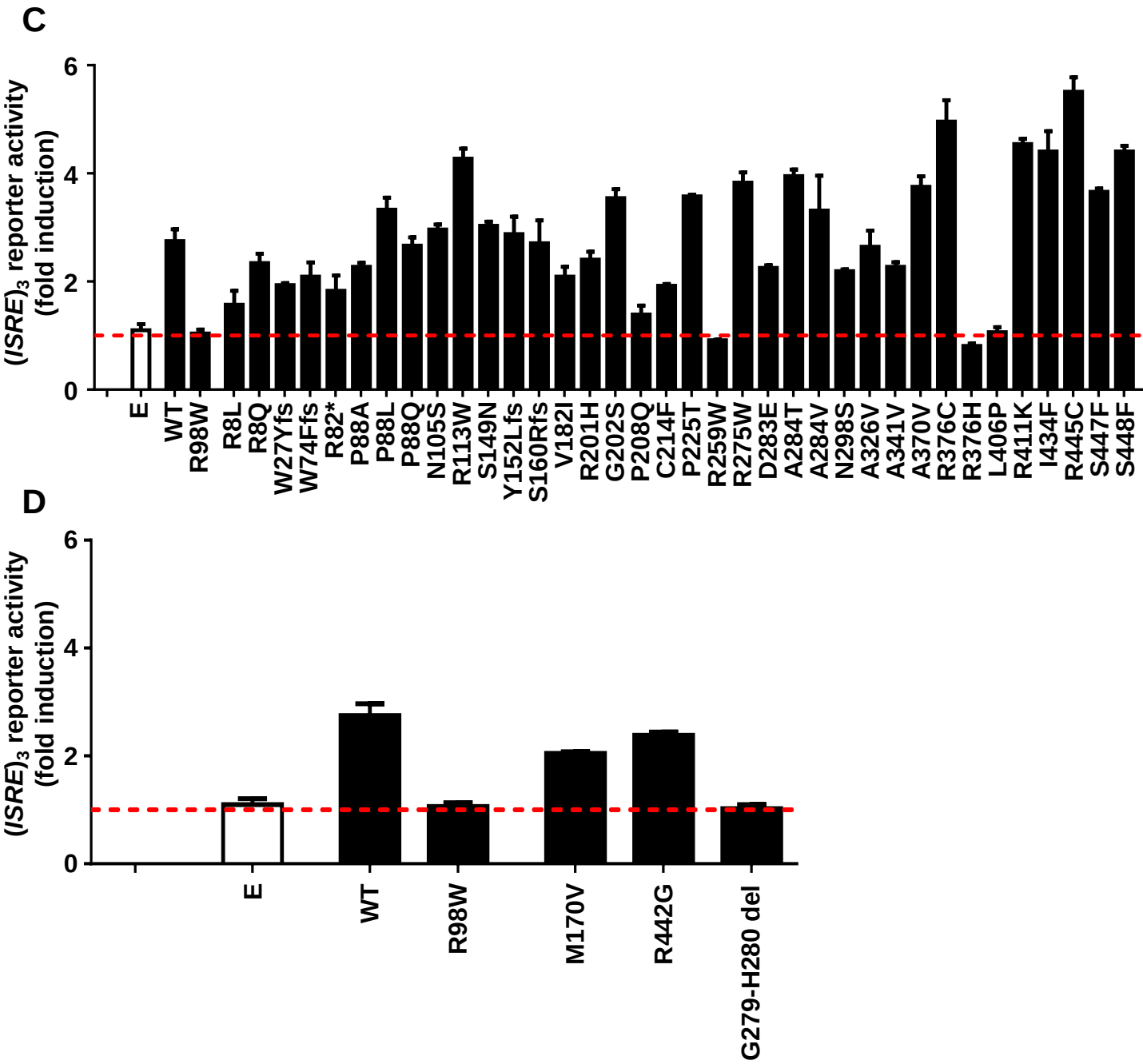
C
(ISRE)3 reporter activity (fold induction)
0
2
4
6
E
WT
R98W
R8L
R8Q
W27Yfs
W74Ffs
R82*
P88A
P88L
P88Q
N105S
R113W
S149N
Y152Lfs
S160Rfs
V182I
R201H
G202S
P208Q
C214F
P225T
R259W
R275W
D283E
A284T
A284V
N298S
A326V
A341V
A370V
R376C
R376H
L406P
R411K
I434F
R445C
S447F
S448F

D
(ISRE)3 reporter activity (fold induction)
0
2
4
6
E
WT
R98W
M170V
R442G
G279-H280 del

A

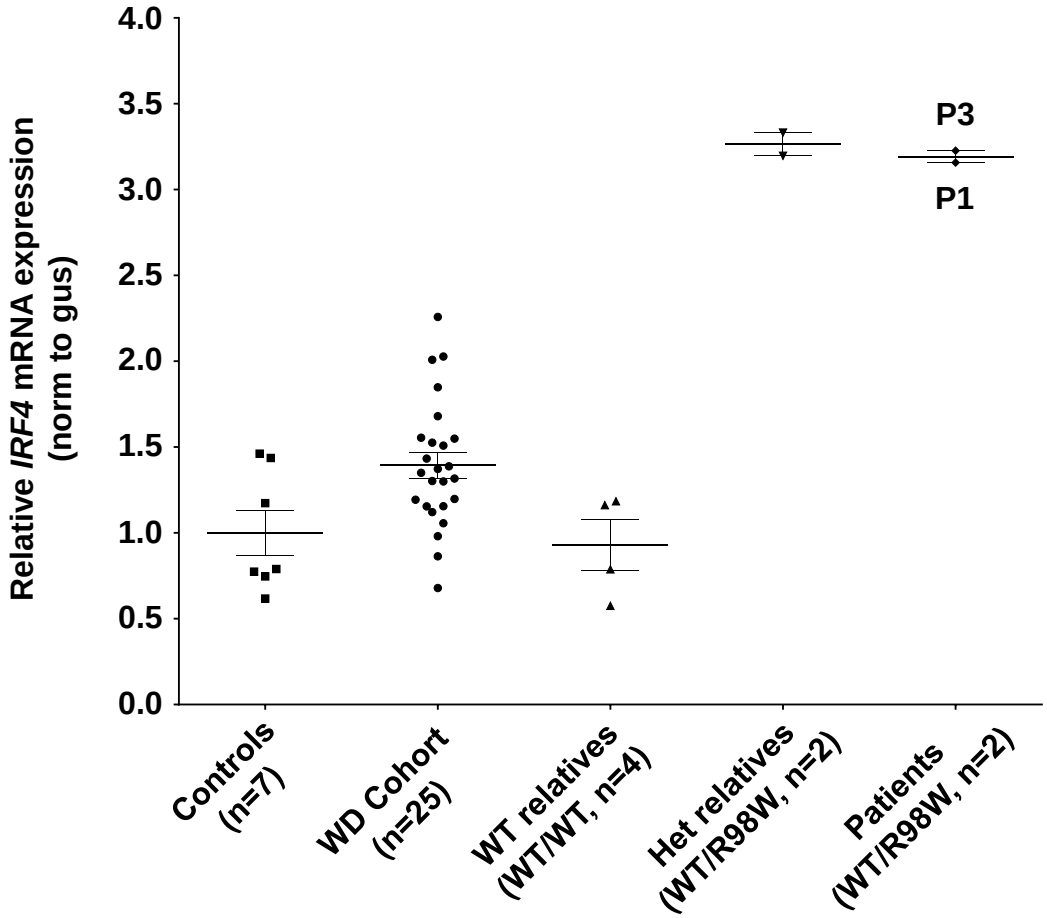
Relative IRF4 mRNA expression (norm to gus)
4.0
3.5
3.0
2.5
2.0
1.5
1.0
0.5
0.0
P3
P1
Controls (n=7)
WD Cohort (n=25)
WT relatives (WT/WT, n=4)
Het relatives (WT/R98W, n=2)
Patients (WT/R98W, n=2)

B

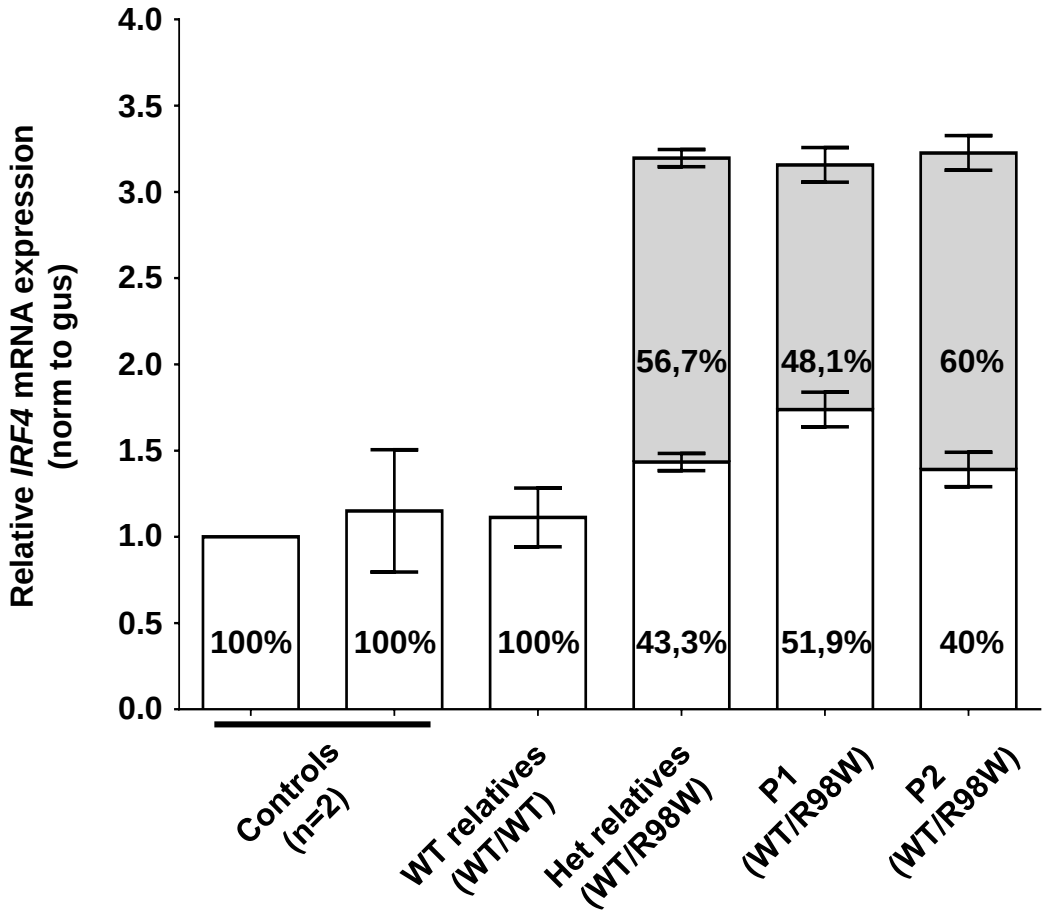
Relative IRF4 mRNA expression (norm to gus)
4.0
3.5
3.0
2.5
2.0
1.5
1.0
0.5
0.0
56,7%
48,1%
60%
100%
100%
100%
43,3%
51,9%
40%
Controls (n=2)
WT relatives (WT/WT)
Het relatives (WT/R98W)
P1 (WT/R98W)
P2 (WT/R98W)

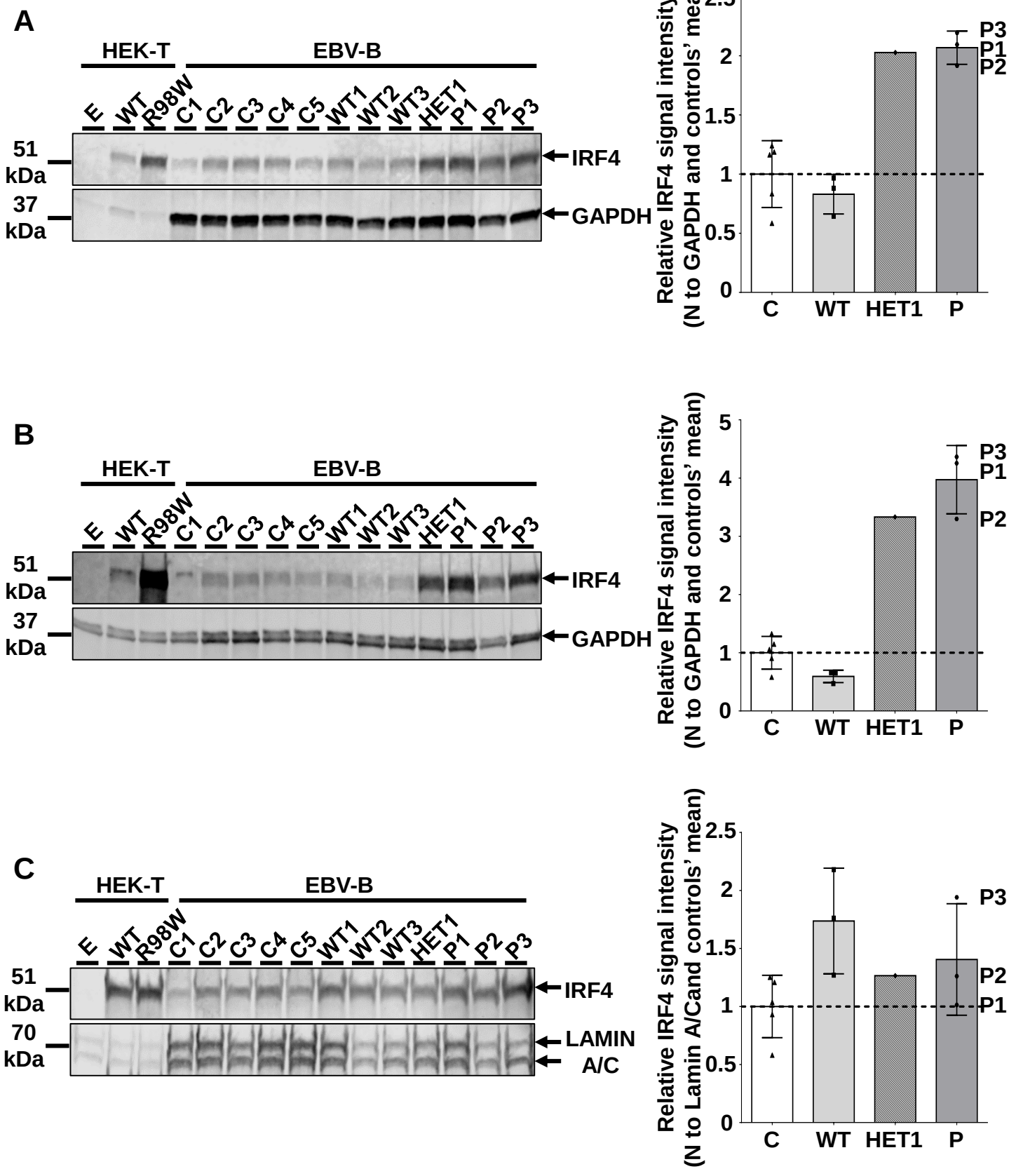
A
HEK-T
EBV-B
E
WT
R98W
C1
C2
C3
C4
C5
WT1
WT2
WT3
HET1
P1
P2
P3
51 kDa
IRF4
37 kDa
GAPDH
Relative IRF4 signal intensity (N to GAPDH and controls' mean)
2.5
2
1.5
1
0.5
0
C
WT
HET1
P
P3
P1
P2
B
HEK-T
EBV-B
E
WT
R98W
C1
C2
C3
C4
C5
WT1
WT2
WT3
HET1
P1
P2
P3
51 kDa
IRF4
37 kDa
GAPDH
Relative IRF4 signal intensity (N to GAPDH and controls' mean)
5
4
3
2
1
0
C
WT
HET1
P
P3
P1
P2
C
HEK-T
EBV-B
E
WT
R98W
C1
C2
C3
C4
C5
WT1
WT2
WT3
HET1
P1
P2
P3
51 kDa
IRF4
70 kDa
LAMIN A/C
Relative IRF4 signal intensity (N to Lamin A/Cand controls' mean)
2.5
2
1.5
1
0.5
0
C
WT
HET1
P
P3
P2
P1

Figure S8

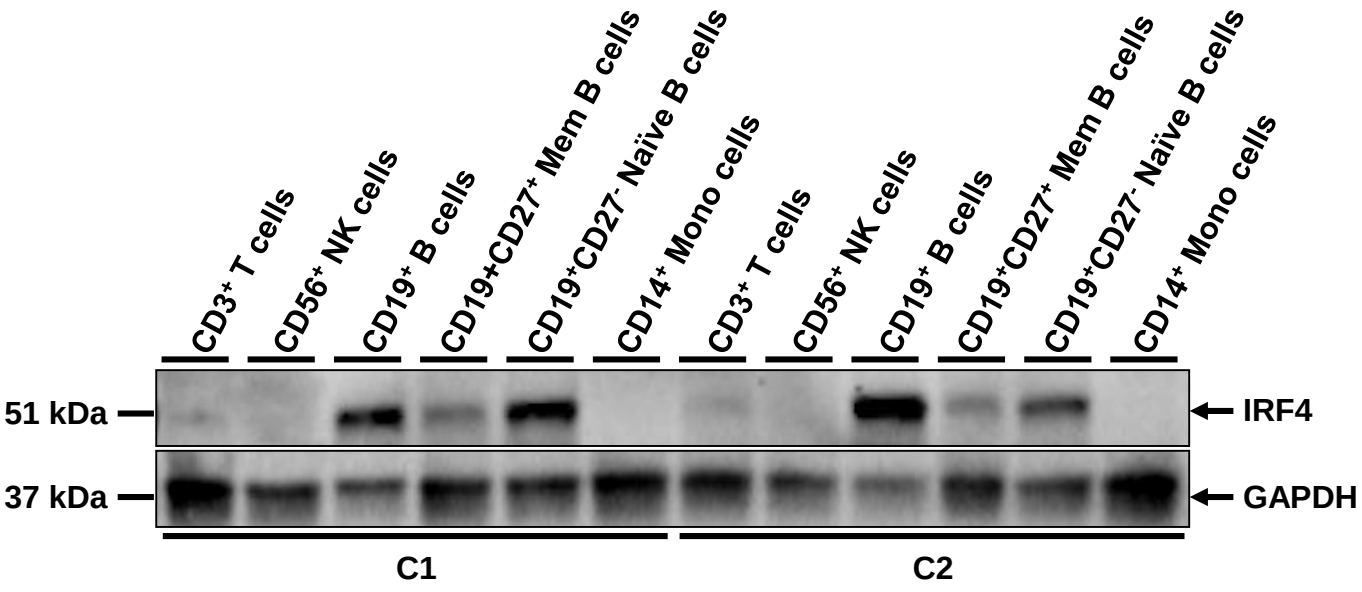
CD3+ T cells
CD56+ NK cells
CD19+ B cells
CD19+CD27+ Mem B cells
CD19+CD27- Naïve B cells
CD14+ Mono cells
CD3+ T cells
CD56+ NK cells
CD19+ B cells
CD19+CD27+ Mem B cells
CD19+CD27- Naïve B cells
CD14+ Mono cells
51 kDa
IRF4
37 kDa
GAPDH
C1
C2

A

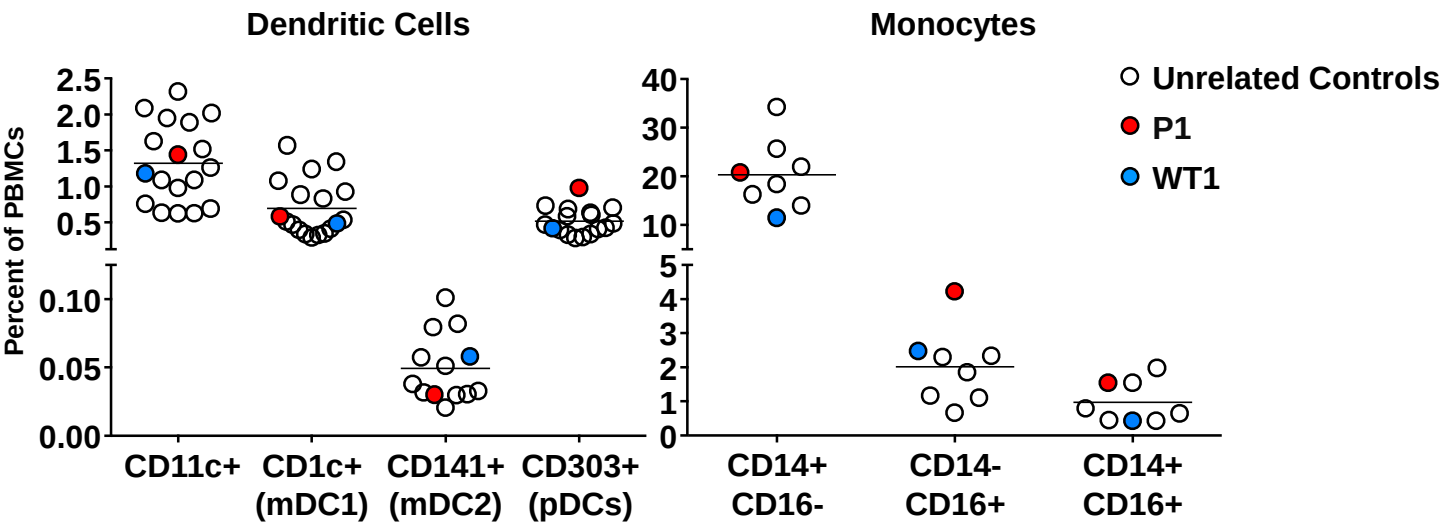

B

Gating Strategy

Population	Characterization
mDC1	HLA-DR+, CD14-, CD16-, Lin (CD3, CD15, CD19, CD56, NKp46)-, CD11c+, CD141-, **CD1c+**
mDC2	HLA-DR+, CD14-, CD16-, Lin (CD3, CD15, CD19, CD56, NKp46)-, CD11c+, **CD141+**, CD1c-
pDCs	HLA-DR+, CD14-, CD16-, Lin (CD3, CD15, CD19, CD56, NKp46)-, **CD303+**
CD14+ CD16- Monocytes	HLA-DR+, Lin (CD3, CD15, CD19, CD56, NKp46)-, **CD14+, CD16-**
CD14- CD16+ Monocytes	HLA-DR+, Lin (CD3, CD15, CD19, CD56, NKp46)-, **CD14-, CD16+**
CD14+ CD16+ Monocytes	HLA-DR+, Lin (CD3, CD15, CD19, CD56, NKp46)-, **CD14-, CD16+**

A

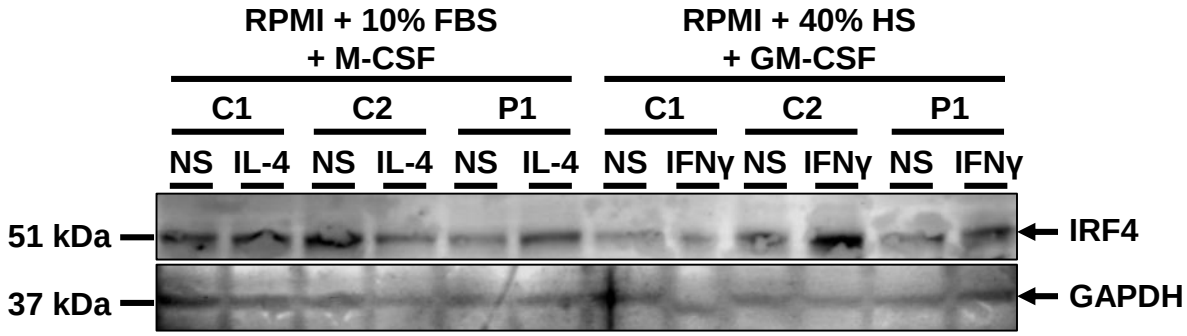
RPMI + 10% FBS
+ M-CSF
RPMI + 40% HS
+ GM-CSF
C1
C2
P1
C1
C2
P1
NS
IL-4
NS
IL-4
NS
IL-4
NS
IFNγ
NS
IFNγ
NS
IFNγ
51 kDa
37 kDa
IRF4
GAPDH

B

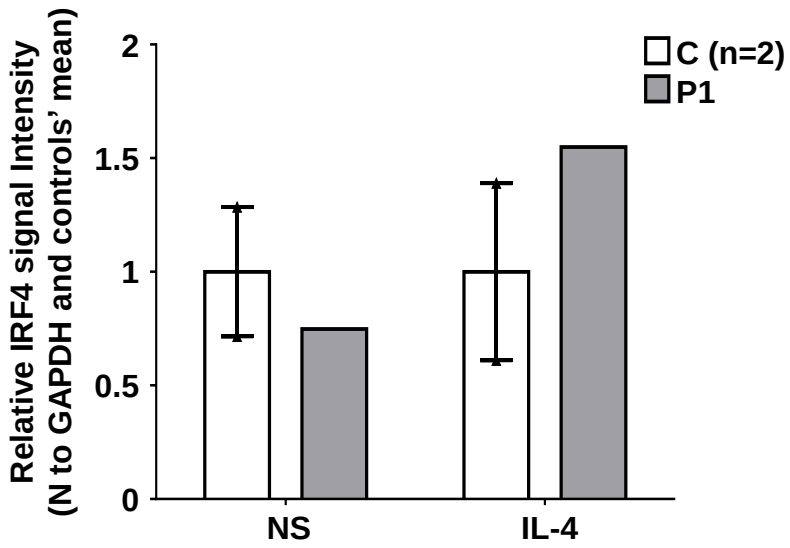
Relative IRF4 signal Intensity
(N to GAPDH and controls' mean)
2
1.5
1
0.5
0
C (n=2)
P1
NS
IL-4

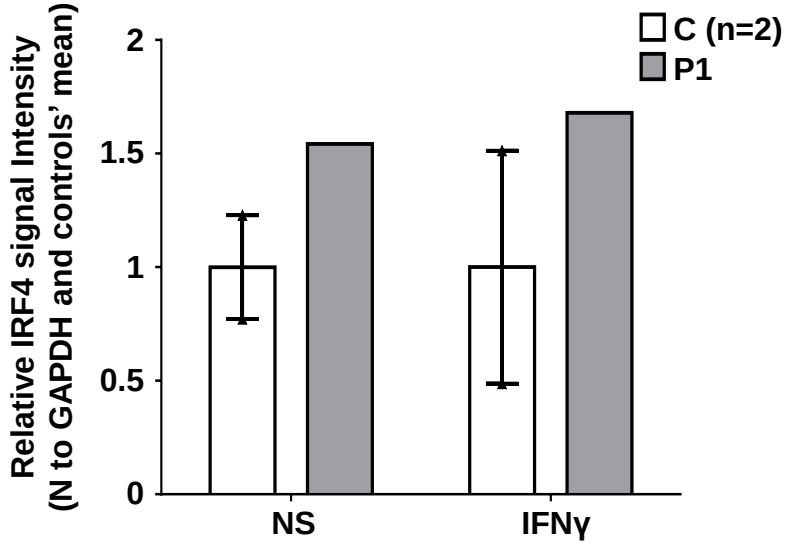
Relative IRF4 signal Intensity
(N to GAPDH and controls' mean)
2
1.5
1
0.5
0
C (n=2)
P1
NS
IFNγ

Figure S10

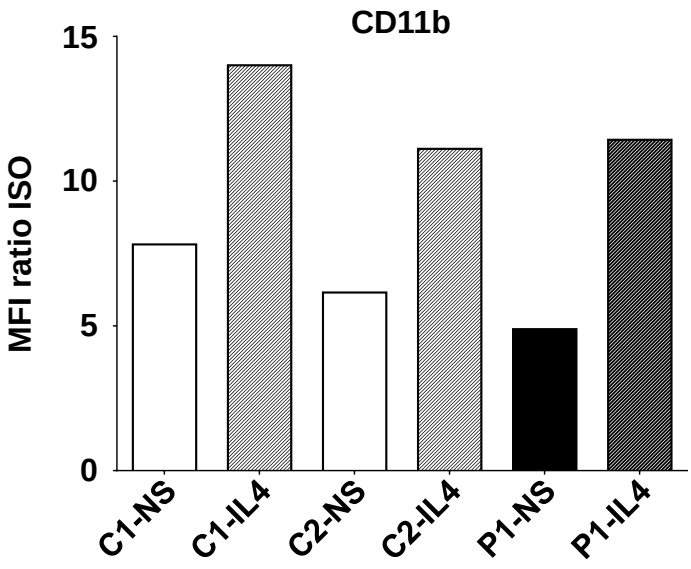
CD11b
MFI ratio ISO
15
10
5
0
C1-NS
C1-IL4
C2-NS
C2-IL4
P1-NS
P1-IL4

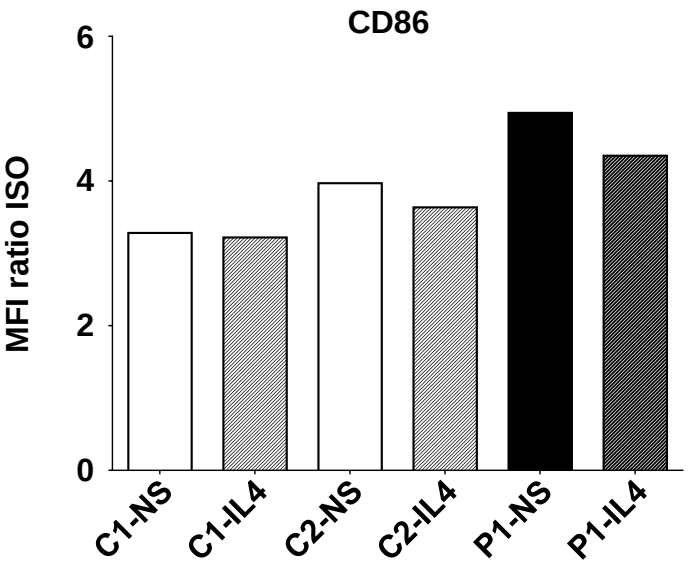
CD86
MFI ratio ISO
6
4
2
0
C1-NS
C1-IL4
C2-NS
C2-IL4
P1-NS
P1-IL4

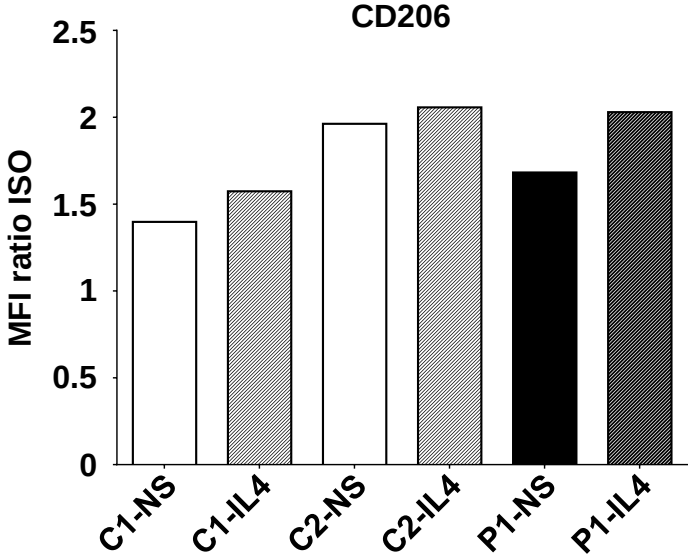
CD206
MFI ratio ISO
2.5
2
1.5
1
0.5
0
C1-NS
C1-IL4
C2-NS
C2-IL4
P1-NS
P1-IL4

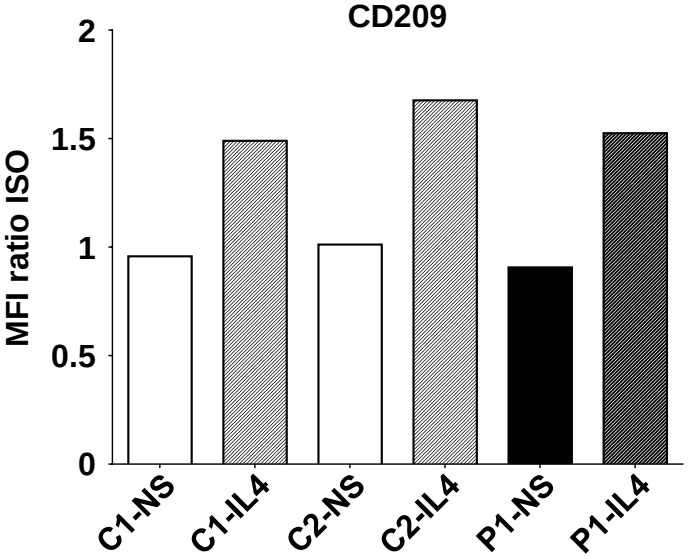
CD209
MFI ratio ISO
2
1.5
1
0.5
0
C1-NS
C1-IL4
C2-NS
C2-IL4
P1-NS
P1-IL4

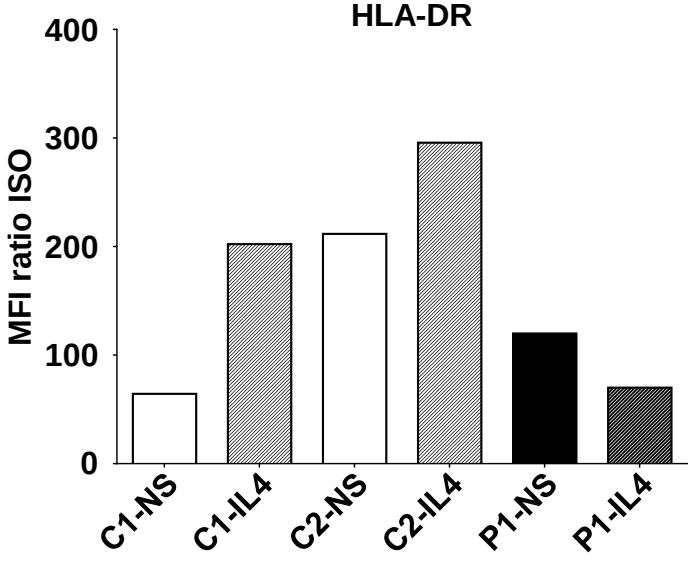
HLA-DR
MFI ratio ISO
400
300
200
100
0
C1-NS
C1-IL4
C2-NS
C2-IL4
P1-NS
P1-IL4

D

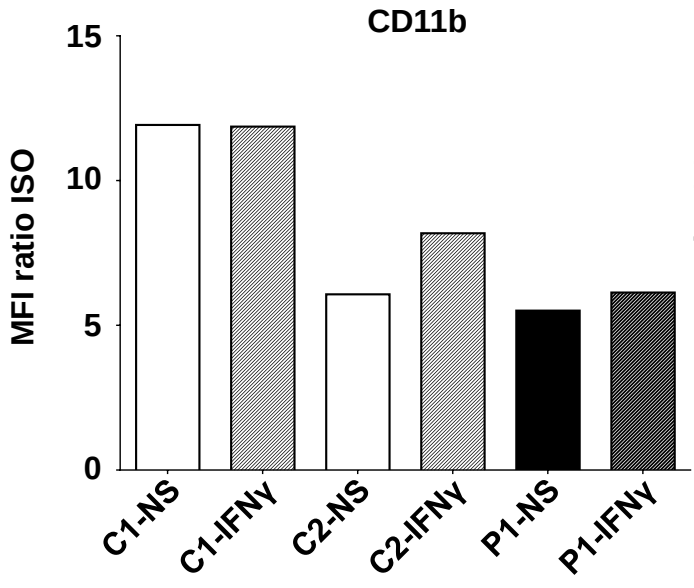
CD11b
MFI ratio ISO
15
10
5
0
C1-NS
C1-IFNγ
C2-NS
C2-IFNγ
P1-NS
P1-IFNγ

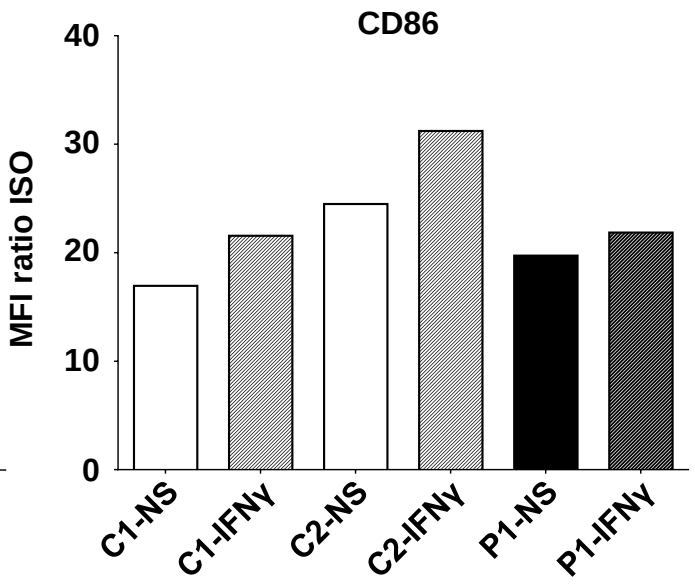
CD86
MFI ratio ISO
40
30
20
10
0
C1-NS
C1-IFNγ
C2-NS
C2-IFNγ
P1-NS
P1-IFNγ

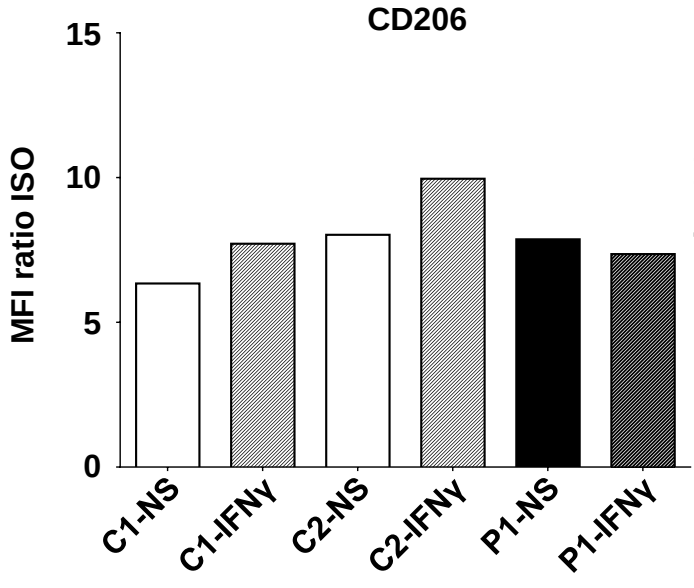
CD206
MFI ratio ISO
15
10
5
0
C1-NS
C1-IFNγ
C2-NS
C2-IFNγ
P1-NS
P1-IFNγ

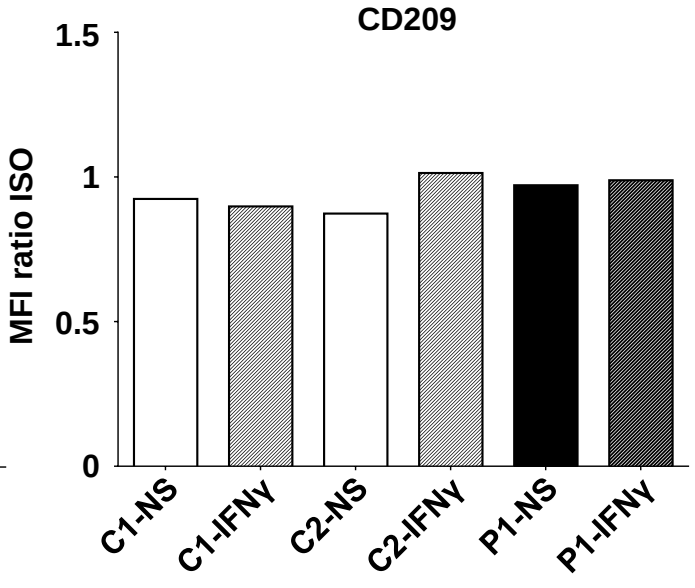
CD209
MFI ratio ISO
1.5
1
0.5
0
C1-NS
C1-IFNγ
C2-NS
C2-IFNγ
P1-NS
P1-IFNγ

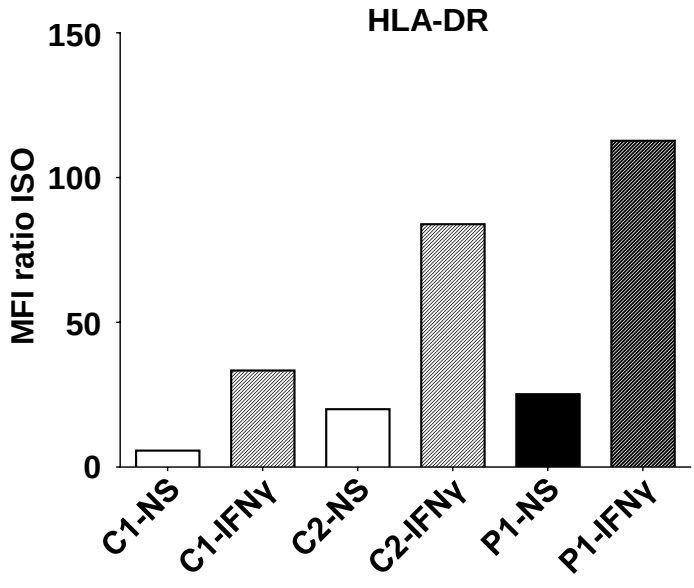
HLA-DR
MFI ratio ISO
150
100
50
0
C1-NS
C1-IFNγ
C2-NS
C2-IFNγ
P1-NS
P1-IFNγ

A

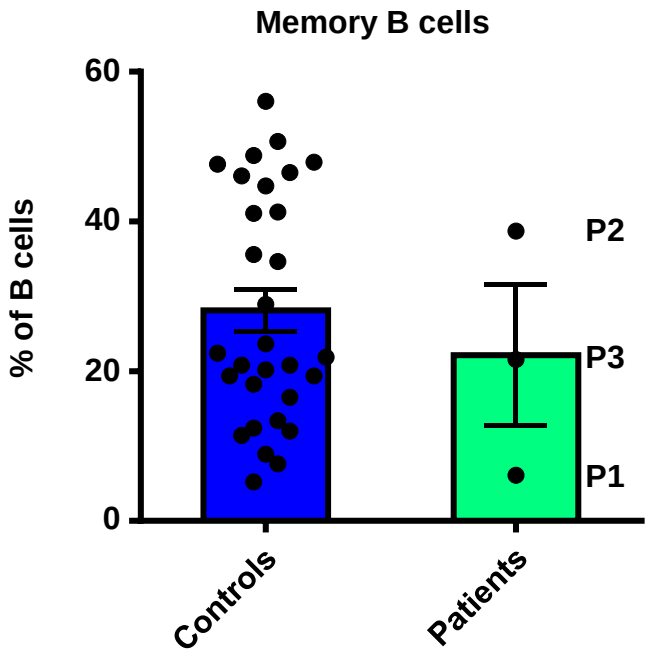
Memory B cells
% of B cells
60
40
20
0
P2
P3
P1
Controls
Patients

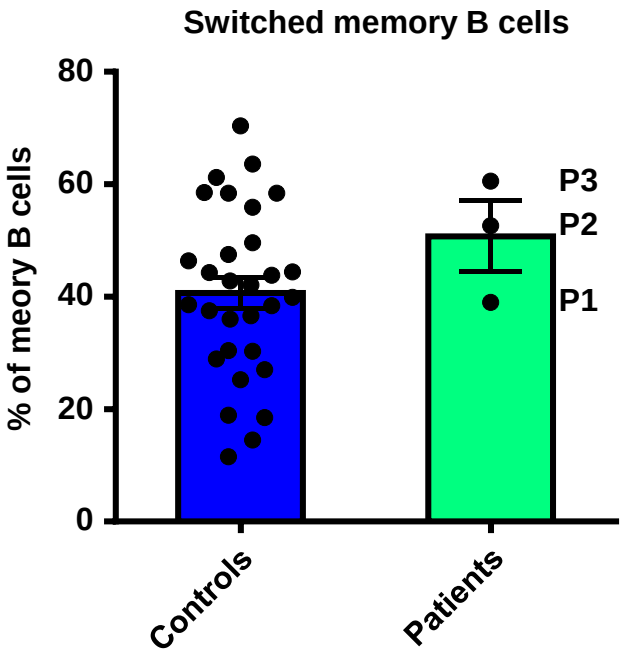
Switched memory B cells
% of meory B cells
80
60
40
20
0
P3
P2
P1
Controls
Patients

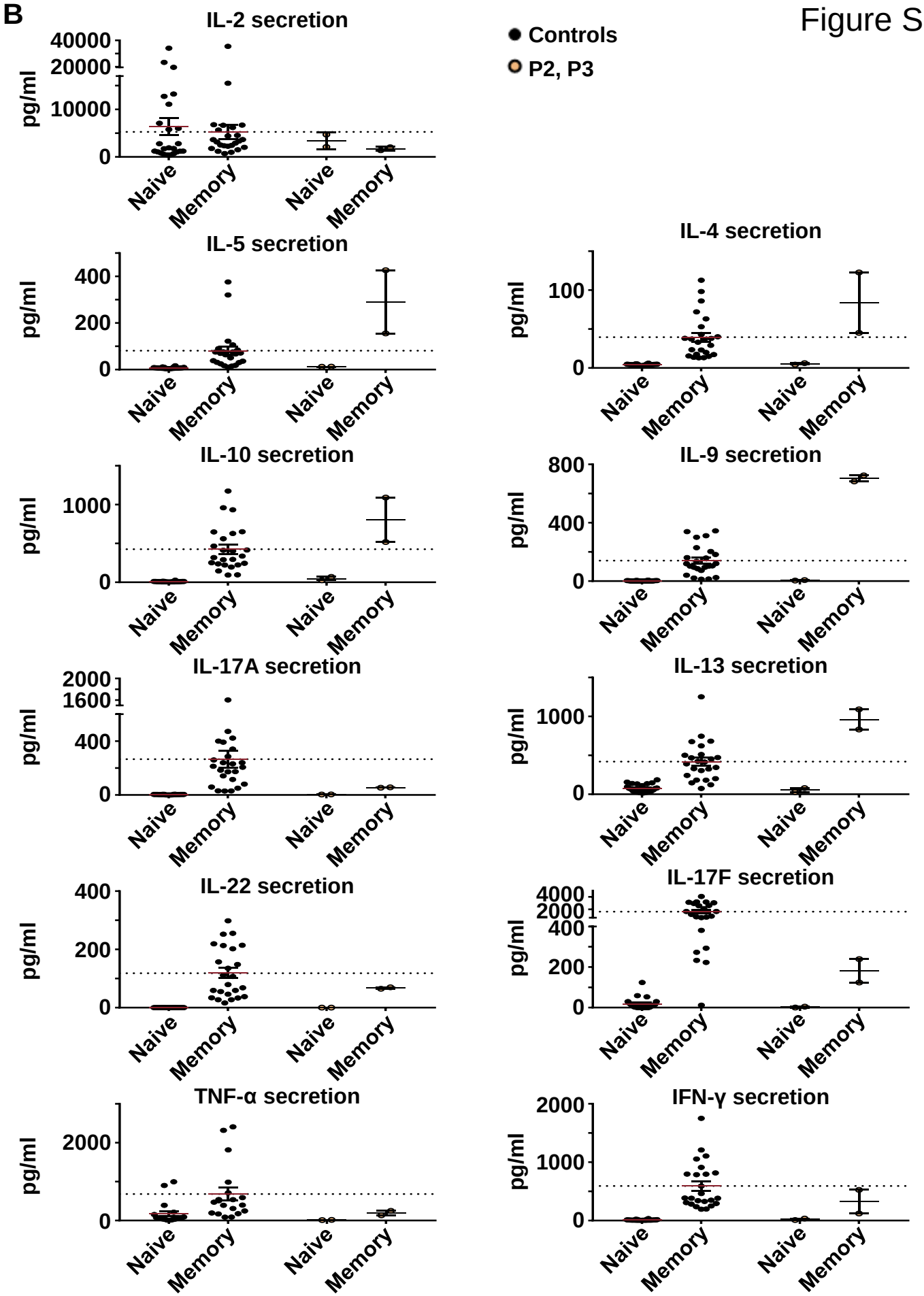
B
Controls
P2, P3
IL-2 secretion
IL-4 secretion
IL-5 secretion
IL-9 secretion
IL-10 secretion
IL-13 secretion
IL-17A secretion
IL-17F secretion
IL-22 secretion
IFN-γ secretion
TNF-α secretion
pg/ml
Naive
Memory

C

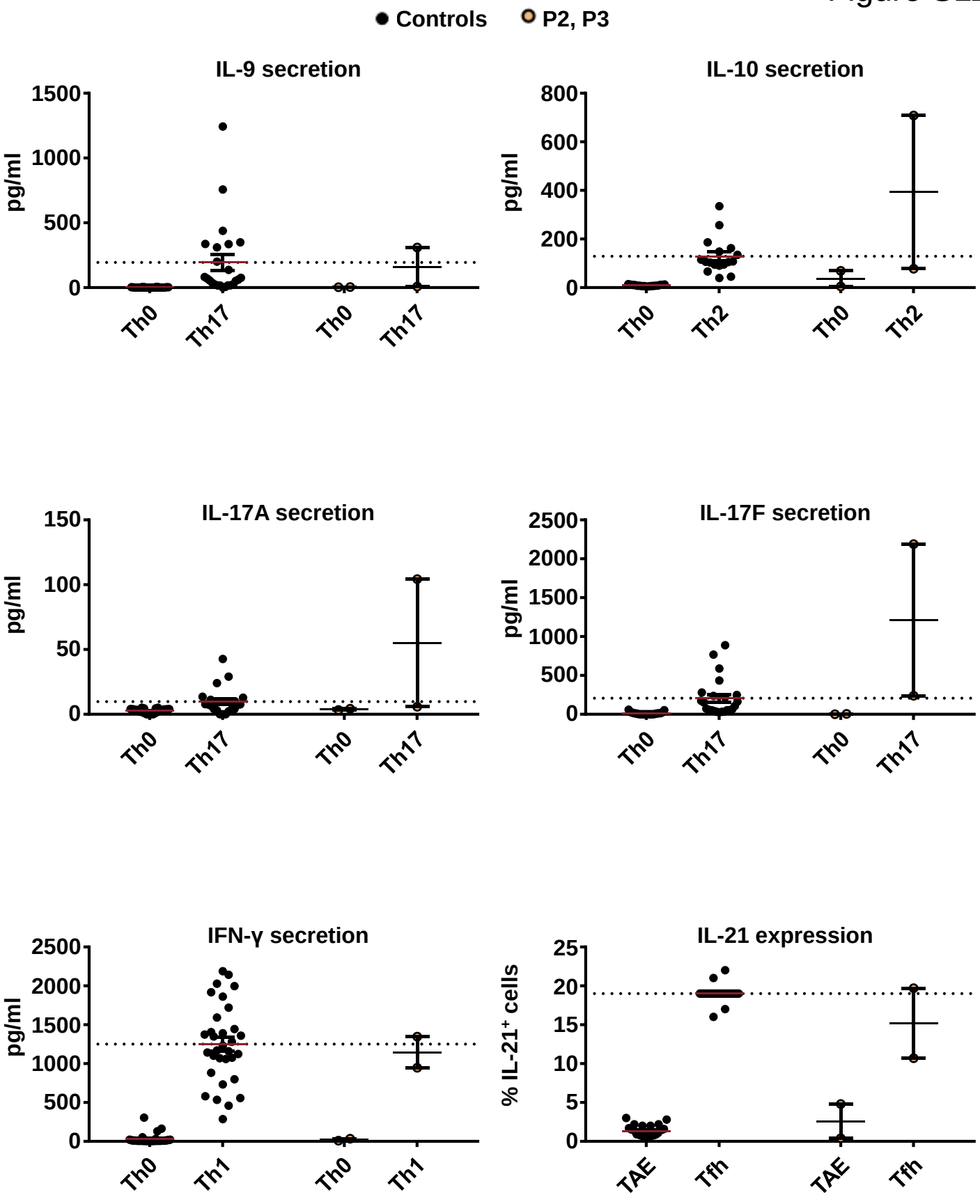
Controls
P2, P3
IL-9 secretion
pg/ml
1500
1000
500
0
Th0
Th17
Th0
Th17
IL-10 secretion
pg/ml
800
600
400
200
0
Th0
Th2
Th0
Th2
IL-17A secretion
pg/ml
150
100
50
0
Th0
Th17
Th0
Th17
IL-17F secretion
pg/ml
2500
2000
1500
1000
500
0
Th0
Th17
Th0
Th17
IFN-γ secretion
pg/ml
2500
2000
1500
1000
500
0
Th0
Th1
Th0
Th1
IL-21 expression
% IL-21+ cells
25
20
15
10
5
0
TAE
Tfh
TAE
Tfh

Figure legends

Figure 1. Autosomal dominant IRF4 deficiency. **A.** Pedigree of the kindred with allele segregation. Generations are designated by a Roman numeral (I, II, III, IV, V and VI), and each individual by an Arabic numeral (from left to right). Each symbol is divided into two parts: the upper part indicates the clinical status for WD (black: affected, white: healthy), the lower part indicates whether Tw was identified by PCR (in saliva, blood, feces or joint fluid) or by PAS staining on bowel biopsy specimens (gray: Tw-positive, white: Tw-negative, "?": not tested). Whipple's disease patients are indicated as P1, P2, P3, and P4; the proband is indicated with an arrow. Genotype status and age (for *IRF4*-heterozygous individuals) are reported below symbols. Individuals whose genetic status could not be evaluated are indicated by the symbol "E?". **B.** Schematic representation of the IRF4 protein showing the DNA-binding domain (DBD), P-rich domain, activation domain, α-helical domain, Q-rich domain, IFR association domain (IAD) and auto-inhibitory domain. The R98W substitution is indicated in red. **C.** Electropherogram of *IRF4* genomic DNA sequences from a healthy control (C) and the patients (P1, P2, P3, P4). The R98W IRF4 mutation is caused by the replacement of an arginine with a tryptophan residue in position 98 (exon 3, c.292 C>T). Corresponding amino acids are represented above each electropherogram. **D.** Alignment of the R98W amino acid in the DBD domain of IRF4 in humans and 11 other animal species. R98 is indicated in red.

Figure 2. Molecular characterization of the R98W *IRF4* mutation (loss of DNA binding). **A.** HEK293-T cells were transfected with an empty pcDNA3.1 plasmid (E) or with pcDNA3.1 plasmids carrying wild-type (WT) *IRF4*, R98W or R98A-C99A *IRF4* mutant alleles. Total cell extracts were subjected to western blotting; the upper panel shows IRF4 levels and the lower panel shows GAPDH levels, used as a loading control. The results shown are representative of

three independent experiments. **B.** (upper panel) HEK293-T cells were transfected with an empty pcDNA3.1 plasmid (E) or with pcDNA3.1 plasmids carrying the wild-type *IRF4* (WT) or R98W *IRF4* mutant alleles. Total cell (1), cytoplasmic (2) and nuclear (3) extracts were subjected to western blotting. Lamin A/C and GAPDH were used as loading controls. (lower panel) IRF4 signal intensity for R98W-transfected cells and WT-transfected cells, in various cell compartments (total, cytoplasmic and nuclear), normalized against the GAPDH signal, as shown by western blotting. The results shown are representative of three independent experiments. **C**. Luciferase activity of HEK293-T cells cotransfected with an $(ISRE)_3$ reporter plasmid plus the pcDNA3.1 empty vector (E) and a plasmid encoding WT or R98W or R98A/C99A mutants. Results are show, as fold induction of activity relative to E-transfected cells. The red dotted line indicates mean activity for E-transfected cells. The mean and standard error of three experiments are shown. **D**. Electrophoretic mobility shift assay (EMSA) of nuclear extracts of HEK293-T cells transfected with E, WT or R98W plasmids. Extracts were incubated with a ^{32}P-labeled *ISRE* probe. Extracts were incubated with specific anti-IRF4 antibody (S) to detect DNA-protein complex supershift, with isotype antibody (I) to demonstrate the specificity of the complex, and with no antibody (-), as a control. The results shown are representative of three independent experiments. **E.** EMSA of nuclear extracts of HEK293-T cells transfected with E, PU.1, WT, R98W, or cotransfected with PU.1 and WT or PU.1 and R98W plasmids. Extracts were incubated with a ^{32}P-labeled λB probe (EICE). Extracts were incubated with specific anti-IRF4 antibody (S) to detect DNA-protein complex supershift, with isotype antibody (I) to demonstrate the IRF4 specificity of the complex and with no antibody (-), as a control. Experiments in the presence of excess of non-radioactive probe (cold probe) demonstrated the probe specificity of the complexes. The results shown are representative of three independent experiments.

Figure 3. IRF4 protein levels in CD4$^+$ T cells.

A.-C. (Left) Total-cell (A), cytoplasmic (B) and nuclear (C) extracts from CD4$^+$ T cells from four unrelated controls (C1 to C4) and two patients (P1 and P3) stimulated with CD2/CD3/CD28-coated beads (Stim) or left unstimulated (NS). Protein extracts from HEK293-T cells transfected with E or WT plasmids were used as controls for the specific band corresponding to IRF4. (Right) Representation of IRF4 signal intensity for each individual relative to the mean signal for unrelated controls (*n*=4) obtained by western blotting (Supp. Figure 8 A-C left) normalized against the GAPDH signal (total, cytoplasmic extracts) or the laminin A/C signal (nuclear extracts).

Figure 4. Overall transcriptional responsiveness of PBMCs following *in vitro* exposure to Tw and BCG and pathway activity analysis for genes responsive to BCG exposure. A. The overall responsiveness of individual subjects following stimulation with BCG and Tw, relative to non-stimulated conditions (along the horizontal axis) is shown as a heatmap. Subjects were grouped by unsupervised hierarchical clustering. **B.** Enriched canonical pathways were ranked according to differences in mean activation *z*-score between genotypes (homozygous vs. heterozygous). The activation *z*-scores for each individual and pathway are shown as heat maps. Pathways predicted to be activated are depicted in orange, pathways predicted to be inhibited are depicted in blue. A lack of prediction concerning activation is depicted in white. Individuals are presented in columns, pathways in rows. The pathways are ranked from most different between genotypes (at the top of the list) to least different (at the bottom). The differences in mean activation *z*-scores between homozygous and heterozygous individuals for each pathway are depicted as bars to the right of the heat maps (the direction of difference is not shown). The Ingenuity Pathway Analysis (IPA) tool was used to generate a list of the most significant canonical pathways and their respective activation *z*-scores.

Supplementary Figures legends

Supplementary Figure 1. Genome-wide linkage and whole-exome sequencing analyses. A. Genome wide linkage analysis was performed by combining Genome-wide array and whole-exome sequencing (WES) data assuming an autosomal dominant (AD) mode of inheritance. LOD (logarithm of odds) scores are shown for the four patients considered together. The maximum expected LOD score is 1.95, based on an AD model with incomplete penetrance. *IRF4* is located within a linkage region (LOD=1.94) on chromosome 6 (indicated by a black arrow). **B.** A refined analysis of WES data identified *IRF4* as the only protein-coding gene carrying a rare heterozygous mutation common to P1, P2, P3 and P4 within the linkage regions.

Supplementary Figure 2. **Analysis *in silico* of *IRF4* variants**. **A.** Minor allele frequency and combined annotation–dependent depletion score (CADD) of all coding variants reported in public database (GnomAD) (http://gnomad.broadinstitute.org) and in-house (HGID) databases. The dotted line corresponds to the mutation significance cutoff (MSC) with 95% confidence interval. The variants studied *in vitro* here are shown in red, in bold typeface. The R98W variant is represented by a blue square.

Supplementary Figure 3. List of variants and strength of purifying selection on *IRF4*. A. Genome-wide distribution of the strength of purifying selection, estimated by the *f* parameter (53), acting on 14,993 human genes. *IRF4* is at the 9.4th percentile of the distribution, indicating that it is more constrained than most human genes. **B**. List of *IRF4* missense and in-frame deletion variants reported in a public database (GnomAD) and studied *in vitro* here. **C.** List of *IRF4* missense and in-frame deletion variants found in the HGID database and studied *in vitro* here.

Supplementary Figure 4. **Functional activity of IRF4.**

Luciferase activity of HEK293-T cells cotransfected with an $(ISRE)_3$ reporter plasmid plus E and WT or various amounts of R98W or R98A/C99A plasmids. Results are showed as fold induction of activity relative to E-transfected cells. The results shown are the mean ± S.D. of three independent experiments.

Supplementary Figure 5. Protein levels and functional impact of *IRF4* variants.

A.-B. HEK293-T cells were transfected with E or WT, R98W or several *IRF4* variants reported in a public database (**A**, see Figure S3B) or in the HGID database (**B**, see Figure S3C). Total cell extracts were subjected to western blotting; the upper panel shows IRF4 levels and the lower panel shows GAPDH levels, used as a loading control. The results shown are representative of three independent experiments. **C.-D.** Luciferase activity of HEK293-T cells cotransfected with an $(ISRE)_3$ reporter plasmid plus E and plasmids containing WT, R98W or several IRF4 variants reported in public databases (**C**, see Figure S3B) or in the HGID database (**D**, see Figure S3C). Results are shown as fold induction of activity relative to E-transfected cells. The red dotted line indicates the mean fold induction in E-transfected cells. The results shown are the mean ± SD of three independent experiments.

Supplementary Figure 6. *IRF4* mRNA levels in EBV-B cells.

A. Total RNA extracted from controls (n=7), patients diagnosed with Whipple's disease (n=25) not related to this kindred, healthy homozygous WT relatives (*n*=4), patients with monoallelic *IRF4* mutations (*n*=2) and asymptomatic heterozygous relatives with monoallelic *IRF4* mutations (*n*=2) was subjected to RT-qPCR for total *IRF4*. Data are displayed as $2^{-\Delta\Delta Ct}$ after normalization according to endogenous GUS control gene expression (ΔCt) and the mean of

controls (ΔΔCt). The results shown are the mean ± SD of three independent experiments. **B.** The *IRF4* mRNA levels reported in Figure S7A are represented on histograms; the percentage within each bar is the deduced frequency of each mRNA obtained by the TA-cloning of cDNA generated from EBV-B cells from controls (*n*=2), healthy homozygous WT relatives (*n*=1), patients with monoallelic *IRF4* mutations (*n*=2) and asymptomatic heterozygous relatives with monoallelic *IRF4* mutations (*n*=1).

Supplementary Figure 7. IRF4 protein levels in EBV-B cells.

A.-C. (Left) Total cell (A), cytoplasmic (B) and nuclear (C) extracts (b) from five healthy controls (C1 to C5), three homozygous WT relatives (WT1, WT2, WT3), three patients (P1 to P3) and one asymptomatic heterozygous relative from the kindred (HET1). Protein extracts from HEK293-T cells transfected with E, WT or R98W plasmids were used as controls for the specific band corresponding to IRF4. (Right) Representation of IRF4 signal intensity for each individual relative to the mean signal for unrelated controls (*n*=5) obtained by WB and represented by black dotted lines (Supp. Figure A left) normalized against the GAPDH signal (total, cytoplasmic extracts) or the lamin A/C signal (nuclear extracts). The results shown are representative of two independent experiments.

Supplementary Figure 8. IRF4 protein levels in PBMC subpopulations.

Total cell extracts from PBMC subpopulations ($CD3^+$ T cells, $CD56^+$ NK cells, $CD19^+$ B cells, $CD19^+CD27^+$ memory B cells, $CD19^+CD27^-$ naive B cells, $CD14^+$ monocytes) from two unrelated healthy controls were subjected to western blotting. The upper panel shows IRF4 levels and the lower panel shows GAPDH levels, used as a loading control. The results shown are representative of two independent experiments.

Supplementary Figure 9. Percentage of dendritic cells and monocyte subtypes within total PBMCs. A. Percentage of $CD11c^+$, myeloid dendritic cells (mDC1 and mDC2) and plasmacytoid dendritic cells (pDCs) (left), and monocyte subtypes (right) among total PBMCs from unrelated controls, a patient (P1) and a homozygous WT relative (WT1). **B.** Gating strategy to define the dendritic cell and monocyte subtypes.

Supplementary Figure 10. IRF4 levels in the patients' monocyte-derived macrophages. **A.** IRF4 protein levels, as determined by western blotting on total cell extracts from M2-like (left panel) or M1-like (right panel) monocyte-derived macrophages (MDMs) from two unrelated healthy controls (C1 and C2) and P1, either left non-stimulated (NS) or stimulated with IL-4 (for M2-like MDMs) or IFN-γ (for M1-like MDMs). **B.** IRF4 signal intensity for each individual relative to the mean signal for controls on western blots. **C.-D.** CD11b, CD86, CD206, CD209 and HLA-DR mean fluorescence intensity (MFI) for M2-MDM (C) and M1-MDM (D) from P1 and two healthy unrelated controls (C1 and C2), either left non-stimulated (NS) or stimulated with IL-4 (for M2-like MDMs) or IFN-γ (for M1-like MDMs).

Supplementary Figure 11. Percentage of memory B cells, *in vitro* differentiation of $CD4^+$ T cells and *ex vivo* cytokine production by $CD4^+$ memory T cells. A. PBMCs from unrelated controls and patients (P1, P2 and P3) were stained with antibodies against CD20, CD10 and CD27, IgM, IgG or IgA. Percentages of memory B cells ($CD20^+$ $CD10^-$ $CD27^+$) were determined, and the proportion of memory B cells that had undergone class switching to express IgG or IgA was then calculated. No significant differences were observed between unrelated controls and patients. **B.** Naïve and memory $CD4^+$ T cells from unrelated controls and patients (P2 and P3) were purified by sorting and cultured with TAE beads. The secretion of IL-2, IL-4, IL-5, IL-9, IL-10, IL-13, IL-17A, IL-17F, IL-22, IFN-γ and TNF-α was measured five days

later. No significant differences were observed between unrelated controls and patients. **C.** Naïve $CD4^+$ T cells from unrelated controls and patients (P2 and P3) were stimulated with TAE beads alone or under Th1, Th2, Th17 or Tfh polarizing conditions. The production of IL-10, IL-21, IL-17A, IL-17F and IFN-γ was measured five days later, in the corresponding polarizing conditions. No significant differences were observed (as in B) between unrelated controls and patients.

Supplementary Table 1. Kindred information summary.
For each subject, Tw carriage status, *IRF4* genotype, clinical status and date of birth (DOB) are reported. NA: not available; Pos: positive; Neg: negative; Tw: *Tropheryma whipplei*; WD: Whipple's disease; E?: genotype not assessed.

	TW carriage (PCR)			**IRF4 genotype**	**Clinical status**	**DOB**
ID	Feces	Saliva	Joint fluid			
III.4 (P3)	Pos. then Neg.	Neg.	NA	WT/R98W	Classical WD	21/05/1925
III.5	Neg.	Neg.	NA	WT/WT	Healthy	14/08/1922
III.6	NA	Pos.	NA	WT/R98W	Healthy	01/04/1935
IV.1 (P4)	Neg.	Neg.	NA	WT/R98W	Althralgia WD	14/04/1947
IV.2	Neg.	Neg.	NA	WT/WT	Healthy	20/07/1951
IV.3 (P2)	Pos.	Pos.	NA	WT/R98W	Classical WD	30/08/1941
IV.4	Pos.	Pos.	NA	WT/R98W	Healthy	23/07/1955
IV.5	Neg.	Neg.	NA	WT/R98W	Healthy	06/11/1951
IV.6 (P1)	Neg.	Neg.	Pos.	WT/R98W	Althralgia WD	17/02/1948
IV.7	Neg.	Neg.	NA	WT/WT	Healthy	17/02/1948
IV.8	Neg.	Neg.	NA	WT/WT	Healthy	09/04/1961
IV.9	NA	NA	NA	WT/R98W	Healthy	26/04/1958
V.1	Neg.	Neg.	NA	WT/WT	Healthy	13/05/1974
V.2	Neg.	Neg.	NA	WT/WT	Healthy	07/05/1978
V.3	Pos.	Neg.	NA	WT/R98W	Healthy	11/09/1965
V.4	Pos.	Pos.	NA	WT/R98W	Healthy	14/07/1962
V.5	NA	NA	NA	WT/WT	Healthy	09/08/1969
V.6	NA	NA	NA	E?	Healthy	NA
V.7	NA	NA	NA	WT/WT	Healthy	
V.8	NA	NA	NA	WT/WT	Healthy	31/08/1994
V.9	NA	NA	NA	E?	Healthy	NA
V.10	NA	NA	NA	E?	Healthy	NA
VI.1	Neg.	Neg.	NA	WT/WT	Healthy	17/02/2004
VI.2	Neg.	Neg.	NA	WT/WT	Healthy	21/09/2006
VI.3	NA	Neg.	NA	WT/WT	Healthy	16/05/2006
VI.4	Neg.	Neg.	NA	WT/WT	Healthy	29/03/2011
VI.5	Neg.	Neg.	NA	WT/WT	Healthy	09/08/1996
VI.6	Pos.	Neg.	NA	WT/R98W	Healthy	04/10/1993
VI.7	Neg.	Neg.	NA	WT/R98W	Healthy	24/08/2002
VI.8	NA	NA	NA	E?	Healthy	NA
VI.9	NA	NA	NA	E?	Healthy	NA

Supplementary Table 2. Non-synonymous variants within the linkage regions found in WES data from patients.

Chr	Pos	ID	Ref	Alt	Function	MAF	Gene
6	394896	NA	C	T	missense	NA	IRF4
11	1010694	rs1128413	C	T	missense	0.393	AP2A2
11	1016609	rs73403291	C	G	missense	0.088	MUC6
11	1016640	rs111704427	G	A	missense	0.193	MUC6
11	1016665	rs77438942	C	T	missense	0.449	MUC6
11	1016704	rs75826443	C	A	missense	0.316	MUC6
11	1016713	rs76406481	T	C	missense	0.325	MUC6
11	1016722	rs144616203	T	G	missense	0.093	MUC6
11	1016724	rs3208810	A	G	missense	0.361	MUC6
11	1016890	rs113508205	G	A	missense	0.199	MUC6
11	1016910	rs113559934	G	A	missense	0.362	MUC6
11	1016914	rs74632841	G	T	missense	0.106	MUC6
11	1016928	rs34053383	C	G	missense	0.475	MUC6
11	1016988	rs72311383	ATGT	A	inframe_deletion	0.073	MUC6
11	1017035	NA	A	AAT	frameshift	0.096	MUC6
11	1017069	rs80333708	G	A	missense	0.399	MUC6
11	1017183	rs34844844	G	T	missense	0.444	MUC6
11	1017220	rs56238842	T	C	missense	0.495	MUC6
11	1017231	rs35840539	A	G	missense	0.495	MUC6
11	1017240	rs62891761	G	A	missense	0.464	MUC6
11	1017294	rs200241162	A	T	missense	0.00437	MUC6
11	1017302	rs35330958	G	C	missense	0.328	MUC6
11	1017325	rs55903826	A	C	missense	0.473	MUC6
11	1017337	rs76686156	T	C	missense	0.328	MUC6
11	1017338	rs78943453	C	A	missense	0.328	MUC6
11	1017384	rs34095361	G	C	missense	0.454	MUC6
11	1017421	rs35549382	G	T	missense	0.246	MUC6
11	1017858	rs79583615	A	G	missense	0.372	MUC6
11	1017963	rs61869008	G	A	missense	0.452	MUC6
11	1017981	rs61869010	T	A	missense	0.453	MUC6
11	1017988	rs112579249	G	T	missense	0.025	MUC6
11	1018024	NA	C	G	missense	0.169	MUC6
11	1018042	rs200364398	A	G	missense	0.173	MUC6
11	1018048	rs12787400	A	G	missense	0.172	MUC6
11	1018059	rs78336072	C	T	missense	0.175	MUC6
11	1018456	rs79920422	G	A	missense	0.484	MUC6
11	1018483	rs78265558	C	G	missense	0.485	MUC6
11	1029320	rs11604757	C	T	missense	0.081	MUC6
8	2046700	rs2294066	C	T	missense	0.151	MYOM2
3	48419897	rs6442117	C	T	missense	0.59	FBXW12
3	48422235	rs6784322	T	A	missense	0.404	FBXW12
3	50332697	rs13100173	G	A	missense	0.369	HYAL3
3	50332697	rs13100173	G	A	missense	0.369	HYAL3
17	56435080	rs9652855	G	C	missense	0.097	RNF43
17	56598991	rs17741424	T	A	missense	0.086	38231
17	59489707	rs77617620	C	T	missense	0.043	C17orf82
17	59489893	rs9907379	T	C	missense	0.689	C17orf82
1	93620393	rs1060622	G	A	missense	0.586	TMED5

10	123844503	rs10887063	C	T	missense	0.179	TACC2
10	123845211	rs11200387	G	A	missense	0.15	TACC2
10	124189197	rs1045216	A	G	missense	0.679	PLEKHA1
10	124214355	rs2736911	C	T	stop_gained	0.131	ARMS2
10	124457452	rs2947594	C	T	missense	0.782	C10orf120
10	124610027	rs1891110	G	A	missense	0.528	FAM24B

Supplementary Table 3. 156 non-synonymous heterozygous coding or splice variants reported in the GnomAD and/or HGID databases.

Chr	Pos	ID	Ref	Alt	fuction	AAChange	CADD	MAF
6	393174	.	C	G	missense	p.Arg8Gly	26.8	6.71E-06
6	393175	rs139884486	G	A	missense	p.Arg8Gln	25.7	0.000189
6	393175	rs139884486	G	T	missense	p.Arg8Leu	28	4.99E-05
6	393231	rs766107516	TGGCTG	T	frameshift	p.Trp27TyrfsTer50	35	5.51E-06
6	393256	rs538907751	G	C	missense	p.Gly35Ala	24.4	4.84E-06
6	393264	rs369688140	C	T	missense	p.Pro38Ser	29.5	3.67E-05
6	393273	rs751037944	G	C	missense	p.Val41Leu	24.7	2.69E-05
6	393284	rs753781892	CGAG	C	inframe del	p.Glu46del	22.9	8.68E-06
6	393292	.	A	G	missense	p.Lys47Arg	22.8	1.90E-05
6	394822	rs754867881	CT	C	frameshift	p.Trp74GlyfsTer28	24	4.10E-06
6	394848	.	C	T	stop gained	p.Arg82Ter	40	4.07E-06
6	394849	.	G	A	missense	p.Arg82Gln	24.4	4.07E-06
6	394859	.	C	G	missense	p.Ile85Met	12.09	3.23E-05
6	394866	rs144593192	C	G	missense	p.Pro88Ala	18.71	3.61E-05
6	394867	rs202124383	C	A	missense	p.Pro88Gln	30	0.000541
6	394867	rs202124383	C	T	missense	p.Pro88Leu	33	4.06E-06
6	394902	rs767879003	G	A	missense	p.Ala100Thr	24.7	4.06E-06
6	394918	rs200303421	A	G	missense	p.Asn105Ser	13.56	5.77E-05
6	394932	rs374588785	C	A	missense	p.Leu110Met	24	1.62E-05
6	394941	rs753842732	C	T	missense	p.Arg113Trp	32	4.06E-06
6	394981	rs745876631	G	A	missense	p.Arg126Lys	22.9	8.24E-06
6	394986	rs771936972	G	A	missense	p.Val128Ile	18.17	4.27E-06
6	395004	rs748154669	A	G	missense	p.Lys134Glu	21.6	4.31E-06
6	395009	rs200504236	T	C	splice donor	c.403+2T>C	23.9	5.22E-05
6	395864	rs11557493	C	G	missense	p.Leu141Val	15.25	1.63E-05
6	395881	rs115613112	G	A	missense	p.Met146Ile	15.67	1.45E-05
6	395885	.	A	G	missense	p.Met148Val	3.441	4.08E-06
6	395886	.	T	C	missense	p.Met148Thr	8.28	3.23E-05
6	395889	rs73717071	G	A	missense	p.Ser149Asn	5.825	0.008454
6	395892	.	A	AT	frameshift	p.Tyr152LeufsTer60	27.8	4.08E-06
6	395894	.	C	T	missense	p.Pro151Ser	13.44	4.08E-06
6	395898	.	A	G	missense	p.Tyr152Cys	10.74	7.24E-06
6	395903	rs764577689	A	G	missense	p.Met154Val	0.009	1.09E-05
6	395903	rs764577689	A	T	missense	p.Met154Leu	0.09	4.08E-06
6	395906	rs776661032	A	C	missense	p.Thr155Pro	0.005	4.09E-06
6	395916	rs750505973	A	T	missense	p.Tyr158Phe	8.071	1.23E-05
6	395919	rs771434117	CT	C	frameshift	p.Ser160ArgfsTer11	21.4	4.10E-06
6	395927	rs766413794	C	G	missense	p.Pro162Ala	5.153	4.12E-06
6	397116	rs767166788	C	G	missense	p.His167Gln	9.287	4.06E-06
6	397123	.	A	G	missense	p.Met170Val	8.301	private
6	397125	.	G	A	missense	p.Met170Ile	21.3	4.06E-06
6	397127	rs755905242	T	C	missense	p.Met171Thr	14.97	2.84E-05
6	397128	.	G	A	missense	p.Met171Ile	18.47	4.06E-06
6	397129	.	C	T	missense	p.Pro172Ser	14.26	4.06E-06
6	397130	rs777399667	C	A	missense	p.Pro172Gln	22.3	4.06E-06
6	397138	.	G	A	missense	p.Asp175Asn	23.6	4.06E-06
6	397154	rs778403209	A	G	missense	p.Asp180Gly	19.46	2.03E-05
6	397155	.	C	G	missense	p.Asp180Glu	1.224	4.06E-06

6	397157	rs747437180	A	G	missense	p.Tyr181Cys	23.6	4.06E-06
6	397159	rs781586995	G	A	missense	p.Val182Ile	14.49	4.06E-06
6	397170	rs770110760	G	C	missense	p.Gln185His	22.3	8.12E-06
6	397172	.	C	T	missense	p.Pro186Leu	23.6	4.06E-06
6	397175	.	A	G	missense	p.His187Arg	16.01	3.23E-05
6	397178	.	C	T	missense	p.Pro188Leu	22.9	1.08E-05
6	397183	rs763272146	A	G	missense	p.Ile190Val	9.874	4.06E-06
6	397184	rs771094772	T	A	missense	p.Ile190Asn	21.8	4.06E-06
6	397186	rs774593906	C	T	missense	p.Pro191Ser	15.87	1.22E-05
6	397201	.	A	G	missense	p.Met196Val	0.002	7.21E-06
6	397205	rs372869810	C	T	missense	p.Thr197Met	17.83	8.12E-06
6	397205	rs372869810	C	T	missense	p.Thr197Met	17.83	8.12E-06
6	397208	rs763891187	T	C	missense	p.Phe198Ser	10.38	8.12E-06
6	397213	.	C	T	missense	p.Pro200Ser	9.286	4.06E-06
6	397216	.	C	T	missense	p.Arg201Cys	25.8	4.06E-06
6	397217	rs753427028	G	A	missense	p.Arg201His	24.2	1.22E-05
6	397219	rs143144957	G	A	missense	p.Gly202Ser	0.004	7.58E-05
6	397234	.	G	A	missense	p.Gly207Ser	20.2	4.06E-06
6	397238	rs757910134	C	A	missense	p.Pro208Gln	23.4	7.22E-05
6	398831	rs538810711	G	T	missense	p.Cys214Phe	16.56	3.61E-05
6	398863	.	C	A	missense	p.Pro225Thr	24.6	6.46E-05
6	398878	rs147454166	G	A	missense	p.Ala230Thr	18.45	1.63E-05
6	398884	rs375133421	G	A	missense	p.Gly232Arg	24.4	4.06E-06
6	398887	rs776593233	G	A	missense	p.Val233Ile	13.26	3.25E-05
6	398888	rs761579830	T	C	missense	p.Val233Ala	16.11	4.06E-06
6	398894	rs765027259	C	A	missense	p.Thr235Lys	16.75	4.07E-06
6	398914	rs772851591	G	A	missense	p.Ala242Thr	24.7	8.15E-06
6	398915	.	C	T	missense	p.Ala242Val	21.5	4.08E-06
6	398925	rs765864636	G	C	missense	p.Leu245Phe	22.7	4.10E-06
6	401425	rs758839744	C	G	missense	p.Asp249Glu	26.2	4.11E-06
6	401430	rs199834880	G	A	missense	p.Arg251Gln	23.8	8.20E-06
6	401438	.	A	G	missense	p.Ile254Val	8.678	4.08E-06
6	401444	rs148760922	C	A	missense	p.Leu256Met	25.7	4.08E-06
6	401448	.	A	T	missense	p.Tyr257Phe	16.05	4.08E-06
6	401453	.	C	T	missense	p.Arg259Trp	35	1.45E-05
6	401454	rs781276700	G	A	missense	p.Arg259Gln	27.1	4.07E-06
6	401492	rs752393433	G	A	missense	p.Glu272Lys	33	4.07E-06
6	401501	rs771669183	C	T	missense	p.Arg275Trp	32	3.23E-05
6	401502	rs139858073	G	A	missense	p.Arg275Gln	27.6	2.53E-05
6	401509	.	CCATGGA	C	indel-inframe	p.Gly279_His280del	20.3	private
6	401510	rs765634575	C	T	missense	p.His278Tyr	22	4.06E-06
6	401520	rs751008894	C	T	missense	p.Thr281Met	22.8	1.63E-05
6	401527	rs114916515	C	G	missense	p.Asp283Glu	0.003	0.000249
6	401528	rs767774669	G	A	missense	p.Ala284Thr	14.13	5.69E-05
6	401528	rs767774669	G	T	missense	p.Ala284Ser	0.642	4.06E-06
6	401529	.	C	T	missense	p.Ala284Val	21.3	6.46E-05
6	401542	.	C	G	missense	p.Asp288Glu	12.06	4.06E-06
6	401545	.	G	C	missense	p.Gln289His	23	3.23E-05
6	401571	rs140099868	A	G	missense	p.Asn298Ser	0.434	0.000148
6	401589	rs756281792	T	C	missense	p.Ile304Thr	0.256	1.44E-05
6	401621	rs780902340	G	A	missense	p.Val315Met	28.2	8.14E-06
6	401627	rs745470687	C	A	missense	p.Leu317Ile	29.4	1.63E-05
6	401637	rs775326241	C	A	missense	p.Ala320Asp	25.2	3.23E-05

6	401637	rs775326241	C	G	missense	p.Ala320Gly	17.79	4.07E-06
6	401642	.	G	A	missense	p.Asp322Asn	26.4	4.07E-06
6	401652	rs773521348	A	G	missense	p.Tyr325Cys	24.3	4.08E-06
6	401655	rs201105575	C	T	missense	p.Ala326Val	23.2	6.88E-05
6	401690	.	G	A	missense	p.Gly338Arg	24.4	4.09E-06
6	401700	rs200311468	C	T	missense	p.Ala341Val	25.8	0.000342
6	401708	rs756088477	A	C	missense	p.Asn344His	16.94	4.10E-06
6	401711	rs753680565	G	A	missense	p.Asp345Asn	26.4	2.18E-05
6	401714	.	C	G	missense	p.Arg346Gly	24.8	4.10E-06
6	401714	.	C	T	missense	p.Arg346Trp	27	4.10E-06
6	401715	rs199596593	G	A	missense	p.Arg346Gln	25.9	2.91E-05
6	401720	.	A	C	missense	p.Asn348His	25.5	4.10E-06
6	401737	rs199919569	C	G	missense	p.Asp353Glu	8.794	4.10E-06
6	401748	rs555752097	A	G	missense	p.Lys357Arg	28	4.10E-06
6	401763	rs779841481	A	C	missense	p.Gln362Pro	22.4	1.09E-05
6	401775	.	C	T	missense	p.Ser366Leu	22.2	3.23E-05
6	405027	rs568315642	C	T	missense	p.Ala370Val	15.04	0.000451
6	405027	rs568315642	C	A	missense	p.Ala370Glu	9.242	3.23E-05
6	405037	rs775948276	C	G	missense	p.His373Gln	13.91	4.06E-06
6	405041	.	G	A	missense	p.Gly375Ser	22.3	3.23E-05
6	405044	rs768893830	C	T	missense	p.Arg376Cys	33	2.03E-05
6	405045	rs377483798	G	A	missense	p.Arg376His	28.6	4.88E-05
6	405045	rs377483798	G	C	missense	p.Arg376Pro	28.3	7.22E-06
6	405045	rs377483798	G	T	missense	p.Arg376Leu	27.5	4.06E-06
6	405051	.	T	A	missense	p.Leu378Gln	23.8	4.06E-06
6	405053	.	C	A	missense	p.Pro379Thr	29.49	4.06E-06
6	405063	.	A	G	missense	p.Gln382Arg	21.3	3.23E-05
6	405064	rs750322004	G	C	missense	p.Gln382His	26	4.06E-06
6	405069	rs142143231	C	T	missense	p.Thr384Ile	19.71	4.06E-06
6	405069	rs142143231	C	T	missense	p.Thr384Ile	19.71	8.12E-06
6	405088	rs751335149	G	C	missense	p.Glu390Asp	27.8	1.44E-05
6	405098	rs201428294	C	A	missense	p.Pro394Thr	25	4.06E-06
6	405098	rs201428294	C	G	missense	p.Pro394Ala	17.89	2.53E-05
6	405130	rs141640145	C	A	missense	p.His404Gln	7.944	4.07E-06
6	406770	.	T	C	missense	p.Leu406Pro	5.648	6.46E-05
6	406772	.	A	T	missense	p.Arg407Trp	2.517	1.14E-05
6	407474	rs199763142	G	A	missense	p.Arg411Lys	23.2	9.29E-05
6	407514	rs760504688	C	A	missense	p.Phe424Leu	22.9	8.14E-06
6	407515	rs763733876	C	G	missense	p.Leu425Val	22.2	4.07E-06
6	407522	.	G	C	missense	p.Gly427Ala	14.31	4.07E-06
6	407527	.	G	A	missense	p.Asp429Asn	28.5	7.23E-06
6	407528	.	A	G	missense	p.Asp429Gly	25.6	3.23E-05
6	407542	rs756736434	A	T	missense	p.Ile434Phe	1.929	9.69E-05
6	407543	rs766230745	TCAG	T	inframe del	p.Ser435del	12.91	7.23E-06
6	407560	.	T	A	missense	p.Tyr440Asn	29.1	4.09E-06
6	407561	.	A	T	missense	p.Tyr440Phe	16.9	4.10E-06
6	407564	rs752069005	A	T	missense	p.His441Leu	22.8	1.23E-05
6	407566	.	A	G	missense	p.Arg442Gly	26.9	private
6	407572	rs559734928	A	G	missense	p.Ile444Val	9.725	1.25E-05
6	407575	rs748516736	C	T	missense	p.Arg445Cys	35	2.10E-05
6	407576	rs756602021	G	A	missense	p.Arg445His	23.8	2.11E-05
6	407576	rs756602021	G	T	missense	p.Arg445Leu	23.8	4.23E-06
6	407578	.	C	T	missense	p.His446Tyr	29.2	4.22E-06

6	407582	rs749474191	C	T	missense	p.Ser447Phe	33	4.25E-06
6	407585	.	C	T	missense	p.Ser448Phe	32	4.27E-06

Supplementary Table 4A. Differentially expressed genes based on transcriptomic data for PBMCs exposed to BCG.

Probe_Id	Genes	C1	C2	HET1	HET2	HET3	P1	P2	P3	WT1	WT2	WT3	WT4
16650325	.	-2.61	-1.86	-2.16	-5.51	-0.94	1.60	6.59	-1.61	4.58	0.60	-2.13	2.61
16651241	.	2.88	-0.97	0.08	-0.38	1.39	3.74	-0.44	1.31	1.60	-6.16	7.29	-0.76
16651491	.	1.56	-3.00	-3.00	-1.94	1.09	-0.60	-2.44	0.83	0.67	4.00	3.20	-2.72
16651635	.	0.74	2.07	0.04	1.45	-1.27	3.35	-0.98	0.89	2.74	-0.83	-5.70	4.04
16651639	.	-0.45	2.61	1.70	1.03	-2.12	0.40	-4.84	-1.50	2.45	-0.31	1.12	0.90
16651905	.	-3.50	-1.07	-4.78	-1.60	1.67	-4.36	1.52	1.67	0.27	-3.99	1.62	-1.43
16653785	.	0.83	-1.90	0.48	0.03	-1.97	1.18	-2.97	-1.19	2.13	-1.53	-3.52	0.06
16653831	.	-1.06	-2.19	-2.03	0.29	0.73	-0.03	-2.33	0.28	1.14	-2.07	0.12	-0.84
16654663	.	0.32	1.14	2.99	0.02	2.77	-2.81	-3.26	2.62	4.84	3.31	1.28	-1.65
16655101	.	-1.07	1.64	-3.61	-1.01	0.78	0.84	0.93	1.71	3.05	-4.28	3.95	2.92
16655337	.	0.33	1.15	-2.49	-1.06	-1.07	-2.77	-1.88	-1.16	-0.96	-2.42	1.33	0.99
16655653	.	-0.07	2.21	-2.27	2.06	-1.11	-0.79	0.34	-2.70	-6.89	0.23	4.02	-3.81
16656923	.	-0.72	-1.34	-0.12	-0.61	-0.52	-1.09	-1.91	0.45	-1.43	-1.42	0.60	-0.77
16657193	.	0.44	1.84	4.66	-0.77	3.19	-3.03	-1.02	4.64	2.86	-3.32	1.21	-2.33
16658579	.	-0.10	-0.98	-0.58	-0.25	-0.17	-1.27	0.09	-1.02	1.33	-0.13	-1.32	-0.62
16658936	.	-0.19	-0.85	0.13	-0.20	0.28	0.46	0.62	-0.18	-0.63	0.82	-1.49	2.54
16661646	RNU11	1.62	0.80	-1.36	1.68	0.28	-1.38	-0.66	1.54	2.83	1.36	0.18	0.11
16661924	.	-0.31	-0.77	-1.03	0.91	1.46	0.76	-0.78	-0.14	0.91	0.90	-2.94	-0.11
16663808	.	0.04	0.36	0.68	-0.15	1.33	-0.57	0.69	0.70	1.82	1.23	-5.99	-0.62
16666237	.	1.28	0.63	0.25	0.09	-0.67	0.23	-0.32	0.10	0.72	-0.84	1.47	-0.41
16666940	.	3.05	3.05	2.60	2.21	2.76	0.29	1.86	0.23	4.04	2.39	2.46	1.43
16668702	C1orf162	-2.44	-2.46	-1.68	-1.86	-2.97	-1.49	-0.41	-1.62	-3.17	-2.20	-2.33	-2.11
16669011	.	2.10	-2.98	2.23	-0.63	-1.05	-0.11	1.23	1.24	3.99	-4.35	2.46	1.80
16669708	NOTCH2NL	-0.92	-0.80	0.03	-0.96	-0.93	1.32	-1.31	-0.19	-1.32	-1.51	-1.28	-1.22
16670383	HIST2H2AA4	1.00	1.10	0.69	0.79	0.78	0.95	0.96	0.80	1.55	1.63	-0.44	1.24
16670673	.	-1.56	-1.05	-0.62	-0.81	-1.01	-1.27	-0.22	-0.80	-0.11	0.19	-2.67	1.80
16671139	S100A9	0.73	0.33	-0.17	0.99	0.03	1.04	-1.02	2.02	-0.69	0.67	-1.60	1.01
16672478	SLAMF8	1.04	1.06	0.58	0.93	0.59	1.02	0.35	0.85	1.47	1.81	-2.69	0.74
16672654	SLAMF7	2.89	2.57	1.82	1.89	2.24	0.76	0.84	1.29	3.00	2.01	0.24	3.02
16676150	BTG2	1.02	0.30	0.40	0.52	0.55	1.06	0.67	1.10	1.18	1.23	-1.67	2.57
16676988	HSD11B1	3.72	4.09	2.59	4.28	2.76	0.73	-1.60	1.67	3.97	4.48	1.23	1.52
16678304	.	0.71	-0.07	-0.87	0.26	1.00	-0.27	-0.23	1.72	1.56	1.52	-3.25	1.16
16678314	.	0.69	-0.29	-0.54	0.02	0.28	0.07	0.29	1.49	0.89	1.58	-8.45	1.95
16678335	.	1.84	-0.04	1.22	0.16	0.47	1.88	1.35	-0.23	2.95	1.20	-4.31	3.26
16678337	.	1.90	0.66	0.98	-0.12	1.46	4.27	-0.02	0.04	1.01	1.15	-5.46	1.11
16678342	.	1.52	-0.02	0.71	-0.68	1.16	1.31	3.10	-0.44	1.67	0.14	-3.58	1.07
16678345	.	1.12	-0.22	0.31	-0.45	0.43	1.36	1.87	-0.90	0.81	0.10	-1.01	0.62
16683445	FUCA1	-3.38	-2.63	-3.07	-3.18	-2.96	-0.89	-0.30	-2.14	-3.51	-3.78	-5.71	-2.34
16685146	.	0.71	0.84	-0.07	0.29	-0.20	-1.17	1.44	-0.03	1.91	0.19	-1.96	0.16
16685148	.	0.21	0.86	0.10	0.06	0.63	-0.79	2.78	0.04	1.57	0.78	-4.19	0.76
16685489	MTF1	1.11	1.15	1.44	1.63	2.19	2.71	-0.76	1.32	1.98	2.61	-0.95	1.90
16689332	GBP1	3.67	3.86	4.26	2.27	3.91	0.61	3.50	-1.59	3.54	3.40	2.50	2.10
16689354	GBP2	1.21	1.83	1.71	0.99	1.67	-0.45	2.86	-0.32	1.88	0.99	1.52	1.80
16689384	GBP4	3.91	3.26	3.70	3.44	4.42	-0.60	3.90	0.50	6.82	2.91	-0.69	4.60
16689400	GBP5	4.01	4.09	3.51	2.99	4.48	1.46	3.56	0.11	4.57	4.02	3.49	3.73
16692553	.	-1.32	-0.83	1.31	-0.01	-1.09	-0.68	-0.72	0.45	2.54	-0.71	1.29	-0.64
16693406	.	0.77	0.22	-0.07	0.80	0.06	0.83	-1.19	1.79	-1.05	0.67	-0.73	0.90
16693522	.	0.34	0.55	0.66	0.82	1.78	-0.10	0.77	-0.07	0.94	1.09	0.74	-1.86
16693523	.	0.33	0.37	0.10	0.57	1.10	-0.70	-0.39	0.57	1.08	0.86	-0.99	-1.50
16693525	.	0.85	-0.11	0.72	0.47	1.73	-1.34	0.94	2.06	1.30	0.96	-1.81	-1.07
16693528	.	0.84	0.15	0.65	0.33	1.09	-0.17	0.67	2.32	1.00	1.10	-1.89	-0.71
16693530	.	0.08	0.65	0.81	1.50	0.97	-0.47	-1.60	1.91	2.65	1.75	-1.85	1.83
16693531	.	-0.29	0.81	0.59	2.06	1.09	-0.60	-0.61	1.43	2.72	1.89	-5.71	1.70
16693532	.	-0.15	0.82	0.49	1.16	0.73	-0.15	-1.18	1.60	1.70	1.31	-2.39	1.67
16695572	PFDN2	0.76	0.93	0.84	0.20	0.93	-0.09	0.26	0.00	3.08	-0.08	-2.23	-1.01
16697095	NCF2	0.61	0.47	0.59	1.09	0.59	1.09	0.12	1.33	0.90	1.44	-1.17	1.52
16697370	PTGS2	4.57	4.84	5.44	4.70	5.77	1.57	1.21	6.22	4.96	5.30	0.50	1.88
16698185	CHI3L1	2.57	3.31	1.38	2.46	3.15	2.21	0.87	2.22	3.14	3.14	-1.62	1.91

16699512	.	2.17	-1.92	-2.10	-0.96	-0.63	-2.36	1.02	-1.81	-0.42	-1.63	1.32	-4.76
16702836	MRC1	-1.10	-0.82	1.09	1.14	-0.06	1.65	-0.47	-0.17	-0.11	-0.16	-3.78	1.32
16702881	MRC1	-1.04	-0.84	1.13	1.18	-0.19	1.75	-0.52	-0.09	-0.08	-0.29	-2.96	1.26
16706413	.	2.07	-1.38	-1.94	-0.66	-1.37	-0.04	1.28	-1.09	2.44	-0.79	-1.55	-0.23
16711456	.	0.10	0.69	0.74	0.29	1.24	1.67	-0.92	-0.44	1.12	1.91	-3.11	1.97
16711458	.	-0.88	0.17	-0.78	-0.65	-0.13	0.69	0.46	-0.42	1.13	0.88	-4.12	-0.88
16713318	.	2.54	1.98	2.33	2.98	2.34	4.08	0.78	3.46	2.09	4.52	3.78	6.74
16713446	.	1.48	-0.51	0.52	-0.03	-2.41	-2.46	-0.24	-0.58	3.99	-2.24	3.02	-0.31
16715241	PSAP	-1.24	-0.98	-1.29	-1.00	-0.84	-0.48	-0.21	-0.73	-0.90	-1.01	-1.92	-0.82
16716341	ANKRD22	5.07	4.54	4.04	3.05	3.95	-0.40	0.63	2.07	5.72	5.54	0.74	1.13
16716590	MYOF	1.44	1.90	1.15	1.52	0.88	1.07	0.32	0.27	1.53	1.35	-2.15	0.43
16717520	SNORA12	-0.58	-1.25	-1.28	-0.76	0.66	0.28	-3.50	0.61	-1.50	-1.06	-4.75	1.49
16718374	.	1.30	-0.94	-0.47	0.63	-0.40	1.63	0.43	-0.37	1.21	-0.13	0.26	1.99
16721670	.	-0.59	-0.53	-0.57	-0.50	-0.34	0.92	-2.77	1.16	0.61	0.04	-6.08	0.72
16721674	.	-1.16	-0.02	-0.35	0.06	-0.07	-0.92	-1.09	0.47	-0.02	-2.10	-1.85	-1.18
16721682	.	-1.12	-0.67	-0.48	-1.06	-0.93	0.65	-0.61	-0.87	1.48	-0.71	-0.91	0.78
16727214	.	-1.06	-1.05	-0.29	0.18	-2.43	2.54	1.53	-1.02	0.06	1.76	-4.35	-1.31
16727216	.	-1.49	-0.13	0.56	-0.41	0.07	-0.47	-0.88	0.35	-1.28	0.91	-0.39	-0.83
16730522	BIRC3	0.93	0.73	0.94	1.16	0.98	1.64	-0.63	1.13	1.58	1.60	-0.24	0.44
16733435	APLP2	-1.02	-0.91	-0.46	-0.16	-0.44	0.14	-0.46	0.12	-0.74	-0.67	-1.23	0.33
16734313	CTSD	-1.39	-1.72	-1.52	-1.09	-0.94	-1.19	-0.53	-0.56	-1.19	-0.94	-4.78	-1.10
16735139	.	-0.90	-0.52	0.54	0.52	-2.22	0.29	3.03	-0.54	-1.17	-0.31	-1.78	1.07
16735143	.	-1.17	-1.01	1.04	0.00	-0.55	-0.70	-1.88	-0.11	0.51	-0.70	-0.96	0.71
16735144	.	-1.47	-1.05	0.61	1.09	-0.39	-1.84	-0.09	-0.13	0.72	-0.15	-5.65	0.73
16735145	.	-1.28	-0.69	0.45	1.32	-0.50	-2.52	-0.75	-0.04	0.07	-0.33	-2.39	2.19
16735802	.	-0.81	0.45	0.42	-0.24	0.73	-0.78	-0.22	-0.34	1.03	0.06	-4.20	-0.61
16735808	.	-0.10	-0.36	0.40	0.09	-1.48	-1.29	-1.84	-0.26	0.69	-1.51	-0.77	-1.94
16735812	.	-0.13	-0.60	0.21	-0.78	-0.28	0.18	0.29	0.76	0.59	-1.18	-5.61	-0.35
16735819	.	0.03	-0.69	0.48	0.23	-0.22	1.43	-1.40	0.60	1.13	1.22	-4.08	0.90
16735835	.	-2.67	-2.88	1.54	0.65	-0.97	4.94	2.07	3.03	-4.09	-6.54	-4.31	3.55
16737102	.	1.35	0.15	0.58	2.40	3.53	0.53	-0.47	0.01	1.29	2.14	1.93	0.79
16742550	.	-0.78	-0.04	-0.46	-0.17	-1.72	2.28	-4.89	-0.54	-2.18	-1.63	-5.07	1.93
16744694	.	-2.11	-0.35	-0.85	1.18	-2.86	1.83	0.72	-1.74	2.04	2.43	-2.12	1.89
16744696	.	-0.49	0.38	-0.02	0.06	-1.99	1.04	-0.05	-1.82	0.83	1.15	-2.99	2.60
16752009	.	-1.40	0.17	0.39	1.25	-0.10	-1.01	-0.93	1.11	-1.87	-0.18	-1.23	1.22
16752018	.	-0.58	-0.62	-0.12	-0.34	0.25	-1.69	0.31	-0.97	-0.82	-0.60	-0.45	1.88
16752645	IL23A	4.26	3.56	1.83	2.24	4.97	0.37	-0.26	1.58	3.26	4.32	1.28	0.79
16754373	GLIPR1	-1.20	-0.85	-0.14	-0.45	-0.94	0.37	-0.93	-0.01	-1.24	-0.72	-2.91	0.62
16754394	.	1.13	-0.23	1.44	1.52	2.06	1.26	0.32	2.24	1.28	3.19	-3.21	1.51
16756078	HSP90B1	-0.94	-0.14	-0.52	-0.44	-0.16	1.10	-0.17	0.14	-0.72	-0.64	-0.78	-0.13
16758622	.	-0.62	-0.20	0.21	-0.32	-0.80	0.41	0.50	-0.72	1.18	-1.58	-1.60	-0.49
16760792	CD163	-5.50	-4.41	-4.06	-2.85	-5.72	-0.99	-3.08	-1.58	-4.17	-2.46	-3.29	-2.00
16761012	A2M	-1.72	-1.72	-0.53	-0.84	-0.44	-1.03	0.99	-1.96	-1.68	-1.61	-3.50	-1.05
16764077	.	-1.38	-0.90	-0.82	0.29	-0.32	0.19	0.84	0.80	1.70	-1.21	-8.96	3.29
16767247	IFNG	7.44	5.86	2.74	0.27	3.57	-0.12	-0.36	-0.91	5.18	5.28	0.24	0.36
16769735	.	0.39	-0.26	-0.57	0.99	-0.80	-1.79	-0.10	-0.61	0.86	-1.18	-3.08	-1.11
16769746	.	-2.60	-0.63	-0.62	0.03	0.34	0.04	1.23	-0.33	-0.06	0.43	-1.33	-0.97
16769749	.	-0.88	-0.57	-0.72	0.96	0.32	0.31	-1.17	1.27	1.75	0.86	-0.73	-0.44
16769756	.	1.51	-2.17	0.41	2.70	0.16	-0.01	-1.72	-0.46	7.07	2.91	-0.36	2.33
16770534	.	-3.36	2.22	-1.62	-0.71	-4.43	-5.00	-3.78	3.41	-4.15	-3.05	5.55	3.28
16771356	.	-0.84	-1.24	-1.53	-0.73	0.73	-1.15	-0.12	-0.63	-1.54	-0.91	-2.00	-0.47
16771482	.	-0.87	-0.10	0.16	0.53	0.78	-0.27	0.30	-0.40	-2.95	1.27	-6.73	-1.86
16771493	.	0.03	-0.07	-2.30	-0.12	-0.76	-0.41	-0.28	1.31	1.46	-0.70	-2.81	2.32
16771496	.	-1.05	1.23	0.28	0.13	-1.36	-2.05	-1.99	2.23	-2.36	-1.18	-4.33	3.24
16771497	.	-1.23	1.15	0.42	1.56	-1.86	-0.89	-5.44	1.46	-0.57	-0.23	-5.82	3.50
16771511	.	-1.28	1.92	-1.08	1.23	0.50	2.59	-0.30	0.00	-2.84	-0.47	-1.81	-2.02
16771512	.	-1.45	1.50	-1.81	1.54	0.55	2.38	-0.40	0.44	-2.76	-0.79	-3.52	-2.99
16771518	.	-1.73	1.00	1.98	-1.28	1.01	-1.89	-0.88	-0.79	-1.98	4.73	-3.33	3.30
16779839	KCTD12	-1.35	-1.19	-1.33	-1.01	-2.22	-1.25	-0.99	-0.98	-1.85	-0.64	-2.93	-0.80
16781591	RNASE6	-4.58	-5.12	-3.02	-1.83	-2.81	-1.39	-0.97	-1.73	-3.32	-2.13	-4.38	-0.53
16788390	.	-0.52	0.00	-0.70	-0.22	-0.65	-1.43	-0.39	-0.79	1.80	-0.59	-3.78	-0.77
16788417	.	2.72	2.68	2.68	2.69	2.13	1.00	3.01	0.45	3.11	1.60	1.85	1.51
16790246	.	-0.89	-1.37	0.19	0.57	-1.16	2.45	-4.59	0.41	4.43	-2.25	-1.79	0.73

16790260	.	1.22	-0.24	0.89	-0.51	1.85	0.45	-1.52	0.78	1.46	2.86	-5.26	-1.37
16791991	NFKBIA	1.41	0.82	0.78	0.64	0.85	1.31	0.11	1.26	0.91	1.02	-0.64	0.39
16794260	.	-0.24	-1.80	-0.40	0.11	-0.41	-0.09	0.31	0.49	3.43	-0.66	-0.61	0.82
16795366	SNORA79	-1.22	-0.87	-0.83	-0.40	-0.77	-0.50	-0.36	-0.21	0.13	-0.84	-0.78	-0.82
16796060	LGMN	-3.03	-2.75	-2.61	-2.55	-1.95	-1.68	0.22	-2.32	-3.04	-2.27	-4.58	-2.02
16796694	WARS	2.93	2.72	2.75	1.83	3.09	1.41	1.84	0.30	3.07	2.81	-0.29	2.83
16800630	C15orf48	2.26	3.13	3.12	2.42	2.21	1.88	0.42	3.50	4.28	3.08	2.07	2.28
16800680	SQRDL	0.94	0.16	1.22	1.19	0.99	0.66	0.35	0.90	1.81	0.95	-1.45	1.35
16807320	.	-1.11	-0.60	0.20	-0.58	-0.74	-0.44	1.34	-0.37	-0.75	-0.62	-1.32	0.82
16811437	HEXA	-1.68	-1.70	-1.17	-1.59	-0.40	-2.94	0.02	-1.18	-2.29	-0.55	-3.58	-1.45
16815137	ATP6V0C	-0.81	-0.97	-0.51	-0.51	-0.08	-0.87	-1.06	-0.84	-0.40	0.39	-2.18	-0.66
16818272	ITGAX	-0.01	0.48	0.63	0.37	0.81	0.93	0.80	0.72	2.02	1.53	-3.18	1.15
16818431	ZNF267	1.05	1.01	0.72	1.07	1.07	0.00	0.80	0.74	1.44	1.15	0.49	0.61
16819207	MT2A	1.58	2.09	1.71	2.01	1.32	3.12	0.05	1.57	3.25	1.48	2.05	2.95
16819244	MT1CP	2.07	2.39	2.48	2.02	1.79	1.53	1.43	2.51	2.62	2.52	0.90	2.08
16819252	MT1F	2.46	2.17	4.01	1.89	2.48	4.99	-0.07	2.76	2.00	2.62	2.97	4.91
16819257	MT1H	6.67	5.00	5.71	3.24	2.03	2.15	-6.95	4.67	7.33	3.45	4.08	2.10
16819264	MT1X	2.94	2.99	0.94	1.00	1.18	3.09	-0.12	3.91	1.63	2.30	-0.28	1.36
16819478	CCL22	1.18	0.96	2.42	2.07	3.09	3.98	-0.38	5.66	3.12	1.12	-0.46	3.43
16823098	.	-0.21	1.56	0.67	0.64	0.29	-0.72	0.54	-0.43	1.07	0.57	-2.46	1.19
16824132	NTAN1	-1.75	-2.44	-1.47	-1.24	-2.29	-0.42	-0.82	-1.15	-1.82	-2.15	-3.75	-0.66
16826738	MT1G	6.55	5.16	4.45	5.61	3.25	4.84	-2.65	3.06	5.43	6.42	4.54	6.31
16828515	.	0.19	0.74	0.51	0.86	0.31	0.34	0.00	-0.32	1.18	-0.33	1.11	-0.60
16828522	.	0.42	0.72	-1.27	0.78	-0.13	2.66	0.64	-1.58	-1.68	1.46	-3.00	4.21
16828527	.	1.38	0.44	-1.43	0.17	0.98	-1.53	-0.50	0.60	2.43	1.73	-6.29	-1.22
16828528	.	0.80	0.63	-1.13	0.56	0.07	-1.00	0.48	-0.19	0.27	0.82	-0.15	0.66
16828529	.	1.69	-1.00	-2.21	2.92	-2.13	-2.51	1.69	-0.60	3.89	3.16	-2.54	0.38
16828531	.	0.92	0.52	-0.90	0.52	0.58	-1.47	0.19	-0.26	0.61	0.79	-1.17	0.39
16828826	COTL1	-1.31	-1.18	-1.11	-0.21	-1.31	0.04	-1.04	-0.29	-1.18	0.54	-3.45	-1.47
16830577	CD68	-0.66	-0.71	-0.65	-0.36	-0.35	-0.31	-0.02	-0.56	-0.76	-0.29	-2.82	-0.20
16833224	CCL8	5.27	5.85	4.58	4.54	3.40	-0.66	0.42	0.79	5.96	6.21	4.77	2.00
16833420	CCL4	2.59	2.29	2.84	2.49	1.75	2.64	1.11	2.22	2.59	2.42	2.44	3.50
16833426	CCL4L2	3.14	2.55	3.13	4.04	3.69	3.22	-0.42	3.02	3.29	3.32	0.83	3.73
16833698	PSMB3	0.76	0.87	0.60	0.59	-0.02	-0.39	0.80	0.76	1.63	1.67	-2.38	0.29
16834764	.	-0.72	-1.67	-0.15	-1.01	-0.52	-2.37	0.96	-1.72	-1.11	-0.16	-3.10	-1.59
16834766	GRN	-1.99	-1.58	-2.11	-1.79	-1.76	-1.39	-0.67	-1.70	-2.41	-2.13	-3.20	-1.25
16835618	.	-0.56	1.47	-0.80	-1.66	0.39	-1.46	0.45	0.23	-0.33	2.43	-4.17	0.74
16835641	.	-0.29	-0.71	1.05	-0.09	0.20	2.99	1.93	-2.54	3.94	0.73	-6.60	3.42
16836624	MIR21	-1.71	1.06	0.02	-0.99	0.47	-1.10	-0.69	-0.18	2.60	0.90	-2.35	-2.07
16838330	SYNGR2	0.02	-0.42	-1.43	-0.48	-0.93	-0.59	-1.19	-0.10	1.18	-0.77	-4.50	-1.99
16839481	.	-1.87	0.14	-1.11	-0.55	1.14	0.03	2.80	-0.37	0.59	-0.13	-2.80	-1.29
16839487	.	0.74	-1.25	-0.11	-1.62	0.44	-0.66	-1.08	0.44	4.55	0.51	-0.94	0.09
16839489	.	-4.43	-1.18	-0.73	-1.86	0.97	2.33	-2.40	-0.09	-1.29	5.51	-5.76	3.90
16839494	.	0.91	-0.02	-0.43	0.25	-0.05	1.36	1.40	0.27	-2.52	0.40	-2.65	2.14
16839497	.	-1.39	-0.12	-0.83	-0.96	0.07	0.44	-0.80	-0.71	0.06	-0.65	-7.93	1.12
16839502	.	-1.06	-1.32	0.42	-0.03	0.17	-1.91	0.85	-1.09	0.27	-0.52	-6.59	-0.81
16839515	.	-0.81	-0.84	0.22	-0.11	-1.10	-1.55	-2.14	1.17	3.83	0.92	-7.87	-0.16
16839516	.	-1.35	-1.38	0.65	-0.82	-0.81	-0.95	-0.20	-0.53	7.35	1.37	-6.19	1.23
16840113	CXCL16	1.57	0.53	0.44	0.86	1.07	0.69	0.69	1.50	2.55	2.24	-1.26	2.49
16840588	.	-1.00	-0.52	-0.02	-0.65	0.13	1.19	-0.59	-1.60	0.82	0.26	-1.85	-1.28
16840591	.	-0.62	-0.64	0.26	-0.19	-0.03	-0.98	-1.05	-0.22	0.14	0.85	-3.60	1.45
16843309	CCL1	5.00	5.02	6.67	6.25	5.21	5.60	-0.28	6.81	4.80	4.97	1.26	3.50
16843602	CCL3L3	3.45	3.65	3.83	4.06	4.12	3.48	0.84	3.85	4.08	4.17	0.75	3.65
16844381	CCR7	1.06	0.74	0.55	0.80	1.13	0.62	0.41	1.31	1.05	1.31	0.12	1.00
16847821	.	-0.93	-0.43	0.22	-0.65	-1.48	1.20	-2.45	-0.39	1.23	-3.24	-4.06	-3.03
16847826	.	0.37	0.13	-0.15	-0.01	-0.44	0.15	-1.23	0.32	2.02	0.66	-4.09	0.96
16847832	.	0.72	0.46	0.74	0.31	0.18	2.88	0.91	0.22	1.14	0.41	-1.24	1.07
16848888	H3F3B	1.21	0.35	0.64	0.99	0.06	-0.72	0.32	2.09	1.38	0.10	-0.70	0.66
16850286	MIR4525	0.41	-0.36	0.55	0.50	-0.25	-0.40	-3.29	0.29	-0.61	-1.56	1.52	-1.17
16852871	SERPINB2	3.96	3.90	4.92	4.89	3.09	6.60	2.15	5.11	4.87	2.65	3.24	6.17
16855166	.	-1.83	1.32	0.06	0.47	-0.40	-1.28	-0.28	-1.68	-1.65	-1.53	-2.64	-2.47
16855493	.	-1.12	-0.58	0.68	0.39	-0.09	-0.01	0.01	-0.94	0.76	1.04	-0.63	-0.75
16855497	.	-0.02	-1.35	-0.67	0.33	-0.11	0.59	-0.92	-0.58	-1.64	-1.62	-1.34	-0.26

16855498	.	-0.58	-1.83	-0.69	0.42	-0.36	1.36	-3.35	-1.14	-1.37	-1.03	-4.49	0.08
16855502	.	-1.08	-0.91	0.01	-0.31	0.08	1.05	-0.20	-0.63	-0.78	0.70	-1.69	-0.23
16855508	.	-1.46	-0.97	-1.06	0.06	0.21	0.44	-1.27	-1.63	0.02	-0.07	-2.81	-0.79
16857612	MCOLN1	-1.25	-1.01	-0.95	-0.52	0.10	-0.06	1.37	-1.28	-1.53	-0.21	-3.31	-1.06
16857916	.	1.19	0.15	-0.20	-0.41	-0.03	1.70	0.05	0.33	1.88	0.09	-2.25	2.72
16858710	JUNB	0.86	0.59	-0.04	1.14	1.37	0.01	0.01	1.41	2.47	1.33	-3.67	1.20
16858774	CALR	-0.63	-0.59	-0.40	-0.35	-0.80	-0.14	-0.02	-0.50	-0.60	0.04	-3.64	-0.14
16859763	IFI30	-1.01	-1.03	-0.92	-0.74	-0.71	-0.52	-0.08	-0.86	-0.82	-0.69	-2.12	-0.61
16859821	.	-1.42	1.63	-0.89	-1.22	-0.86	1.72	5.97	-3.49	5.13	-1.87	-3.84	0.91
16859822	.	-0.99	0.81	0.15	-0.62	-0.54	-0.02	0.98	-1.87	1.72	-0.66	-0.63	0.00
16860971	HAMP	-2.67	-2.66	-3.18	-2.99	-4.03	-3.50	-0.73	-2.68	-4.25	-3.46	-5.35	-2.35
16861380	CAPNS1	-0.04	-0.62	-0.49	-0.35	-0.68	0.65	0.91	-0.31	0.70	-0.38	-3.30	-0.62
16861384	.	0.18	-0.84	-0.86	-0.58	-0.31	1.04	0.71	-1.71	3.87	0.73	-7.15	0.26
16861390	.	-0.65	-0.71	-0.61	-0.38	-1.41	-0.65	1.65	0.15	-0.53	-1.07	-1.47	-0.47
16861392	.	-0.27	-1.05	-0.33	-0.19	-0.42	0.63	1.40	-0.35	0.87	-0.39	-6.87	1.37
16861887	ECH1	-1.33	-0.51	-0.53	0.27	-0.83	-2.34	0.32	0.09	1.62	-1.64	-3.87	-1.63
16863124	APOC1	-5.56	-6.12	-4.40	-3.08	-3.42	-3.07	-1.22	-3.63	-2.23	-3.50	-3.86	-3.96
16864756	FPR3	-1.13	-1.13	-0.54	-0.20	-1.50	0.18	0.22	-0.91	-0.76	-0.19	-3.48	0.11
16866174	UBE2CP5	2.17	-0.24	0.17	0.39	1.20	-0.22	-1.71	-1.13	-1.17	-2.28	3.15	-0.89
16866283	.	-0.03	0.68	-0.34	0.85	-0.02	1.17	0.17	-0.06	-0.09	1.01	-4.47	-0.64
16866562	.	-1.06	-0.64	-0.72	-0.17	-0.23	-0.78	-0.51	0.57	-0.94	-0.54	-1.34	0.43
16867217	.	-0.26	-0.50	-0.05	-0.04	0.30	0.59	0.82	0.84	0.75	1.04	-3.54	1.50
16869487	.	-0.63	-0.68	-0.41	0.06	-0.14	-0.03	-0.33	-0.36	0.77	-0.61	1.16	-0.75
16869684	ADGRE2	-0.85	0.47	1.28	1.71	0.81	2.20	-0.19	0.94	3.23	2.15	-4.18	2.27
16871546	TYROBP	-0.76	-0.78	-0.62	-0.29	-0.60	-0.47	-0.14	-0.31	-0.61	0.04	-2.66	-0.12
16872452	BLVRB	-1.20	-1.58	-0.84	-1.67	-1.22	-1.97	-0.28	-1.73	-1.55	-1.23	-2.16	-1.09
16873060	PLAUR	2.57	2.12	2.33	2.43	2.37	0.92	0.73	2.55	2.77	3.00	-0.08	1.17
16874001	.	-0.70	-0.03	-0.81	-0.65	1.35	0.06	0.28	0.52	1.23	0.45	-3.27	1.29
16880942	PLEK	1.49	0.95	0.49	0.91	0.94	0.49	1.28	0.24	1.14	1.29	-0.30	1.80
16884372	MERTK	-3.14	-4.64	-2.91	-2.54	-5.21	-1.72	-1.32	-0.56	-4.65	-1.85	-3.43	-1.80
16884629	IL1RN	1.95	1.23	2.73	2.88	3.48	2.74	-0.19	2.67	2.05	2.32	-0.31	1.57
16885625	FAR2P3	-0.15	-0.05	-1.33	-1.24	-0.13	-0.31	-1.32	0.75	0.73	-1.41	1.69	-1.05
16886174	KYNU	0.71	1.01	1.38	1.43	0.85	2.15	0.19	1.79	2.64	1.67	-2.11	2.59
16886491	TNFAIP6	5.56	5.61	4.39	4.94	5.31	2.32	-0.55	5.49	5.45	6.34	4.03	2.89
16889725	.	1.24	-3.03	0.11	-0.79	-1.23	-0.29	-4.09	-0.16	3.83	-7.85	-6.83	-4.40
16893456	.	1.52	-3.41	0.91	0.18	-1.99	-2.12	2.18	-0.55	3.90	-0.93	-4.35	1.71
16893467	.	0.33	-1.50	-0.92	-0.31	1.12	-2.45	1.01	1.62	0.76	0.63	-3.89	-2.07
16898487	.	-1.28	1.28	1.16	1.07	-3.04	-1.32	-0.45	0.28	1.21	2.11	-6.67	3.62
16900096	IGKC	0.22	0.06	2.17	0.03	1.36	-1.03	-3.73	0.79	1.65	0.59	-4.83	0.62
16900475	.	-0.67	-0.11	0.48	0.70	0.14	-2.87	1.22	0.23	-0.63	0.23	-0.75	-1.68
16900484	.	-1.49	-2.23	-0.83	-0.57	-0.84	0.73	4.71	-0.35	-1.76	0.34	0.40	0.78
16900485	.	-0.42	-0.87	-0.64	-0.14	-0.36	-0.05	0.42	0.49	1.10	0.05	0.84	1.29
16900487	.	-0.49	-1.03	0.27	-0.50	0.17	1.04	-0.93	0.02	-1.61	-0.16	-3.86	1.12
16900509	.	-0.37	0.64	0.37	0.08	1.25	-1.92	-1.79	-0.05	2.24	0.56	-1.97	-4.20
16900519	.	0.79	-0.55	-1.60	-0.61	-0.66	1.64	1.37	0.03	-1.36	0.10	-5.97	-1.07
16900520	.	0.37	-0.61	-0.63	-0.25	-0.62	-1.57	2.73	1.18	0.67	-0.12	-3.11	1.41
16900522	.	0.10	-0.18	0.12	1.16	-1.01	-4.12	1.91	0.45	1.65	-1.09	-7.03	-0.65
16900525	.	0.52	-0.93	0.08	-0.17	0.62	0.41	2.44	-0.05	4.04	2.74	-3.34	0.51
16901974	IL1A	6.43	5.59	6.27	6.65	7.12	3.86	-0.01	6.79	6.77	7.19	3.05	4.30
16901986	IL1B	4.91	4.89	4.91	6.10	6.42	5.74	-1.98	6.76	5.29	6.12	3.62	5.55
16906534	STAT1	1.03	1.34	1.33	2.07	0.84	-0.43	1.70	-0.60	1.08	1.44	0.82	1.91
16914352	CTSA	-1.58	-1.00	-0.85	-1.23	-0.85	-1.05	0.70	-0.89	-0.61	-0.27	-4.29	-1.07
16914395	MMP9	0.58	0.76	1.18	1.23	0.44	1.95	-0.09	1.88	2.17	1.14	-2.40	1.29
16917939	CST3	-1.09	-1.10	-1.45	-0.77	-1.25	-1.12	-0.70	-1.36	-1.87	-0.10	-2.37	0.12
16919242	MAFB	-1.32	-1.37	-0.80	-1.48	-1.76	-0.38	0.39	-1.03	-1.64	-0.55	-2.22	0.34
16920169	B4GALT5	1.86	1.20	0.79	0.16	0.94	-1.40	1.40	-0.18	1.91	1.46	-1.38	-0.26
16924145	BAGE2	-1.07	-1.31	-0.23	-0.61	-1.05	1.32	-0.45	-0.83	1.49	-1.07	-1.80	0.17
16929562	HMOX1	-2.83	-2.15	-2.02	-1.64	-1.24	-2.00	-0.19	-1.54	-0.79	-0.96	-3.22	-1.92
16930938	RNU12	2.03	-0.62	0.70	0.90	0.74	-0.45	0.30	0.33	-3.45	-1.60	1.64	1.77
16941344	ALAS1	1.47	1.74	2.21	1.03	1.51	-0.05	0.47	0.74	2.59	1.73	0.72	1.57
16948561	.	-0.96	-0.93	-0.97	-0.53	-1.04	-0.57	-1.03	-0.85	-0.14	-0.81	-1.96	-0.55
16967771	CXCL8	4.16	3.09	5.33	5.56	3.07	2.52	0.30	4.60	6.53	4.26	2.23	2.79
16967843	EREG	4.10	3.16	3.83	5.17	4.05	5.26	0.30	6.61	4.39	5.14	0.87	3.79

16970074	SNORA24	0.03	-0.61	-0.77	-1.00	-1.92	-1.54	-1.39	-1.75	-0.65	-0.61	-1.34	-0.24
16976827	CXCL5	5.53	4.82	6.47	7.57	6.14	7.01	-0.82	8.74	3.31	6.91	3.45	6.57
16976844	CXCL2	2.41	1.24	2.47	2.14	0.92	1.36	1.72	1.61	2.42	1.70	3.20	1.61
16977045	CXCL9	2.78	5.40	3.08	5.53	6.24	-2.92	3.19	-3.88	5.64	3.40	5.46	5.97
16977052	CXCL10	2.28	4.27	3.64	3.33	3.16	0.99	2.03	-3.14	2.31	2.52	2.26	4.68
16977343	.	-2.65	0.35	2.56	-0.92	1.92	1.23	-3.05	-0.46	0.45	-1.96	-2.80	4.29
16977358	.	0.72	-0.94	-2.31	-0.74	-0.30	0.44	4.61	-0.69	6.18	-0.04	-2.90	0.59
16979917	SLC7A11	3.02	2.73	3.40	3.88	2.83	3.00	0.23	4.81	5.34	3.26	-1.73	3.73
16983266	.	1.33	-1.36	0.45	-0.15	0.58	2.21	2.48	2.09	-1.03	-0.40	1.58	2.94
16984010	IL7R	0.81	-0.18	0.43	1.08	0.80	1.19	-0.78	0.74	2.50	0.59	-1.13	1.39
16986203	HEXB	-1.52	-1.55	-0.90	-0.62	-1.22	-1.12	-0.89	-0.69	-0.37	-1.41	-1.76	-1.05
16988537	.	-1.19	-5.16	-3.99	-1.31	-0.56	-1.46	0.68	-2.07	-3.81	-0.09	-1.96	-1.14
16990120	.	-0.62	0.86	-0.84	-0.05	0.05	-0.83	-1.74	-1.36	3.23	-0.95	-7.16	-1.16
16990127	.	-0.23	-0.69	0.28	-0.52	-0.63	-0.88	-1.00	-0.07	-0.62	-0.15	-2.49	-1.00
16990132	.	0.49	-0.62	0.33	0.63	-0.56	-1.72	-5.38	-0.72	-1.14	-0.80	-4.62	2.77
16990136	.	-1.45	-0.83	-0.05	0.61	-0.40	1.55	-2.15	-1.31	1.43	0.15	-0.12	-1.69
16993416	.	-0.80	-0.88	0.01	-0.13	0.10	0.04	-0.05	0.51	-1.07	0.00	-2.78	-0.24
16993420	.	-0.08	-0.87	-0.34	-0.13	-0.53	1.05	-1.37	-1.00	-0.20	-0.77	-3.60	1.19
16993421	.	-0.72	-0.85	0.14	-0.62	0.28	-0.21	0.34	-0.47	-0.78	-0.53	-2.84	0.28
16993422	.	0.62	-0.97	0.01	-0.06	0.40	-0.28	0.50	-0.90	-0.34	-0.77	-6.38	-0.26
16993424	.	-0.62	-1.06	-0.70	0.73	0.34	0.33	0.13	-0.09	1.05	-0.28	-3.87	-0.30
16993430	.	-0.98	-1.12	-0.09	-0.30	0.13	0.47	0.44	-1.04	-0.03	-0.44	-4.70	-0.66
16995601	FYB	-0.59	-0.36	-0.85	-1.16	-1.55	-0.77	-0.19	-0.64	-0.37	-1.06	-2.88	-1.78
16995866	FLJ32255	0.91	1.64	-0.18	0.57	0.93	0.80	-0.78	-0.39	1.54	1.95	-1.90	0.08
16996813	CD180	-3.04	-2.52	-1.83	-2.04	-2.38	-2.44	-0.74	-2.66	-3.84	-3.50	-2.91	-0.61
16996983	NAIP	-1.62	-1.48	-1.35	-1.40	-2.08	-0.23	-0.07	-0.76	-3.03	-1.58	-2.56	-0.03
16997644	.	-1.49	1.04	1.45	-1.15	-1.56	0.25	-2.12	1.36	-4.01	-1.54	0.42	-4.24
16997919	.	-2.25	-3.47	0.37	-1.60	1.84	0.55	0.36	-0.22	4.01	3.67	0.96	1.56
16999776	IRF1	1.79	2.01	2.32	2.41	2.61	0.50	2.92	0.13	2.93	2.02	0.12	0.97
17000485	HSPA9	0.59	0.40	0.62	0.51	0.71	0.45	-0.30	-0.42	0.96	0.63	-1.63	0.58
17001545	CSF1R	-1.73	-1.64	-0.81	-0.30	-1.67	0.60	-0.33	0.33	-2.00	-0.75	-4.01	0.26
17004518	LY86	-1.75	-1.67	-2.48	-2.34	-0.66	0.01	0.06	-3.66	-3.79	-1.49	-2.73	-0.60
17005001	CD83	1.81	1.80	2.27	1.75	2.25	0.43	1.06	0.79	2.60	1.73	0.92	0.89
17005569	HIST1H1E	0.62	0.39	-0.62	0.42	-0.23	1.96	0.52	1.30	0.50	1.00	-3.67	0.63
17006296	.	0.90	0.16	0.80	1.12	0.06	1.73	0.52	0.45	0.20	0.88	-5.05	-1.45
17006297	.	-0.01	-0.81	0.69	-1.17	-0.17	6.52	3.57	0.79	2.06	-0.60	-3.64	0.38
17006304	.	-0.29	1.06	-0.70	0.92	1.04	-1.59	-4.16	0.33	2.92	-2.01	-1.12	-1.86
17006307	.	-0.17	-1.63	-0.71	-0.27	0.94	-2.08	-0.91	1.43	-0.85	-0.66	-6.57	-2.57
17006319	.	-1.24	0.52	2.00	2.32	1.70	-0.45	0.05	-0.07	2.22	3.05	-3.13	2.24
17006659	TNF	4.54	4.76	3.80	3.84	6.45	2.56	-0.15	3.00	5.27	4.43	1.96	1.55
17006683	AIF1	-1.23	-0.86	-1.26	-1.00	-1.65	-0.27	-0.36	-0.24	-1.11	-0.88	-0.38	0.02
17009218	.	1.49	0.57	-0.34	0.71	1.70	0.05	-0.36	0.20	0.52	1.85	-1.45	-0.70
17011939	FAM26F	2.57	1.89	0.44	0.91	2.68	0.56	1.37	-0.69	3.80	3.38	3.16	2.10
17012946	TNFAIP3	1.49	1.06	1.69	0.68	1.92	0.92	0.06	1.54	1.77	1.33	-1.19	0.26
17016503	HIST1H3I	0.50	0.91	0.27	-0.68	0.78	0.78	3.64	0.38	3.26	2.38	-6.03	0.21
17017018	IER3	2.30	2.22	2.54	3.46	3.00	2.12	0.56	3.32	2.48	3.18	-0.49	1.99
17017178	.	-1.10	-1.07	0.39	-0.81	0.76	-1.33	-2.42	-1.97	4.01	0.44	-5.72	2.69
17017188	.	-0.82	0.19	0.10	-0.14	0.56	-0.26	-0.25	-0.66	-1.33	1.26	-6.34	-0.72
17017192	.	-1.34	-0.32	-1.02	-0.20	0.00	-1.04	0.33	-0.35	-0.87	2.03	-5.08	-0.55
17017193	.	-0.63	0.25	-0.96	0.68	0.87	-0.62	0.61	-0.02	-0.85	2.01	-2.15	-1.34
17017979	TAP1	1.67	0.98	1.06	0.93	1.49	0.84	0.79	-0.09	1.84	1.73	0.10	1.48
17019728	PLA2G7	-0.84	-0.65	-0.24	0.01	-0.80	-0.09	-0.25	-0.27	-0.69	-0.67	-0.63	0.06
17022357	.	-0.64	-0.96	-0.07	-0.62	-1.52	1.16	-3.07	-0.13	-0.02	1.49	-6.16	1.60
17022949	.	2.54	2.84	1.91	1.24	2.88	-0.98	3.10	-0.54	3.02	1.88	5.57	3.10
17026267	.	4.82	4.72	4.07	3.95	6.74	2.67	0.15	3.11	5.79	4.80	-0.04	1.84
17027144	.	1.67	0.98	1.06	0.93	1.49	0.84	0.79	-0.09	1.84	1.73	0.10	1.48
17027794	.	4.54	4.76	3.80	3.84	6.45	2.56	-0.15	3.00	5.27	4.43	1.96	1.55
17027817	.	-1.23	-0.86	-1.26	-1.00	-1.65	-0.27	-0.36	-0.24	-1.11	-0.88	-0.38	0.02
17028326	.	0.63	-0.23	0.66	0.24	-0.04	0.83	1.27	0.02	0.79	0.72	-0.64	1.17
17028909	.	2.11	2.03	2.45	3.22	2.82	1.86	0.50	3.19	2.38	2.82	-0.04	2.04
17029788	.	1.67	0.98	1.06	0.93	1.49	0.84	0.79	-0.09	1.84	1.73	0.10	1.48
17030620	.	4.54	4.76	3.80	3.84	6.45	2.56	-0.15	3.00	5.27	4.43	1.96	1.55
17030643	.	-1.19	-0.89	-1.28	-1.03	-1.66	-0.27	-0.35	-0.23	-1.07	-0.85	-0.77	0.01

17031687	.	2.11	2.03	2.45	3.22	2.82	1.86	0.50	3.19	2.38	2.82	-0.04	2.04
17032476	.	1.67	0.98	1.06	0.93	1.49	0.84	0.79	-0.09	1.84	1.73	0.10	1.48
17033337	.	4.54	4.76	3.80	3.84	6.45	2.56	-0.15	3.00	5.27	4.43	1.96	1.55
17034143	.	2.11	2.03	2.45	3.22	2.82	1.86	0.50	3.19	2.38	2.82	-0.04	2.04
17034791	.	1.67	0.98	1.06	0.93	1.49	0.84	0.79	-0.09	1.84	1.73	0.10	1.48
17034947	.	-1.38	0.89	0.19	-0.32	-0.15	-0.10	-2.54	1.74	-0.14	1.51	-4.55	2.64
17035418	.	4.54	4.76	3.80	3.84	6.45	2.56	-0.15	3.00	5.27	4.43	1.96	1.55
17035441	.	-1.11	-0.93	-1.26	-1.09	-1.66	-0.22	-0.32	-0.33	-0.93	-0.83	-0.12	-0.01
17037271	.	1.67	0.98	1.06	0.93	1.49	0.84	0.79	-0.09	1.84	1.73	0.10	1.48
17038117	.	4.54	4.76	3.80	3.84	6.45	2.56	-0.15	3.00	5.27	4.43	1.96	1.55
17038140	.	-1.23	-0.86	-1.26	-1.00	-1.65	-0.27	-0.36	-0.24	-1.11	-0.88	-0.38	0.02
17038297	.	1.08	0.75	1.13	0.66	1.36	-0.62	0.54	0.48	0.56	0.99	-1.97	0.29
17039184	.	2.23	2.03	2.48	3.48	2.99	2.06	0.54	3.19	2.43	2.98	-0.40	1.99
17039977	.	1.67	0.98	1.06	0.93	1.49	0.84	0.79	-0.09	1.84	1.73	0.10	1.48
17040712	.	4.54	4.76	3.80	3.84	6.45	2.56	-0.15	3.00	5.27	4.43	1.96	1.55
17040735	.	-1.23	-0.86	-1.26	-1.00	-1.65	-0.27	-0.36	-0.24	-1.11	-0.88	-0.38	0.02
17041752	.	2.11	2.03	2.45	3.22	2.82	1.86	0.50	3.19	2.38	2.82	-0.04	2.04
17044253	GPNMB	-4.07	-3.70	-3.21	-3.23	-2.49	-2.14	-0.57	-2.92	-3.14	-2.65	-3.73	-2.29
17044432	.	-0.81	1.21	0.54	0.20	-0.48	1.51	-0.15	-0.84	1.38	0.11	-2.06	1.57
17044438	.	-0.63	-0.06	-1.36	0.07	-1.12	-0.22	-0.10	-0.69	0.69	-0.19	-2.58	-0.59
17046911	NCF1B	0.94	1.90	1.43	0.74	0.82	1.96	1.40	0.98	1.30	2.08	2.01	1.64
17047459	SNORA14A	-0.73	-0.91	-0.25	-0.76	-0.73	0.85	-0.31	-1.48	-0.81	-0.39	-2.11	-0.85
17055786	LOC541472	6.61	4.93	4.29	3.24	6.11	2.42	1.59	5.40	5.21	5.86	0.05	2.50
17056984	INHBA	5.60	5.74	6.07	5.66	6.29	4.05	0.36	6.00	5.79	5.63	2.85	3.80
17057035	PSMA2	0.63	0.69	0.26	0.45	0.86	0.56	0.50	-0.60	0.86	0.37	-0.75	-0.12
17058719	NCF1C	1.21	2.01	0.73	0.91	1.70	3.26	2.15	0.97	1.12	2.46	-1.93	1.79
17061125	RASA4B	-4.04	2.58	-4.46	-1.88	0.13	0.62	-1.09	-1.79	-2.94	-1.95	-0.34	-4.67
17063722	CLEC5A	1.87	0.73	2.16	3.03	2.27	1.35	-1.11	4.05	3.79	2.65	-1.46	1.52
17066961	ADAMDEC1	0.74	0.92	0.83	0.29	-0.46	2.37	0.06	1.27	1.44	0.39	-0.46	2.57
17068296	IDO1	5.30	4.69	4.19	3.24	4.03	-0.06	1.89	2.21	5.93	4.59	3.28	1.32
17068317	.	6.18	5.02	6.09	3.18	6.00	0.15	0.39	3.90	7.08	5.54	8.03	3.15
17068606	.	-4.27	-1.62	-0.65	-1.19	-0.54	2.57	-1.10	0.79	0.44	-1.80	-3.72	-2.13
17068624	.	-1.21	-0.72	-0.82	-1.13	0.61	0.20	2.55	0.57	1.10	0.06	-4.87	0.41
17068633	.	-0.60	-0.23	-0.40	-0.48	-0.64	1.24	-0.50	-0.94	-0.89	-1.00	0.95	-0.15
17069063	LYN	0.54	1.02	0.90	0.88	0.10	1.82	0.49	0.82	0.63	1.46	-1.22	1.09
17074721	.	-1.11	3.51	1.57	4.42	4.13	3.00	2.93	-1.67	-1.37	2.53	1.44	3.62
17081297	.	-0.91	0.01	-1.31	-0.49	-1.28	-0.36	-1.56	-0.62	-0.24	-1.05	1.66	-0.82
17083229	.	0.91	1.21	-0.55	-0.10	0.87	-1.20	-1.52	-0.14	-1.54	-0.88	-1.11	-0.51
17083357	CD274	5.43	4.24	4.74	4.75	3.54	0.67	1.72	3.35	5.49	4.26	1.75	2.06
17097052	TXN	1.51	1.51	1.17	1.15	1.97	0.92	0.66	0.68	1.33	1.31	1.17	0.77
17097643	TNFSF15	3.28	5.43	5.58	4.88	5.79	1.42	3.83	4.40	5.20	4.06	1.18	2.18
17099707	FCN1	-2.93	-2.43	-1.74	-1.31	-1.28	-0.82	-2.06	-2.55	-2.47	-2.31	-1.49	-0.60
17100655	.	-1.23	-1.27	0.34	0.33	-1.04	0.50	0.04	-2.52	0.77	-0.28	0.64	-0.91
17101111	IL3RA	3.12	2.32	3.35	3.29	3.76	2.89	0.85	2.22	4.66	3.83	0.00	3.71
17104675	.	-0.70	-1.47	0.89	0.76	0.98	-0.55	3.83	-1.34	6.28	1.79	-4.36	0.04
17104678	.	-0.07	-0.51	-0.03	-0.31	0.40	0.19	0.75	0.53	2.44	2.27	-1.25	1.44
17104683	.	1.36	-0.76	-1.08	0.04	-1.39	0.82	-0.29	-0.27	1.51	-0.09	-2.90	0.63
17104684	.	1.71	-0.61	-0.60	-0.03	-1.04	2.04	-1.47	-0.45	1.50	0.37	-8.14	-0.21
17114697	.	0.98	0.99	-1.42	-0.74	-0.45	0.14	-0.23	-0.18	0.49	-2.01	1.67	-0.81
17115692	MPP1	-1.53	-1.85	-2.10	-1.66	-2.42	-1.02	-0.48	-1.75	-1.25	-1.56	-3.10	-1.82
17115868	IL3RA	3.10	2.58	3.35	3.27	3.82	2.68	0.86	2.21	3.92	3.91	-0.13	3.66
17115925	CD99	-1.16	-1.06	-0.84	-1.11	-1.02	-0.52	-0.75	-0.37	-1.11	0.31	-3.13	-0.78
17117453	.	0.59	0.34	0.34	0.59	0.62	0.77	-0.28	1.25	1.20	0.84	-2.82	1.93
17117680	.	-0.59	-0.66	0.09	-0.34	-0.20	-0.48	-1.58	-0.10	0.05	0.31	-3.93	-0.86
17117736	.	3.85	4.50	3.14	2.74	2.40	4.93	-0.17	4.03	5.50	4.94	2.67	3.61
17117867	.	-3.95	-3.56	-0.67	-2.38	-1.43	-2.19	0.30	-2.12	-2.59	-1.73	-3.65	-1.47
17118001	BRK1	-0.59	-0.98	-0.21	0.12	-0.43	-1.00	0.87	-0.81	1.96	-0.18	-1.42	-1.30
17118058	LOC728093	-2.00	-0.95	-5.48	-1.13	-4.84	-3.40	-0.21	-1.02	-3.97	-2.11	-0.79	0.13
17118066	LOC441081	-2.00	-0.95	-5.48	-1.13	-4.84	-3.40	-0.21	-1.02	-3.97	-2.11	-0.79	0.13
17118068	.	-1.76	-1.08	-4.34	-0.95	-4.12	-2.75	-0.34	-0.60	-3.42	-1.73	-0.43	0.16
17118104	.	-2.00	-0.95	-5.48	-1.13	-4.84	-3.40	-0.21	-1.02	-3.97	-2.11	-0.79	0.13
17118127	LOC102724994	-2.00	-0.95	-5.48	-1.13	-4.84	-3.40	-0.21	-1.02	-3.97	-2.11	-0.79	0.13
17118144	.	-2.57	-3.10	-1.73	-0.72	-3.74	-1.28	-2.30	-0.76	-2.62	-1.89	-4.96	-1.82

17118269	.	2.80	1.90	3.39	2.67	1.89	2.14	0.32	2.22	2.30	2.74	3.02	2.90
17120642	.	-1.26	-0.42	-0.78	-0.65	0.94	-0.20	-0.42	0.20	-1.31	-0.14	-1.75	1.11
17120866	.	-1.87	-0.04	0.71	-0.05	-1.37	0.14	-0.17	0.61	-1.09	-0.28	-3.73	-2.49
17121252	.	-1.01	-0.23	-0.15	-0.01	-0.11	0.02	0.09	-0.67	1.13	0.37	-2.45	0.89
17121378	.	-0.37	-1.06	0.32	-0.08	0.53	-0.74	0.59	-0.33	1.88	0.15	-3.18	-0.75
17121380	.	-0.41	-1.74	0.67	-0.08	0.61	-1.43	1.10	-0.22	1.53	0.31	-2.95	-0.80
17121504	.	-0.65	-1.52	1.20	-0.11	0.45	-2.02	0.91	-0.06	1.03	0.69	-2.50	-0.27
17121622	.	-0.80	-0.60	-1.34	-0.25	0.21	0.82	-1.00	-1.58	-1.43	-0.52	-1.00	0.08
17121624	.	-0.80	-0.60	-1.37	-0.20	0.23	0.89	-0.92	-1.56	-1.55	-0.50	-1.00	0.05
17122488	.	1.61	2.52	0.12	0.47	3.40	-0.68	0.25	0.05	5.40	2.38	-3.63	0.43
17122504	.	0.59	1.43	1.77	0.47	2.21	-0.27	-1.11	0.69	0.98	1.07	-2.01	-0.23
17122506	.	0.99	1.65	0.74	0.68	1.76	-0.04	-0.35	1.49	1.60	0.80	-0.16	1.52
17122508	.	1.01	1.63	0.88	0.74	1.61	0.07	-0.08	1.42	1.66	0.87	-0.13	1.44
17122638	.	1.45	-1.08	0.63	-1.72	-0.10	-2.35	-1.53	0.03	1.13	-1.18	-1.83	1.27
17123206	.	-0.03	0.00	0.01	0.61	1.04	1.31	-0.84	-0.38	-1.22	1.50	-4.62	2.24
17124068	.	-2.04	-2.24	-2.48	-1.96	-2.38	-1.80	-0.71	-0.61	-2.67	-1.50	-3.23	-1.69
17124274	.	0.46	-1.56	-0.63	-0.31	0.06	-2.18	0.69	-0.23	-1.69	-1.27	-2.51	0.73
17124336	.	-2.50	-0.75	0.40	-1.22	-1.26	-1.63	0.54	-0.59	4.11	-4.48	-1.01	1.44
17124748	.	1.76	-0.77	1.33	0.67	1.54	1.15	-0.25	0.04	2.12	0.68	-3.90	-0.61
17125294	.	-0.79	-0.14	-0.32	-0.33	-0.35	-2.05	0.13	-1.87	0.68	-1.90	-1.61	0.37
17126000	.	0.52	-0.59	-2.36	1.64	0.69	-1.90	1.61	0.49	3.70	2.33	-4.60	-0.06
17126024	.	1.02	-0.86	1.37	-0.01	0.03	0.62	1.27	0.18	-0.24	0.17	-1.49	2.61
17126032	.	-1.97	-2.09	-1.13	-1.14	-1.63	-0.10	0.59	-0.93	-1.32	-1.66	-0.22	-0.64
17126050	.	-1.08	-0.71	-0.60	-1.03	-0.79	0.43	0.38	-0.64	-0.97	0.18	-2.56	-0.56
17126052	.	-0.32	-0.51	0.36	0.50	0.75	-1.93	-0.90	0.16	1.74	-0.59	-1.82	0.83
17126142	.	-1.97	-2.09	-1.13	-1.14	-1.63	-0.10	0.59	-0.93	-1.32	-1.66	-0.22	-0.64
17126152	.	-0.75	-0.43	0.14	0.81	0.12	-0.06	0.56	0.68	1.81	0.02	-2.74	1.16
17126156	.	-1.08	-0.71	-0.60	-1.03	-0.79	0.43	0.38	-0.64	-0.97	0.18	-2.56	-0.56
17126162	.	-0.32	-0.51	0.36	0.50	0.75	-1.93	-0.90	0.16	1.74	-0.59	-1.82	0.83

Supplementary Table 4B. Differentially expressed genes based on transcriptomic data for PBMCs exposed to Tw.

Probe_Id	Genes	C1	C2	HET1	HET2	HET3	P1	P2	P3	WT1	WT2	WT3	WT4
16650647	.	-1.33	-0.08	0.55	-0.11	-0.02	-2.39	-0.06	-1.93	-3.58	1.55	-1.81	0.97
16651905	.	-3.30	-1.32	-4.44	-3.02	-0.38	-4.24	2.57	-1.24	2.04	-4.76	0.66	-0.25
16652101	.	3.55	0.82	1.69	0.39	0.57	1.08	1.50	4.45	4.90	-7.55	2.40	-2.41
16653707	.	1.66	-2.88	1.37	0.85	2.59	0.10	1.68	4.39	1.30	-4.11	4.95	-4.14
16653785	.	0.70	-1.66	1.17	1.36	0.46	-0.94	-1.24	0.06	1.01	0.99	-1.47	0.50
16653795	.	-0.84	0.53	-0.75	0.54	0.60	1.73	0.50	0.93	-1.21	1.45	0.25	-1.17
16654693	.	-3.80	-0.07	1.15	2.22	-2.32	-0.34	-1.92	-0.22	3.08	-1.70	-0.15	-0.72
16657037	.	0.01	1.67	1.22	-0.76	0.72	-7.52	2.28	-0.23	6.56	1.54	-2.14	1.97
16658933	.	0.23	-1.09	-0.49	0.86	0.39	-0.36	-1.57	0.83	0.65	2.11	0.62	2.68
16658936	.	0.74	-0.63	0.17	0.44	0.02	2.56	0.29	-0.22	0.10	-0.39	0.94	1.50
16663808	.	-1.39	-0.36	0.24	-0.32	0.93	1.17	0.26	-0.38	1.51	1.00	0.04	-0.61
16678342	.	-0.62	-0.08	0.17	-1.41	1.25	-2.67	2.38	-0.03	1.12	-0.22	-0.89	-1.08
16693644	.	-0.59	-0.96	-0.24	-1.15	-0.34	1.08	1.30	-0.37	2.18	0.68	-1.63	0.10
16699512	.	2.81	-4.16	-0.78	-0.25	3.93	-1.86	0.65	2.14	-0.19	-3.01	0.87	-1.12
16718373	.	1.11	-0.90	-0.71	0.97	-0.29	-0.28	0.09	1.08	2.59	1.38	0.12	1.89
16732028	LOC105369519	-0.87	-0.95	-0.05	-0.08	0.34	-2.11	0.07	1.72	1.87	0.34	0.77	-2.22
16735142	.	1.96	1.67	1.19	0.09	-0.91	-0.32	0.84	2.57	3.55	1.15	-2.65	-1.28
16735819	.	-0.74	-0.89	-0.26	0.16	0.12	0.56	-0.32	0.72	0.73	1.13	-0.18	1.12
16735835	.	0.42	0.80	0.41	2.54	-2.38	-0.73	4.84	4.26	-3.65	-1.97	0.38	4.69
16740560	.	-0.65	-0.50	0.36	0.36	0.42	0.18	-0.56	0.04	0.64	0.80	0.74	0.34
16745154	.	0.82	-0.82	-0.53	0.47	0.09	0.07	0.02	-0.29	1.86	-0.23	-0.56	3.40
16747336	SCARNA10	0.89	0.29	-0.70	0.02	0.37	-0.20	1.30	0.51	0.84	-1.44	0.04	-0.73
16751995	.	1.36	-2.10	2.56	-4.08	4.43	-1.29	0.09	-0.67	-1.04	1.41	-1.30	-0.67
16752007	.	-1.31	0.81	2.90	0.16	0.06	1.62	0.99	1.68	5.58	-0.33	1.62	0.74
16755523	.	0.31	-0.83	0.42	-0.15	0.01	1.03	-0.72	0.45	1.96	-0.21	-0.67	1.73
16764077	.	-1.27	-0.56	1.04	0.92	0.06	-3.16	-0.61	0.90	1.92	-0.31	-2.67	3.99
16769725	.	-1.53	1.81	-0.92	1.44	0.83	0.60	-4.09	-0.76	-1.59	-2.26	0.22	-4.09
16769727	.	-1.29	-0.47	0.85	0.31	-0.81	1.14	-1.04	1.92	-0.76	-1.15	-0.82	-2.14
16769728	.	-0.82	-0.86	-0.88	1.73	-0.24	-1.92	0.43	1.42	-1.79	0.98	-2.09	5.19
16769749	.	-0.08	-1.03	-0.02	0.08	0.05	-1.87	0.24	1.35	2.11	-0.24	-0.97	-0.98
16769758	.	-1.16	-0.62	2.16	0.87	2.15	-3.75	-5.68	-0.53	4.47	1.98	-1.91	1.08
16771317	.	-0.17	0.94	-0.85	1.09	0.82	0.77	0.40	1.40	7.33	1.29	-1.83	-0.35
16771492	.	-2.11	-1.93	2.03	-0.28	2.37	-1.87	-1.29	0.65	-1.90	2.48	-0.82	1.43
16771510	.	0.12	1.16	-1.12	0.11	0.48	0.36	1.84	0.36	1.62	0.60	0.58	-1.99
16771559	.	-0.83	-1.76	-1.80	-1.22	1.40	-1.97	-1.07	0.36	5.80	0.65	-1.56	2.13
16790473	.	0.05	0.18	-0.41	-0.89	0.02	-0.02	0.34	-0.29	1.50	0.89	-0.60	-0.70
16794260	.	-0.73	0.02	0.44	-0.29	0.13	2.22	-1.34	0.99	3.21	-0.75	-0.05	-1.39
16823043	SNHG19	1.06	1.10	2.45	1.09	-0.59	-2.24	1.63	-1.37	-0.35	0.53	-1.93	-3.87
16823105	.	-0.81	-0.88	0.29	0.15	-0.40	-0.17	0.54	1.89	-0.49	0.85	1.71	1.00
16828270	.	-0.94	0.26	1.43	0.43	1.08	-0.01	-0.82	0.74	0.60	-0.28	1.66	0.61
16828528	.	0.89	0.85	-0.50	0.61	-0.03	1.40	1.07	0.45	-0.20	-0.31	-0.95	0.94
16828531	.	0.86	0.65	-0.71	0.43	0.51	0.36	0.49	0.50	0.45	-0.40	-1.07	1.10
16835618	.	-0.06	-1.07	1.66	-1.36	1.43	0.22	-0.67	0.93	5.53	1.56	1.60	-2.34
16835641	.	0.27	0.80	-0.32	-1.26	-0.29	3.90	2.49	-0.36	4.45	1.03	-0.97	3.40
16836624	MIR21	-1.84	-1.38	1.11	-0.14	0.92	-1.59	-0.70	-0.23	2.26	-0.18	1.11	-2.35
16839474	.	-0.41	0.72	0.63	0.24	-0.24	-1.83	1.61	-0.53	0.80	-0.87	-0.74	1.92
16839477	.	-1.60	-1.12	0.87	1.14	0.32	-1.85	0.93	0.76	-3.53	-1.81	-0.94	-1.26
16839481	.	-0.87	0.53	0.79	-0.25	0.90	-3.50	0.23	1.03	-1.21	0.61	1.17	-1.64
16839489	.	-3.93	2.15	0.79	-0.73	0.85	-0.54	-0.75	0.31	0.28	3.46	0.79	6.30
16839492	.	-1.45	0.68	0.23	-0.63	-0.34	3.09	-0.36	0.85	-1.72	0.45	0.73	4.71
16839494	.	1.34	-0.72	-0.16	0.64	0.53	2.70	0.20	-0.05	-2.29	0.64	-1.14	1.79
16839506	.	-2.63	-1.15	-0.16	0.23	-0.17	-2.67	0.88	0.39	1.14	1.61	1.37	-1.63
16839513	.	-0.66	-0.69	-0.33	-0.70	0.46	-0.83	-0.31	0.10	2.50	0.63	0.21	-0.71
16839515	.	-0.84	-1.14	1.71	0.05	-0.53	-0.92	-0.26	-0.16	3.09	0.91	-1.13	0.19
16840589	.	-2.62	0.60	0.96	0.31	0.87	0.50	-1.11	0.67	-0.29	1.08	-0.88	-2.81
16842465	.	-2.74	2.06	2.24	-0.96	-0.86	-1.72	0.23	3.34	-2.64	-2.61	2.33	-2.14
16842466	.	-0.44	0.99	1.53	-1.25	-0.99	-0.13	0.17	1.20	-2.32	-2.90	1.74	-2.22
16847247	.	3.41	-2.06	1.77	2.75	2.02	-0.87	0.89	1.19	5.20	-0.68	1.46	-2.23

16847319	MIR4737	-3.30	-0.02	3.15	-0.26	0.29	-0.89	2.03	-0.72	0.68	-2.86	-1.57	-2.04
16852308	SCARNA17	-0.42	0.59	-0.63	0.53	-0.93	-1.70	-0.45	-0.42	-0.41	-0.86	1.83	-2.00
16857916	.	0.26	-0.04	-1.28	-0.25	-0.27	1.02	-0.13	0.21	1.39	-1.05	0.85	2.06
16859821	.	-1.04	-0.09	-0.63	1.02	0.05	-3.23	3.29	0.39	4.46	-0.84	1.14	-0.27
16859824	.	-0.71	0.99	0.14	-1.48	-0.60	4.68	-1.09	3.43	-1.33	0.65	1.18	3.24
16861887	ECH1	0.62	-0.24	-0.28	0.45	-0.62	-0.61	2.38	-0.23	1.02	-0.50	-0.87	-0.67
16893456	.	1.90	-1.32	0.81	1.13	1.68	-4.12	-1.30	0.51	2.62	1.23	-0.63	1.59
16898487	.	-1.05	0.70	3.24	2.82	-0.75	-2.79	2.73	0.68	0.17	1.84	-4.70	1.84
16900096	IGKC	-0.59	-0.81	-1.13	-0.18	0.98	3.37	-0.41	1.39	1.21	0.79	-0.17	1.06
16900461	.	0.07	-0.89	-0.46	-0.50	0.29	1.38	1.67	-0.46	2.39	0.98	0.49	-1.15
16900505	.	-1.06	-0.26	-1.54	-0.65	-0.46	-1.06	-0.80	0.94	1.20	-0.93	1.62	0.33
16900506	.	-1.45	-0.92	-0.19	-1.42	0.86	-1.22	0.41	0.58	4.77	1.10	1.50	1.77
16900520	.	-0.61	-1.03	-1.21	-0.36	-0.17	-0.20	1.49	0.58	-0.69	-0.67	0.71	1.57
16900530	.	-1.68	1.14	0.24	-0.68	2.07	-2.20	0.33	0.40	-0.03	-0.03	-0.80	-2.17
16915993	PPDPF	-1.08	-1.23	0.64	-0.25	0.08	-0.38	-0.21	0.11	0.65	-0.31	0.59	1.68
16934240	.	-1.99	-1.06	1.60	-0.15	0.02	-0.47	-0.41	0.21	-0.84	-1.70	-2.76	-0.21
16934244	.	-1.55	-1.79	1.61	-0.59	0.14	-0.64	-0.66	0.42	-1.39	-2.41	-3.01	-0.05
16934245	.	-1.40	-0.54	-1.58	-0.05	0.62	-2.10	-1.11	0.63	-0.69	-2.54	-0.17	-1.18
16934595	.	1.34	1.26	-0.80	-1.78	-0.39	1.70	-0.39	-0.09	4.87	-5.23	1.27	-7.36
16934598	.	1.00	-1.06	1.23	-0.11	0.02	6.14	-0.57	-0.80	1.58	-0.67	-0.25	1.50
16934602	.	0.04	-1.33	-0.04	-0.07	-0.47	-2.96	0.30	0.86	2.09	-0.62	-0.19	0.81
16934603	.	0.14	-0.86	1.17	-0.58	-0.06	-2.08	0.46	0.65	1.98	-0.76	-1.43	-0.15
16961037	SCARNA7	-2.22	1.02	-2.26	1.35	-2.27	4.58	-0.47	-0.69	0.78	0.22	-2.31	-1.37
16983266	.	-0.49	-1.65	-2.46	0.02	0.93	1.01	0.46	1.29	-2.78	-2.22	0.20	2.09
16988537	.	-0.33	-1.65	-3.89	-1.23	-1.62	-1.51	-0.32	-1.83	-1.92	-3.89	-1.59	-2.43
16989865	.	-0.14	-1.53	0.27	-0.33	0.25	-3.85	1.00	0.48	-2.07	-0.96	0.37	2.26
16990120	.	0.43	-0.50	-0.10	0.49	-0.23	1.08	-1.18	-0.86	3.68	-0.71	-0.81	-0.84
16997644	.	-2.33	-0.44	1.61	0.42	-1.00	1.41	1.34	0.96	-2.05	-1.88	0.06	-2.11
17006290	.	1.47	0.06	0.63	0.72	1.58	-1.62	0.80	0.22	1.19	-1.40	0.10	-2.06
17006294	.	0.32	-0.34	0.60	-0.01	0.12	-2.54	0.08	0.19	1.14	-1.31	-0.60	0.76
17006295	.	0.09	-1.23	-0.02	-0.10	-0.02	-0.46	0.76	0.11	1.33	-1.11	-1.22	0.81
17006296	.	0.77	-0.84	1.34	0.08	-0.22	-4.68	-0.40	-0.41	0.61	-1.76	-0.16	-2.33
17006305	.	-1.21	-2.08	-3.30	-0.83	-0.24	-3.51	0.53	-0.03	3.19	-0.58	0.50	-2.34
17006306	.	-1.29	-2.60	1.21	-1.64	-1.04	-1.34	1.53	0.71	6.02	-3.72	-0.03	0.88
17006308	.	-1.59	-0.44	-0.42	-1.35	1.21	-1.30	1.34	0.23	2.20	-0.74	0.88	-0.17
17016372	HIST1H1C	0.08	-0.18	0.24	-0.26	0.75	0.96	0.23	1.16	2.01	1.11	0.67	-1.34
17016503	HIST1H3I	-1.23	-0.39	0.52	-0.69	0.25	-2.58	-2.26	0.08	2.78	1.23	-0.45	-2.91
17017177	.	0.46	-0.77	-0.49	-0.64	0.78	-1.45	-0.08	0.09	1.33	0.98	1.09	0.10
17017194	.	-4.83	-0.81	3.34	1.08	1.27	-0.88	0.46	-1.11	1.99	3.95	2.61	6.54
17017197	.	0.79	-0.86	1.26	0.34	-0.70	-2.40	0.71	0.17	5.90	-1.69	-0.44	4.28
17018387	.	-0.72	-0.79	0.75	0.45	0.43	-2.84	0.54	0.18	4.74	1.47	-1.47	2.83
17041697	.	-0.22	-0.69	-0.07	0.24	0.01	-0.35	0.64	-0.11	0.59	-0.51	-0.69	0.82
17047459	SNORA14A	0.97	0.71	0.06	-0.40	-0.72	1.03	0.76	0.13	-0.29	0.05	-1.28	-1.48
17061125	RASA4B	-2.13	2.69	-1.90	-0.58	1.01	2.04	-1.45	-0.85	-1.78	2.23	2.23	-5.88
17068624	.	0.59	-0.01	0.02	-0.53	-0.91	-0.75	0.89	1.17	0.61	-0.87	0.00	3.76
17100655	.	1.29	0.94	0.46	0.71	-1.34	-0.27	0.02	-0.39	-0.98	-0.64	0.55	0.46
17100810	.	-0.09	-0.69	-1.52	-0.15	0.19	0.05	0.30	-0.34	1.35	-1.05	0.92	1.48
17104684	.	-0.70	-0.66	-0.20	0.63	-1.08	-1.07	-0.31	-0.06	0.71	0.86	-0.54	-0.55
17118001	BRK1	0.56	-0.61	-0.70	0.01	0.02	-1.19	1.82	-1.01	1.99	-0.98	0.33	-2.36
17118426	.	-0.65	1.14	0.11	0.20	-0.12	0.01	-0.64	0.36	3.42	1.35	0.40	1.57
17118850	.	0.86	1.06	-0.25	-0.02	0.06	-0.44	0.71	0.19	3.34	-0.58	0.42	2.19
17120164	.	0.05	0.63	-0.22	0.18	0.40	-2.58	0.12	-0.27	0.18	-0.77	-0.95	-1.29
17121378	.	-0.70	-0.30	-0.05	-0.18	0.43	-0.41	0.42	-0.10	1.79	-0.27	0.62	-0.61
17121380	.	-0.66	-1.08	0.36	-0.30	0.40	-0.38	0.02	-0.04	1.64	-0.19	0.93	-1.22
17121504	.	-0.40	-2.05	0.86	-0.31	-0.05	-0.22	-0.60	0.06	1.55	0.22	1.46	-2.10
17124336	.	-0.62	-0.21	-0.57	0.10	-0.90	0.52	0.81	0.41	3.06	-1.17	0.92	1.55
17124536	.	2.59	-1.58	0.92	0.65	-0.69	-5.38	0.34	2.85	5.23	-2.26	-1.19	2.99
17124748	.	1.16	0.35	0.64	0.43	0.80	1.94	1.66	-0.33	5.98	1.98	0.27	-1.11
17125856	.	-1.10	-2.39	-1.27	-1.52	1.35	-1.96	-1.24	0.15	2.78	-1.58	-1.19	1.53
17126000	.	-1.43	-1.42	-2.62	0.31	0.00	-1.15	1.71	-0.91	3.36	1.17	-2.27	0.09
17126152	.	-0.37	-0.66	0.58	0.14	-0.41	0.29	-0.28	1.23	1.28	-0.14	0.79	1.17

Supplementary Table 5. Immunophenotyping of patients (P1, P2 and P3) and a WT homozygous relative.

	P1	P2	P3	P1'sister	Normal range
Phenotype	WD	WD	WD	Healthy	
IRF4 genotype	R98W/WT	R98W/WT	R98W/WT	WT/WT	
lymphocytes number/µl	1100	2400	1200	2400	
T Lymphocyte Immunophenotyping (%)					
CD3+	71	77	58	77	51-82
CD4+	49	42	33	55	31-63
CD8+	21	30	25	19	9-34
CD45RO+/CD4+	48	81	85	40	
CD45RA+/CD4+	52	19	15	60	20-86
CD31+/CD4+	31	17	8	25	
CD31+/CD45RA+/CD4+	24	6	3	20	20-28
CCR7+CD45RA+/CD8+	20	7	6	15	29-57
CCR7+CD45RA-/CD8+	17	7	12	2	3-14
CCR7-CD45RA-/CD8+	39	49	27	44	20-41
CCR7-CD45RA+/CD8+	24	37	55	40	11-26
B Lymphocyte Immunophenotyping (%)					
CD19+	8	11	6	9	4-21
NK Lymphocyte Immunophenotyping (%)					
CD16+CD56+	21	12	36	12	5-33